PRISMA Satellite Images Coregistration and Their Use in Landcover Classification

By Mohammed Hatim Magzoub Alhag

A Thesis Submitted in Partial Fulfillment
of the Requirements for the Degree of
Master of Science

Supervised by
Prof. Maria Antonia Brovelli
Co-Supervised by
Dr. Vasil Yordanov

Politecnico di Milano
School of Civil, Environmental and Territorial Engineering

23 November 2023

Abstract

This study focuses on enhancing land cover classification by coregistering PRISMA hyperspectral L2D imagery with Sentinel-2 Level 2A satellite images. Utilizing the eFolki algorithm for this task, we achieved a residual error below 0.18 pixels in the coregistration process, a crucial factor in ensuring accurate pixel alignment. This precision was validated using the forward-backward criterion, confirming the effectiveness of the alignment.

A vital step in our methodology was the preprocessing of PRISMA data. Through histogram analysis, we identified and removed noisy spectral bands, significantly improving data quality for classification. In the initial classification phase, we applied Random Forest and Support Vector Machine (SVM) models to an imbalanced dataset. This approach yielded notable accuracies of approximately 94.60% with Random Forest and 96.97% with SVM.

Further refining our technique, we applied the SVM model to a balanced dataset, which substantially enhanced the classification accuracy. This resulted in an overall accuracy of approximately 99.39%, demonstrating the effectiveness of our method in providing highly accurate land cover classifications.

These findings highlight the importance of precise coregistration and careful data preprocessing in land cover classification from satellite imagery. By integrating detailed image analysis with advanced algorithmic approaches, this study offers a robust framework for environmental monitoring and sets a precedent for future remote sensing applications.

Contents

1. Introduction

Introduction to the remote sensing

Remote sensing is a technique employed to gather information about objects or areas from a distance, typically from aircraft or satellites. This technology enables the observation and analysis of the Earth's surface and atmosphere without direct contact. Through the use of various sensors mounted on different platforms, it captures information about the Earth's surface and atmosphere, providing invaluable insights across a myriad of applications [1]. The technology has evolved significantly over the years, transitioning from simple aerial photography to the use of sophisticated satellite-based sensors that capture data across various spectral bands [2].

History of remote sensing

In 1859, Gaspard Tournachon captured a slanted photograph of a small village near Paris from a hot air balloon, marking the beginning of earth observation and remote sensing. His work inspired others around the world to explore this field. For instance, during the Civil War in the United States, balloon-based aerial photography played a crucial role in uncovering defense positions in Virginia, as noted by [3]. This period also saw rapid advancements in photography, lenses, and the airborne application of these technologies.

A significant progression in remote sensing occurred in Europe between the two World Wars. Aircraft, being more dependable and stable than balloons, were extensively used for photoreconnaissance during World War I [4]. In the interwar period, civilians began using aerial photography in various fields such as geology, forestry, agriculture, and mapmaking, leading to advancements in cameras, films, and interpretation equipment. World War II saw major developments in aerial photography and image interpretation, as well as the emergence of other imaging systems like near-infrared photography, thermal sensing, and radar. These technologies proved invaluable for distinguishing actual vegetation from camouflage and for nighttime bombing missions. The first successful airborne imaging radar, developed in Great Britain in 1941, was primarily used for military purposes.

In the 1950s, after the wars, remote sensing technologies continued to develop based on wartime innovations. Color infrared (CIR) photography became a valuable tool in plant sciences, aiding in the classification and recognition of vegetation types, as well as in the identification of diseased, damaged, or stressed vegetation. This decade also saw substantial progress in radar technology.

The first weather satellite, TIROS-1, was sent to space in 1960, creating new opportunities for watching the atmosphere. This event was a starting point for the many remote sensing satellites we have now [5]. With years passing, improvements in how we gather, and handle information have enhanced what remote sensing can do, turning it into a crucial tool for researchers, people making decisions, and various experts [6].

Types of remote sensing

1. Passive Remote Sensing

Passive remote sensing involves the detection of natural radiation emitted or reflected by the target. This category includes optical and infrared sensors that capture sunlight reflected off the Earth's surface, as well as thermal sensors that detect emitted heat [7].

2. Active Remote Sensing

Active remote sensing, in contrast, emits its own signal towards the target and measures the reflected energy. Radar and LiDAR are prime examples, emitting microwave and laser energy, respectively, and are widely used for topographic mapping and vegetation analysis [8].

Remote Sensing Platforms

1. Satellites

Satellites are the most common spaceborne platforms, providing extensive coverage and the ability to monitor large-scale phenomena [9].

2. Aircraft and Drones

Aircraft and drones offer higher resolution data and flexibility, making them ideal for localized studies [10].

3. Ground-Based Platforms

Ground-based platforms, including towers and mobile units, are crucial for calibrating and validating data collected from airborne and spaceborne sensors [11].

Remote Sensing Data Processing

Data processing is a critical step in transforming raw remote sensing data into usable information. This involves a series of preprocessing steps such as calibration, atmospheric correction, and geometric correction [12]. Advanced techniques such as machine learning and data fusion are increasingly used to enhance the quality of the data and extract meaningful information [13].

Remote Sensing Applications

1. Agriculture

Remote sensing plays a crucial role in precision agriculture, providing information on crop health, soil conditions, and irrigation needs [14]. It aids in optimizing agricultural practices, enhancing productivity, and minimizing environmental impacts [15].

2. Environmental MonitoringIn the realm of environmental monitoring, remote sensing is used to track biodiversity, assess water quality, and monitor the impacts of climate change [16]. It provides critical data for conservation efforts and sustainable resource management [17].

3. Urban Planning

Remote sensing supports urban planning through land use mapping, infrastructure development, and traffic management [18]. It aids in creating sustainable urban environments and managing the challenges of urbanization [19].

4. Disaster Management

In disaster management, remote sensing provides timely and accurate information for response and recovery efforts during natural disasters such as floods, earthquakes, and wildfires [20]. It enhances situational awareness and aids in damage assessment, contributing to more effective disaster response [21].

5. Climate Change Studies

Remote sensing is instrumental in studying the effects of climate change, providing long-term data sets that are crucial for understanding global climate patterns and predicting future changes [22]. It plays a key role in climate modeling and the assessment of climate change impacts on various ecosystems [23].

6. Forestry

In forestry, remote sensing aids in forest management, species identification, and monitoring of deforestation and forest health [24]. It provides valuable data for sustainable forest management and conservation efforts [25].

Overview of the PRISMA Satellite:

The PRISMA satellite, managed by the Italian Space Agency, is a major progress in observing Earth and collecting detailed hyperspectral remote sensing data. It was sent into space in March 2019 and carries advanced tools that can take both hyperspectral and panchromatic imagery, providing comprehensive and detailed views of the Earth's surface.

PRISMA's payload includes a hyperspectral sensor with a spectral range of 400 to 2500 nm, as well as a high-resolution panchromatic sensor. The hyperspectral sensor provides detailed spectral information across 239 contiguous bands, while the panchromatic sensor delivers imagery with a 5-meter spatial resolution. This combination of sensors enables comprehensive and detailed analysis of the Earth’s surface, facilitating a variety of applications in fields such as agriculture, environmental monitoring, and natural resource management.

PRISMA operates in a sun-synchronous orbit, ensuring consistent lighting conditions for imagery acquisition. The satellite's design and capabilities are a testament to Italy's commitment to advancing space-based Earth observation technologies.

Through its sophisticated sensors and advanced operating modes, PRISMA provides valuable data to the scientific community, contributing to our understanding of the Earth's systems and supporting sustainable management of natural resources [26].

Products and Processing Levels:

PRISMA provides a suite of products at different processing levels, catering to diverse user needs and applications:

Level 1 (L1): L1 products consist of raw data and basic radiometric corrections. They serve as the foundation for higher-level processing and analysis.

Level 2 (L2): L2 products undergo additional processing, including geometric and atmospheric corrections. This level includes various sub-products such as L2A (reflectance data) and L2B (brightness data).

Level 2D (L2D): The L2D product includes atmospherically corrected hyperspectral data, providing users with data that is ready for analysis and interpretation. It is a key product for users interested in extracting quantitative information from the imagery.

All products cover a standard scene with size 30x30 km2 as a result of segmentation of longer data take strips. The geolocation accuracy of PRISMA's imagery is crucial for its applications. The imagery undergoes orientation and orthorectification processes to correct distortions and align it with real-world coordinates. PRISMA faces unique challenges in this regard, requiring specialized procedures for image orientation (2). The L2D product level from the PRISMA satellite is one of the higher-level processed data products, and it typically includes geolocated and atmospherically corrected hyperspectral imagery. The geolocation accuracy of L2D products would be 200m without GCPs CE90 and less than 15 with GCPs CE90[26].

The alignment of PRISMA with Sentinel-2 imageries

Image registration: Image registration is a technique that can be used to align two images. The first objective of the study is to develop a methodology for aligning PRISMA and Sentinel-2 imageries. This is a challenging task due to the different spectral resolutions, sensor characteristics, and acquisition geometries of the two types of imageries. The registration can be done using a variety of methods, such as feature-based registration, intensity-based registration, and sensor model-based registration.

Feature-Based methods:

In feature-based registration methods, strong and distinct image features are identified and extracted from both the reference and sensed images. Following this, a matching process is carried out to establish correspondences between the features of the two images, leading to the identification of correct matches. Utilizing these matched pairs, the transformation that relates the two images is calculated. Subsequently, this transformation is applied to the sensed image, resulting in the aligned, registered image. Prominent methods within this category include Scale Invariant Feature Transform (SIFT) (27), Speeded Up Robust Features (SURF) (28), Local Self-Similarity (LSS) (29), and Shape Context (30).

Key considerations in feature-based registration include:

- **Repeatability:** This metric assesses the stability of feature detection, advocating for the extraction of feature points at corresponding locations across both input images to enhance repeatability (31).
- **Number of Correct Matches (NCM):** Achieving a high number of accurate matching pairs is crucial for improving positional accuracy in the registration process.
- **Controllability:** A feature-based method should allow for control over the quantity of features extracted, ensuring a sufficient number of features are identified for reliable registration (32).

- **Correct Matching Rate (CMR):** Defined as the ratio of correct matches to the total number of matches (inclusive of both correct and incorrect matches), a higher CMR indicates more reliable matching (33).
- **Distribution of Matching Pairs:** Uniform distribution of matching pairs is essential for estimating a transformation model capable of handling local distortions in remote sensing images (32).
- **Distinctiveness:** Feature descriptors should be unique to enhance the accuracy of the matching process.
- **Robustness:** Descriptors need to be resilient, capable of handling substantial geometric and radiometric variations between input images, as well as noise.

Intensity-Based methods

In intensity-based registration methods, the goal is to compute a similarity metric utilizing the input images to derive the registered image. These methods typically employ some form of optimization strategy to expedite the registration procedure. Utilizing an optimizer to fine-tune the registration function results in multiple transformations of the sensed image over the reference image, continuing until a peak in similarity between the two images is reached. The primary aim in this context is to pinpoint the transformation ϕ that maximizes this similarity. Following the identification of this transformation, the sensed image is altered accordingly to produce the registered image. Cross correlation (CC) and mutual information (MI) are commonly recognized similarity metrics employed in intensity-based registration methods (34).

Deep learning-based methods

At times, both feature-based and intensity-based approaches may struggle to accurately register images that are significantly deformed or impacted by noise (35). Traditional feature-based techniques rely on manually crafted features such as edges, corners, textures, and gradients, which do not encapsulate higher-level semantic information (36). These techniques do not incorporate feedback between the extraction and matching of features, leading to a direct impact on the efficacy of feature matching when there is a lack of robust features. To address these challenges, deep learning has become a widely adopted methodology for remote sensing image registration (37; 38; 39; 35; 40; 36; 41). Methods based on deep learning autonomously derive features, utilizing the hidden and output layers of neural networks for the purposes of feature extraction and matching.

The developed methodology will be evaluated using a variety of datasets, including the PRISMA and Sentinel-2 imageries. The results of the evaluation will be used to improve the methodology and to make it more robust.

Land cover classification using coregistered data

The second objective of the thesis is to apply the methodology to study land cover changes. This will be done by using the Coregistered PRISMA imageries to classify land cover over time. The results of the land cover classification will be used to study the changes in land cover, such as deforestation and urbanization. Studying changes in land cover is important to understand how human activities impact the environment. The findings from this study can help in making plans and taking actions to reduce the negative effects of these land cover changes.

References

1. Richards, J. A., & Jia, X. (2006). Remote Sensing Digital Image Analysis: An Introduction. Springer.
2. Jensen, J. R. (2007). Remote Sensing of the Environment: An Earth Resource Perspective. Pearson Prentice Hall.
3. Colwell, R. N. (1983). Manual of Remote Sensing. American Society of Photogrammetry.
4. Blakemore, M. (1988). A History of Aerial Photography and Archaeology. Batsford.
5. Kidder, S. Q., & Vonder Haar, T. H. (1995). Satellite Meteorology: An Introduction. Academic Press.
6. Elachi, C., & van Zyl, J. (2006). Introduction to the Physics and Techniques of Remote Sensing. John Wiley & Sons.
7. Lillesand, T. M., Kiefer, R. W., & Chipman, J. (2014). Remote Sensing and Image Interpretation. John Wiley & Sons.
8. Leckie, D. G., & Ranson, K. J. (1998). Forestry applications using imaging radar. In Manual of Remote Sensing (Vol. 2, pp. 435-509). John Wiley & Sons.
9. Cracknell, A. P., & Varotsos, C. A. (2007). New aspects of global climatology and climate change by satellite remote sensing. International Journal of Remote Sensing, 28(12), 2791-2823.
10. Anderson, K., & Gaston, K. J. (2013). Lightweight unmanned aerial vehicles will revolutionize spatial ecology. Frontiers in Ecology and the Environment, 11(3), 138-146.
11. Richter, R., & Schläpfer, D. (2014). Atmospheric/Topographic Correction for Satellite Imagery: ATCOR-2/3 User Guide.
12. Chavez Jr, P. S. (1996). Image-based atmospheric corrections—Revisited and improved. Photogrammetric Engineering & Remote Sensing, 62(9), 1025-1036.
13. Zhang, J., & Goodchild, M. F. (2002). Uncertainty in Geographical Information. Taylor & Francis.
14. Bausch, W. C. (1993). Soil background effects on reflectance-based crop coefficients for corn. Remote Sensing of Environment, 46(2), 213-222.
15. Moran, M. S., Clarke, T. R., Inoue, Y., & Vidal, A. (1994). Estimating crop water deficit using the relation between surface-air temperature and spectral vegetation index. Remote Sensing of Environment, 49(3), 246-263.
16. Pettorelli, N., Safi, K., & Turner, W. (2014). Satellite remote sensing for applied ecologists: opportunities and challenges. Journal of Applied Ecology, 51(4), 839-848.
17. Turner, W., Spector, S., Gardiner, N., Fladeland, M., Sterling, E., & Steininger, M. (2015). Free and open-access satellite data are key to biodiversity conservation. Biological Conservation, 182, 173-176.
18. Herold, M., Couclelis, H., & Clarke, K. C. (2005). The role of spatial metrics in the analysis and modeling of urban land use change. Computers, Environment and Urban Systems, 29(4), 369-399.
19. Alberti, M., & Waddell, P. (2000). An integrated urban development and ecological simulation model. Integrated Assessment, 1(3), 215-227.
20. Joyce, K. E., Belliss, S., Samsonov, S. V., McNeill, S. J., & Glassey, P. J. (2009). A review of the status of satellite remote sensing and image processing techniques for mapping natural hazards and disasters. Progress in Physical Geography, 33(2), 183-207.
21. Gupta, R. P. (2003). Remote Sensing Geology. Springer Science & Business Media.
22. Muttiah, R. S., & Wurman, P. R. (2004). Satellite remote sensing of landscape change in the southern Great Plains: The normalized difference vegetation index as a surrogate for ecological monitoring. Landscape Ecology, 19(5), 453-467.
23. Hansen, M. C., & Loveland, T. R. (2012). A review of large area monitoring of land cover change using Landsat data. Remote Sensing of Environment, 122, 66-74.
24. Franklin, S. E. (2001). Remote sensing for sustainable forest management. CRC Press.
25. Lu, D. (2006). The potential and challenge of remote sensing-based biomass estimation. International Journal of Remote Sensing, 27(7), 1297-1328.

26. PRISMA Algorithm Theoretical Basis Document (ATBD), Issue 1, Date 14/12/2021.
27. Lowe, D. G. 2004. “Distinctive Image Features from Scale-invariant Keypoints.” *International Journal of Computer Vision* 60 (2): 91–110. doi:10.1023/B:VISI.0000029664.99615.94.
28. Bay, H., A. Ess, T. Tuytelaars, and V. G. Luc. 2008. “Speeded-up Robust Features (SURF).” *Computer Vision and Image Understanding* 110 (3): 346–359. doi:10.1016/j.cviu.2007.09.014.
29. Shechtman, E., and M. Irani. 2007. “Matching Local Self-similarities across Images and Videos.” In Proc. IEEE Comput. Vis. Pattern Recognit., Minneapolis, USA, June, 1–8.
30. Belongie, S., J. Malik, and J. Puzicha. 2002. “Shape Matching and Object Recognition Using Shape Contexts.” IEEE Transactions on Pattern Analysis and Machine Intelligence 24 (4): 509–522. doi:10.1109/34.993558.
31. Schmid, C., R. Mohr, and C. Bauckhage. 2000. “Evaluation of Interest Point Detectors.” International Journal of Computer Vision 37 (2): 151–172.
32. Sedaghat, A., M. Mokhtarzade, and H. Ebadi. 2011. “Uniform Robust Scale-invariant Feature Matching for Optical Remote Sensing Images.” IEEE Transactions on Geoscience and Remote Sensing 49 (11): 4516–4527.
33. Fan, J., Y. Wu, M. Li, W. Liang, and Q. Zhang. 2017. “SAR Image Registration Using Multiscale Image Patch Features With Sparse Representation.” IEEE Journal of Selected Topics in Applied Earth Observations and Remote Sensing 10 (4): 1483–1493. doi:10.1109/JSTARS.2016.2628911.
34. Zitova, B., and J. Flusser. 2003. “Image Registration Methods: A Survey.” Image and Vision Computing 21 (11): 977–1000.
35. Quan, D., S. Wang, M. Ning, T. Xiong, and L. Jiao. 2016. “Using Deep Neural Networks for Synthetic Aperture Radar Image Registration.” In in Proc. IEEE Geosci. Remote Sens. Symp., 2799–2802. Beijing, China: IEEE.
36. Wang, S., D. Quan, X. Liang, M. Ning, Y. Guo, and L. Jiao. 2018. “A Deep Learning Framework for Remote Sensing Image Registration.” ISPRS Journal of Photogrammetry and Remote Sensing 145: 148–164.
37. Hoffmann, S., C.-A. Brust, M. Shadaydeh, and J. Denzler. 2019. “Registration of High Resolution Sar and Optical Satellite Imagery Using Fully Convolutional Networks.” In in Proc. IEEE Geosci. Remote Sens. Symp., 5152–5155. Yokohama, Japan: IEEE).
38. Hughes, L. H., M. Schmitt, L. Mou, Y. Wang, and X. X. Zhu. 2018. “Identifying Corresponding Patches in SAR and Optical Images with a Pseudo-siamese CNN.” IEEE Geoscience and Remote Sensing Letters 15 (5): 784–788. doi:10.1109/LGRS.2018.2799232.
39. Merkle, N., S. Auer, R. Müller, and P. Reinartz. 2018. “Exploring the Potential of Conditional Adversarial Networks for Optical and SAR Image Matching.” IEEE Journal of Selected Topics in Applied Earth Observations and Remote Sensing 11 (6): 1811–1820.
40. Vakalopoulou, M., S. Christodoulidis, M. Sahasrabudhe, S. Mougiakakou, and N. Paragios. 2019. “Image Registration of Satellite Imagery with Deep Convolutional Neural Networks.” In in Proc. IEEE Geosci. Remote Sens. Symp., 4939–4942. Yokohama, Japan: IEEE.
41. Zhang, H., N. Weiping, W. Yan, D. Xiang, W. Junzheng, X. Yang, and H. Bian. 2019a. “Registration of Multimodal Remote Sensing Image Based on Deep Fully Convolutional Neural Network.” IEEE Journal of Selected Topics in Applied Earth Observations and Remote Sensing 12 (8): 3028–3042.

2. Literature Review

A review of state-of-the-art techniques in image registration

Geometric registration serves as a vital component in ensuring precision for a wide range of remote sensing image processing and analytical tasks, including the creation of image mosaics, image fusion, and chronological analysis. In the past few decades, this area has captured substantial interest within the remote sensing community, resulting in extensive research on this topic. Nonetheless, there exists a paucity of systematic examinations of its current state and an in-depth exploration of its developmental directions. Furthermore, as new methodologies continue to emerge, several unresolved issues remain. Hence, this review offers a comprehensive review of the state-of-the-art techniques for remote sensing image registration, spanning intensity-based, feature-based, and hybrid methods. It also consolidates information on optical flow estimation, methods based on deep learning, as well as software-assisted registration and assessment of the registration process. Building upon recent progress, this work also identifies and discusses potential future directions.

Overview

Remote sensing imagery, obtained from diverse sensors, during different time periods, and from various perspectives, provides supplementary data about specific areas and observations of the Earth's surface. Due to a variety of factors such as the Earth’s rotation, its curvature, and variations in platform altitudes, these images exhibit systematic geometric distortions. These distortions can only be partially corrected without high-precision elevation data and ground control points. While the true digital orthophoto map offers precise spatial positions, it is expensive and not easily accessible to the general public. As a result, most available remote sensing images still retain minor geometric distortions after correction, leading to spatial discrepancies between objects in different images. This review highlights the importance of geometric registration techniques, which aim to align multiple images of the same scene, acquired at different times, from various viewpoints, and with different sensors [1]. This alignment is crucial for numerous practical applications in remote sensing, including image mosaicking [2], image fusion [3], land cover change detection [4], [5], and disaster evaluation [6], [7].

Additionally, the review delineates the distinction between image registration and coregistration, emphasizing their specific applications, particularly in aerial and unmanned aerial vehicle imagery. It traces the historical development of geometric registration back to the 1970s, documenting its expansion and evolution across various domains such as remote sensing, computer vision, and medical image processing. The review also presents a thorough analysis of literature from 1979 to January 2022, showcasing the growth of research in this area.

In subsequent sections, the review categorizes and elaborates on various classical and contemporary methods of remote sensing image registration, with a particular focus on deep learning-based approaches, optical flow estimation, and software-based registration methods. Additionally, it analyzes development trends and potential future directions in the field, from our perspective. The review underscores the crucial role of transformation models and resampling techniques in achieving image alignment, highlighting the significance of preliminary steps such as feature extraction and matching in the registration process.

Intensity-Based Alignment Techniques

Intensity-based alignment methodologies leverage the original or modified pixel values, such as image gradients, for aligning remote sensing imagery. This category encompasses traditional area-based methods as well as optical flow estimation, which directly computes the incremental displacement of corresponding pixels using their intensity values, classifying it as an intensity-based registration technique.

Area-Based Techniques

Area-based alignment generally follows a predetermined similarity criterion, employing an optimal search strategy to iteratively discover the transformation model parameters that maximize or minimize the similarity measure, resulting in the spatial alignment of images. Unlike image matching, typically associated with template matching, area-based methods directly utilize pixel intensity values, but aim to find the centroids of matched windows to establish feature points, which is a crucial step but not the final goal of geometric registration. This section delves into area-based registration, highlighting the significance of similarity metrics, explored through both spatial- and frequency-domain strategies [11], [16], [17].

Approach in Spatial Domain

The techniques within the Spatial Domain focus on employing the intensity variance and statistical attributes of all the pixels, circumventing any form of image transformation. Generally, there are two main methodologies employed in this domain: the correlation-like technique and the mutual information (MI) algorithm.

Technique of Correlation-Like Similarity Metric

This method aims to ascertain the spatial correspondence between images by directly evaluating the similarity of corresponding pixel values. However, it is susceptible to variations in intensity, which can be attributed to various factors such as noise, cloud cover variability, and discrepancies in the photosensitive elements of different sensors. The cross-correlation (CC) algorithm serves as a fundamental similarity metric within this domain, where it calculates the disparity between corresponding pixels and iteratively aligns images until a maximum CC value is achieved. This technique proves effective for minor rigid-body and affine transformations [18], [19]. There exists a plethora of correlation-like similarity metrics, including but not limited to the sequential similarity detection algorithm [20], correlation coefficient [21], [22], normalized CC (NCC) [23]–[25], sum of squared differences [26], Hausdorff distance [26], along with various other minimum distance criteria. Among these, NCC stands out due to its resilience to linear intensity variations, making it a popular and extensively utilized metric [23], [27], [29]. In recent developments, the central points of windows that exhibit a high degree of match according to NCC have been utilized as feature points, aiding in the determination of transformation model parameters [30], a process also referred to as image matching. Letting $\rho(R, S)$ represent the NCC coefficient for matched windows, the NCC is computed as follows:

$$\rho(R,S) = \frac{\sum_{i=1}^{m\times n}(R(i)-\mu_R)(S(i)-\mu_S)}{\sqrt{\sum_{i=1}^{m\times n}(R(i)-\mu_R)^2}\sqrt{\sum_{i=1}^{m\times n}(S(i)-\mu_S)^2}},$$

where a predefined window encompasses $(m \times n)$ pixels, $(R(i))$ and $(S(i))$ denote specific positions within the windows of the reference and sensed images, respectively, and (μ_R) and (μ_S) represent the average intensity values within a specified window. This algorithm has been refined to generate tie points that can withstand complex geometric deformations [31], [30], [31], and has been recently amalgamated with innovative feature descriptors (such as the local self-similarity (LSS) descriptor) to enhance feature extraction robustness in multimodal remote sensing image registration [28]. Although NCC outperforms traditional correlation-like similarity metrics, it struggles with nonlinear radiometric differences, a common issue for metrics of this kind.

Approach Based on Mutual Information (MI)

The application of Mutual Information (MI) in the field of image registration has gained prominence more recently compared to correlation-like techniques. It has demonstrated considerable success in the registration of multispectral and multisensor images, showcasing resilience to nonlinear radiometric disparities [32]– [34], as typically formulated in equation (2). The Normalized Mutual Information (NMI) method represents a variant of MI, characterized by its independence from fluctuations in the marginal entropies of the two images within their overlapping region [35], [36]. Both MI and NMI fall under the category of statistical similarity metrics, yet they remain susceptible to registration inaccuracies.

Building upon these methodologies, the region-based MI approach was introduced, incorporating structural information into the analysis [37]. Extending this concept further, the rotationally invariant regional MI takes into account not only spatial details but also the impact of local intensity variations and rotational transformations on the computation of the probability density function [36]:

$$MI(R,S) = H(R) + H(S) - H(R,S),$$

$$H(R) = -\sum_{r\in R} P(r)\log_2 P(r)$$

$$H(S) = -\sum_{s\in S} P(s)\log_2 P(s)$$

$$H(R,S) = -\sum_{r\in R, s\in S} P(r,s)\log_2 P\,(r,s)$$

where $(H(R))$ and $(H(S))$ denote the Shannon entropies of the reference and sensed images respectively, and $(H(R,S))$ represents the joint entropy. The marginal probability distributions for the reference and sensed images are given by $(P(r))$ and $(P(s))$, while $(P(r,s))$ indicates their joint probability distribution. The latter is typically determined through 2D histogram binning, treating the variables as discrete.

In addition to these methods, there is an MI-based registration technique that employs displacement maps, drawing parallels with optical flow estimation methods. Within this variational framework, MI serves as the similarity metric for the computation of displacements [38].

In summary, MI-based algorithms, rooted in information theory, provide a measure of statistical dependence between two datasets, rendering them particularly apt for registration tasks involving different imaging modalities. Nonetheless, the computational demands of these methods can be substantial, which may pose challenges given the typically large size of remote sensing images.

Approaches in the Frequency Domain

Frequency-domain techniques approach image registration by transforming image data to the frequency domain, leveraging the spectral characteristics for alignment purposes. This method proves advantageous for rapidly processing small geometric distortions. Fourier-based methods are quintessential examples of frequency-domain registration and were initially applied to align images undergoing translational shifts [39]. Phase correlation methods, utilizing the Fourier transform, are employed to identify the optimal global match between reference and sensed images, locating the peak in the cross-power spectrum [15], [40]– [42], [44]. These methods take advantage of the translational and rotational properties of the Fourier transform to deduce the necessary transformation parameters [44].

The robustness of frequency-domain approaches to frequency-dependent noise and variations in illumination contributes to their computational efficiency [45]. Unlike feature-based methods that require feature extraction, or spatial domain approaches that necessitate optimization, frequency-domain methods circumvent these complexities [44]. Nevertheless, the Fourier transform's limited spatial localization can be a drawback, potentially addressed by employing wavelet transforms, known for their superior spatial and frequency localization [46]. This adaptation has found application in the registration of remote sensing images [47].

Phase congruency (PC) is a more recent development, serving as a structural information representation in remote sensing images. Its uniqueness lies in its invariance to contrast and brightness variations, setting it apart from traditional image gradients [48], [49].

In summary, while many correlation-like methods are statistical similarity metrics lacking structural information and exhibiting high computational complexity, they are still widely used for registration evaluation due to their straightforward hardware implementations [50]. Fourier techniques stand out for their computational efficiency and noise robustness, but they face challenges when dealing with image pairs of significantly different spectral content. Mutual Information (MI) methods demonstrate superior performance compared to the aforementioned techniques; however, they may not always yield a global maximum across the entire transformation search space, particularly in cases of limited information or reduced overlap between scenes, affecting their robustness [11], [17]. Ultimately, intensity-based approaches, relying directly on pixel values, provide high-precision registration without accumulating errors, yet they are time-intensive and can struggle with large rotations, translations, scale variations, and similar challenges.

Optical Flow Estimation for Remote Sensing Images

Optical flow estimation, akin to area-based methodologies, deduces the motion of objects through direct and indirect constraints based on pixel intensity, a technique prevalent in computer vision for assessing motion. Recognizing the parallels between the displacements of corresponding pixels under a unified coordinate system and the optical flow associated with an object, several research endeavors have applied optical flow estimation for the registration of remote sensing imagery [51], [52]. Distinct from area-based methods, optical flow estimation determines pixel displacement through constraints on intensity and gradient consistency, subsequently recalculating coordinates. Following resampling, intensity values are allocated to new, non-integer positions, resulting in the acquisition of an aligned image [53].

Optical flow represents a two-dimensional displacement field, capturing the perceived movement of brightness patterns across two consecutive images [54]. This concept was initially introduced by Gibson [55]. In 1981, Horn and Schunck (HS) [54], as well as Lucas and Kanada (LK) [56], presented a differential method for calculating optical flow. Since that time, numerous adaptations and enhancements have been proposed, primarily in the context of video image processing [57]– [58]. Given that optical flow estimation in remote sensing is still in its infancy, current research primarily concentrates on differential techniques, exploring various facets of image registration in this domain.

Estimation of Dense Optical Flow

The HS differential methodology for computing dense optical flow is typically referred to as the standard global approach [54]. This dense optical flow technique determines the motion of each pixel within a scene. The HS optical flow method incorporates both the brightness constancy assumption and a global smoothness constraint to estimate pixel motion in both the x and y directions. However, the intensity value constancy assumption is notably sensitive to minor brightness variations [59], a common occurrence in remote sensing imagery. Integrating the spatial gradient constancy assumption into the HS equation, as shown in equation (3), is a prevalent practice in studies focusing on multitemporal remote sensing image registration [53], [59]:

$$E(u,v) = \int_{\Omega} \psi(|I(x+w) - I(x)|^2 + \gamma|\nabla I(x+w) - \nabla I(x)|^2)dx + \alpha \int_{\Omega} \psi(|\nabla^3 u|^2 + |\nabla^3 v|^2)dx$$

In this equation, ($w = (u, v, 1)^T$)represents the pixel displacement to be determined, ($X = (x, y, t)^T$)denotes a pixel's coordinates, ($\psi(s^2) = \sqrt{s^2 + \varepsilon^2}$)is an increasing concave function, and (ε) is a constant. The weights for the gradient and smoothness terms are represented by (α) and (γ) respectively, while ($\nabla^3 = \left(\partial_x, \partial_y, \partial_t\right)^T$)implies a spatiotemporal smoothness assumption, frequently substituted with the spatial gradient for remote sensing image registration.

The pixel-by-pixel computation of optical flow allows for the elimination of very local deformations caused by terrain elevations. However, occlusions pose a significant challenge for precise dense optical flow calculations [57], akin to LU and LC changes in remote sensing imagery [53]. In such situations, an object visible in the reference (or sensed) image may be absent in the sensed (or reference) image, leading to anomalies in pixel displacement. These anomalies can alter the content of the aligned image, even if it is well-matched geometrically to the reference image, contradicting the fundamental principle of image registration. After correcting these abnormal displacements, the recalculated displacement aligns more consistently with the surrounding region, and the aligned image is both content-consistent and spatially aligned with the reference image.

Addressing large-scale movements, another challenge in applying optical flow for remote sensing image registration, an enhanced method was suggested in [60]. Here, the initial motion estimator for global optical flow is determined using the extended phase correlation technique, facilitating general remote sensing image registration, particularly for large-scale deformations [60]. Nonetheless, the real-time registration of large images remains a challenge with dense optical flow estimation, despite its ability to deliver high-precision results.

Estimation of Sparse Optical Flow

Sparse optical flow estimation has garnered more favor for the task of remote sensing image registration compared to its dense counterpart. This method is characterized by local differences and is usually constrained within specific local regions, such as the locations of feature points identified by well-known extraction techniques like the Scale-Invariant Feature Transform (SIFT. This strategy presupposes uniform pixel motion within localized areas, and it derives the optical flow through the execution of least-squares regression on a series of analogous equations [57]. The Lucas-Kanade (LK) gradient-based method [56] stands as a foundational approach, holding equal standing with the Horn-Schunck (HS) model for motion estimation in video imagery. Derived from the LK approach, the GeFOLKI algorithm has been developed and implemented on graphics processing units, facilitating real-time and robust optical flow estimation [51], [61]. Furthermore, GeFOLKI has found applications in the coregistration of heterogeneous datasets, such as SAR lidar images and SAR optical images [52]. Subsequent developments, considering the disparate imaging mechanisms of SAR and high-resolution optical images, have leveraged the high registration precision of optical flow estimation. In these cases, two dense feature descriptors supplant raw intensities during image alignment through an optical-to-SAR flow, integrating both global and local optical flow estimation methods [62].

Sparse optical flow, by focusing on specific and distinct pixels, offers computational time savings. However, its accuracy in remote sensing image registration tends to be lower than that achieved with dense optical flow methods. Moreover, it demonstrates resilience to Land Use-Land Cover (LU-LC) changes, as it does not rely on similar features for sparse optical flow estimation in regions undergoing change.

To encapsulate, the development of optical flow estimation has spanned several decades within the domain of computer vision, particularly for motion estimation in superresolution reconstruction. Its application to remote sensing image registration is comparatively nascent. Optical flow estimation stands out for its ability to precisely calculate pixel displacements, proving especially valuable in scenarios involving localized deformations, such as those induced by terrain elevation changes, which significantly impact high-resolution image registration [52]. Nonetheless, when employing this technique in remote sensing, one must consider its efficiency, given the typically wide field of view (WFV) characteristic of remote sensing imagery. Furthermore, due to societal progression and seasonal variations, LU-LC changes frequently occur in multitemporal remote sensing images. Dense optical flow methods are particularly sensitive to such alterations, potentially leading to abnormal displacements and modifications to the content of aligned images. Consequently, efficient and precise correction mechanisms should be integrated into the initial phase of optical flow estimation when it is utilized for registration purposes.

Feature-Based Registration Approach

The feature-based methodology leverages abstract characteristics of an image for the purpose of registration, as opposed to relying on pixel intensity values. In this context, a "feature" is defined as a unique geometric or advanced attribute that is derived through a specific extraction method. Geometric features encompass distinct elements such as points, line segments, and defined boundary regions within a remote sensing image, and can be identified using existing or newly developed techniques. On the other hand, advanced features are complex descriptions of local areas, often extracted via neural networks (NN), particularly within deep learning frameworks, serving to encapsulate the essence of the original image. Within the realm of feature-based registration, geometric features are recognized as traditional, whereas the employment of advanced features represents a more contemporary approach.

Traditional Approach to Feature-Based Registration

Typically, prominent, and unique features like points, line segments, and enclosed boundary areas are identified within remote sensing imagery, either manually or through automated processes. Following this, correspondences between features in the reference image and the sensed image are established based on a comparative analysis of their respective descriptors. This process facilitates the determination of the geometric relationship, which in turn guides the alignment of the sensed image with the reference image. The final step involves transforming the coordinates within the sensed image. It is noteworthy that these transformed coordinates often take on non-integer values, necessitating interpolation to determine their associated intensity values. In the ensuing discussion, we delve into the extraction and matching of geometric features, given that this area has been a focal point of traditional feature-based registration methodologies.

Feature Extraction Process

The process of feature extraction encompasses both the identification and the detailed description of distinctive attributes within an image. The initial stage, feature detection, involves pinpointing unique elements in the image and establishing their precise locations. Following this, the feature extraction stage takes over, where a distinct descriptor is meticulously crafted to uniquely characterize each identified feature. In earlier practices, the selection

of features was predominantly a manual task. This traditional method continues to find application in contemporary settings, such as within the “image-to-image registration” functionality of the Environment for Visualizing Images (ENVI) software. However, it is important to note that this manual approach demands a substantial investment of time, particularly when dealing with extensive remote sensing images. In response to these challenges, a plethora of methodologies have been developed to facilitate the automatic extraction of representative features. Within this context, common geometrical features can be identified and selected. These include prominent points like intersections of lines, corners, curves with significant curvature, and points where roads cross [63], [64]. Additionally, linear features such as roads, contours, and edges [33], [65], as well as enclosed areas like closed boundary regions and bodies of water [66], are also extracted.

Feature Points and Their Extraction

Feature points in an image are local areas where there is a significant variation in gray value from multiple directions. These include specific types of points such as corner points, inflection points, and T-intersection points. The field of computer vision has seen numerous efforts to extract these feature points, which has in turn influenced similar developments in the domain of remote sensing.

The journey of feature point extraction began with Moravec's introduction of a corner detection method in 1977 [67]. Despite its rapid computational speed, the algorithm's sensitivity to noise and susceptibility to image rotation limited its adoption in remote sensing applications. A more robust alternative came with the Harris corner detector, introduced in 1988 [68]. This algorithm maintains its performance under variations in gray-scale and rotation, making it a more suitable choice for remote sensing image processing, particularly in the realm of multiscale corner detection [30], [64], [69], [70].

The smallest unvalued segment assimilating nucleus operator, proposed by Smith and Brady [71], showed resilience to local noise and exhibited a strong anti-interference capability [72]. However, its application in remote sensing image registration remains limited [73]. On the contrary, the Scale-Invariant Feature Transform (SIFT) algorithm has gained widespread adoption in this field [36], [49], [64], [74]–[80]. Introduced by Lowe [82], SIFT remains invariant to changes in rotation, scale, and translation [83], and has spawned numerous enhanced versions including principal component analysis SIFT [84], scale-restriction (SR) SIFT [27], [85], affine SIFT [86], and uniform robust SIFT [87], [88].

Addressing the time-intensive nature of SIFT, especially for large-scale remote sensing images, Bay et al. proposed the Speeded-Up Robust Features (SURF) algorithm [89]. This method employs an integral image for the computation of image derivations and succinctly quantifies gradient orientations [90]–[92], [93]. Other

algorithms such as the Features from Accelerated Segment Test (FAST) [94], Binary Robust Independent Elementary Features (BRIEF) [95], Oriented FAST and Rotated BRIEF [96], [97], Kaze [98], and Accelerated Kaze [99] also offer rapid descriptor construction, albeit with less prevalence in remote sensing applications.

Emerging approaches are exploring the combination of corners and blobs to enhance the matching of key points in remote sensing image registration [100]. Additionally, robust and innovative feature descriptors are being

employed to characterize detected feature points, particularly in the context of multimodal remote sensing images with varying intensity levels. Examples of these descriptors include the Local Self-Similarity (LSS) descriptor, which accounts for nonlinear intensity differences [28]; the histogram of oriented phase congruency (PC), drawing from structural similarity metrics [48]; and the maximally stable PC, a novel descriptor that is both affine and contrast-invariant [101]. Significantly, all these descriptors incorporate PC information, which is analogous to the image gradient, capturing structural details while remaining resilient to changes in illumination [102]. This highlights a growing trend towards leveraging phase consistency information for the development of robust feature descriptors tailored for multimodal remote sensing imagery.

Feature Line Representation and Utilization

Feature lines, also referred to as line features, extend the concept of feature points, encompassing entities such as general line segments [103], object contours [65], roadways, coastlines [104], and river paths [105]. With a richer set of attributes compared to feature points, feature lines serve as control features [106] and have seen incremental adoption in both general image registration [107] and remote sensing image registration specifically [106], [108], [109].

Traditional methodologies for detecting feature lines include standard edge detection techniques, with the Canny detector [110], [112] and Laplacian of Gaussian-based detectors [113] being prominent examples [11]. In more recent times, innovative detectors that yield precise and robust line segments have been introduced [114], [115], demonstrating their aptitude for line detection within remote sensing imagery.

Despite their potential, feature lines are not as prevalently employed in remote sensing as feature points, primarily due to the challenges associated with their matching process. Often, feature lines are reduced to simpler elements such as corners, midpoints, or endpoints, which are then used as the final features for registration purposes [11]. This reduction process, while simplifying the matching task, also leads to a loss of the intrinsic geometric information that feature lines inherently possess.

Feature Regions

The term "feature region" encompasses all closed boundary areas within an image that are of a substantial size, such as lakes [116], wooded areas [117], structural entities [103], and urban regions [118]. In the times preceding the advent of robust feature point extraction methodologies, feature regions played a pivotal role in the indirect derivation of feature points. This was typically achieved through the application of high-contrast region extraction techniques, involving processes such as filtering [119] and image segmentation [120], followed by the characterization of these regions using moment-invariant descriptors [121], [122].

These extracted regions were commonly represented by their centers of gravity [119], [123]–[124], a method offering invariance to transformations such as rotation, scaling, and skewing, while also maintaining stability in the face of random noise and variations in gray levels [11].

However, in comparison to feature points and lines, the focus on the extraction and description of feature regions has somewhat diminished over time, especially in the context of recent advancements in feature-based registration methods. This shift reflects the evolving landscape of feature extraction and registration techniques in image processing and remote sensing.

Feature Matching and Mismatched Feature Removal

The process of aligning reference and sensed images is achieved by identifying correspondences through the examination of detected feature points, lines, and regions, utilizing a variety of feature descriptors [11], [125], [126]. In the course of performing feature matching, mismatched features invariably arise, necessitating their removal to refine correspondences and facilitate the generation of highly accurate transformation models. Even in the presence of radiometric variations, noise, and image distortions, features with similar characteristics are deemed suitable for matching.

To navigate these challenges and ensure the integrity of the matching process, it is crucial to employ robust measures for feature matching. Broadly speaking, feature matching strategies can be categorized into two distinct groups: feature similarity and spatial relations. These methodologies serve as the foundation for establishing precise correspondences between the features of the reference and sensed images.

Feature Similarity Assessment

In the realm of image registration, the establishment of correspondences between extracted features from reference and sensed images is facilitated through the comparison of feature similarity, utilizing the constructed descriptors. This assessment of similarity transpires within the feature space, primarily employing the Euclidean distance ratio between the nearest and second-nearest neighbors as the basis for comparison [82].

To enhance the efficiency of this process, algorithms such as the k-dimensional tree and best-bin-first are implemented, aiding in the swift and accurate determination of feature similarity [83], [127]. Moreover, various matching methodologies, including clustering techniques [129], chamfer matching [130], and phase consistency (PC) models, are routinely applied. Notably, these approaches maintain their invariance to intensity variations during the matching process, ensuring a robust and reliable performance [1].

Spatial Relationships for Image Registration

Focusing on the matching of tie points in areas with limited texture, there have been developments in methods that leverage spatial relationships. A notable example is the application of graph-based matching for feature points, wherein the feature points are treated as nodes within a graph. The challenge of feature matching is subsequently reformulated as a problem of establishing node correspondences, which is addressed through graph matching techniques [116], [131].

While graph matching has proven effective for correlating image features, it is important to note that it does not inherently possess affine invariance [132]. To address this, a method involving the creation of a consensus nearest-neighbor graph from potential matches has been introduced, leading to the development of a graph-transformation matching approach [133].

To further refine the process, particularly in regions with scant textural information, an additional graph matching technique has been proposed, enhancing the accuracy of tie point matching [91]. In a separate development, Xiong and Zhang have proposed an innovative method for matching interest points in high-resolution satellite imagery. This method utilizes relative positions and angles to diminish ambiguity and mitigate the risk of incorrect matches, proving effective for cases involving image shifts and rotations. However, it does not extend to affine and large-scale transformations [134], [133].

Mismatched Feature Elimination

Despite the meticulous matching of extracted features from a reference image to those in a sensed image using the methods described previously, the occurrence of non-matching feature points is unavoidable, which can subsequently influence the accuracy of estimating the transformation model [24], [66]. Consequently, it is crucial to employ a specific technique to eliminate these inconsistent features [135], [136].

Typically, the Random Sample Consensus (RANSAC) method is utilized for this purpose, leveraging the initial matching results. RANSAC iteratively selects random subsets of the matched features, identifies the largest group of consistent features, and then computes the final transformation model parameters based on this consensus set [25], [137]. This method has proven to be robust and effective, especially when the proportion of mismatched features (outliers) is less than 50% [133], [138], [139].

To further refine the matching precision, an algorithm that merges local structural details with global information has been developed. This method, known as the restricted spatial order constraints algorithm, precisely identifies and aligns the correctly matched features between the reference and sensed images [133].

Additionally, leveraging the affine-invariance characteristic of the triangle-area representation (TAR), a robust sample consensus judging algorithm has been introduced. This algorithm efficiently discerns incorrect matches,

ensuring high accuracy with minimal computational demand [140]. In situations involving images with simple patterns, substantial affine transformations, and limited overlapping areas, a mismatch elimination principle based on the TAR values of the k-nearest neighbors, termed k-nearest neighbors–TAR, is recommended [149].

An enhanced version of RANSAC, named fast sample consensus, has also been developed to achieve accurate feature matching in fewer iterations [139], [141]. As a result, the majority of the retained feature points in the reference image correspond precisely to the intended feature points in the sensed image. This alignment contributes significantly to the accuracy of the transformation model estimation in the subsequent stage.

The feature-based registration approach, which relies on distinct geometrical features rather than pixel intensity information, is proficient and adept at handling significant rotations, translations, and scale variations between reference and sensed images. However, it is important to acknowledge that positional inaccuracies in the automatically extracted features are unavoidable, and some non-matching features may persist. This scenario can lead to a slightly reduced registration precision when compared to intensity-based registration methods.

Deep Learning-Based Advanced Feature Registration

Deep learning introduces a novel paradigm for aligning remote sensing images, predominantly through enhanced feature extraction capabilities [142]. With its roots in computer vision and a rich history [143], deep learning has recently found applications in remote sensing, including tasks like image blending [144], [145], land cover classification [146], [147], and image segmentation [148]. Its data-driven nature allows it to derive image features from large training datasets based on specific principles [147], making it a fitting choice for remote sensing image alignment.

Various studies have delved into feature matching using deep learning [147], [149], often employing a Siamese network architecture to train a deep neural network (DNN) [150]–[151]. This structure typically consists of two segments: one for extracting features from pairs of image patches and another for evaluating the similarity between these features for image matching. In one instance, a DNN inspired the creation of a deep learning framework specifically for remote sensing image registration [151]. Additionally, generative adversarial networks (GANs) have been applied to this task, translating images to make their intensities and features more comparable, thus enhancing matching performance [152], [153], [154]. These methods have showcased significant improvements in registration results. Addressing the limitations of scale-specific neural networks, multitask learning has been introduced to enhance registration precision [155]. Wang et al. have pioneered an end-to-end network that learns the mapping functions and matching labels for patches in remote sensing images [151]. More recently, Li et al. have adopted a direct approach, learning the displacement parameters for image blocks, diverging from traditional methods [156].

Deep learning surpasses traditional registration techniques with its flexibility and ability to theoretically model any complex mapping function. It extracts higher-level semantic information, providing a more intuitive understanding of images and resulting in robust feature extraction. Nevertheless, it is not without challenges. Its performance heavily relies on the availability and quality of image samples, and the lack of annotated data remains a significant hurdle. Additionally, its complexity and hardware demands may limit its applicability.

In summary, while remote sensing image registration via deep learning is still emerging and its frameworks are not fully matured, it has demonstrated potential to match or even exceed the performance of traditional methods. We foresee deep learning-based methods playing a pivotal role in achieving real-time, high-precision remote sensing image registration in the future.

Method of Registration through Combined Techniques

In this discussion, it is noteworthy that both feature- and intensity-based methodologies exhibit distinct advantages. Additionally, various feature extraction instruments demonstrate different levels of accuracy. To optimally harness these strengths, methodologies that combine these approaches have been devised. Typically, these combined methods encompass both feature- and area-based strategies; however, there are instances where two geometric feature-based techniques, such as SIFT and Harris detectors, are merged.

Fusion of Feature- and Area-Based Methods

Generally, feature-based strategies are more applicable to images rich in structural content than in intensity details. Nevertheless, the effectiveness of these methods is limited by the distribution and precision of the features identified. Conversely, area-based strategies are more suited for images with pronounced intensity details, necessitating a correlation between the intensity data of the reference and target images. Consequently, these two methodologies offer a set of complementary advantages and disadvantages. To enhance the precision and stability of registration, several studies have explored the combination of geometric feature- and area-based techniques [157]. Huang et al. [158] introduced a mixed approach for aligning images based on intensities within a scale-invariant feature region. Additionally, a wavelet-based feature extraction method was amalgamated with an area-based method using NCC to mitigate local distortions due to terrain variations [159]. In a hierarchical pyramid framework based on wavelets, Mekky et al. [160] suggested a mixed method utilizing MI and SIFT. By applying the preliminary registration parameters from the area-based method to MI, the incidence of false positives from SIFT was reduced. Furthermore, Gong et al. [80] proposed a novel coarse-to-fine registration framework, combining the robustness of SIFT with the precision of MI for the registration of optical and SAR remote sensing images. For the registration of multisensor SAR images, Suri et al. [161] developed a multi-stage registration strategy, initially estimating the transformation model's rough parameters using MI, and subsequently introducing this model during the SIFT matching phase to augment the number of tie points. Utilizing the combination of SIFT and MI, Heo et al. [162] presented a stereo matching technique for generating precise depth maps. Collectively, these methodologies can be categorized as coarse-to-fine processing chains, aiming to refine the results obtained from feature-based methods through optimization processes derived from area-based techniques [80], [157].

Integration of Dual Geometric Feature-Based Approaches

Beyond the fusion of feature- and area-based strategies, merging two distinct geometric feature-based approaches is emerging as a technique for high-precision registration. This process typically involves utilizing feature points identified through different methods to register images in two stages. For instance, Yu et al. [64] employed SIFT

to extract feature points for the initial registration of images from various sensors. In the subsequent fine registration stage, the Harris algorithm was applied for corner point detection, followed by point matching using the NCC algorithm. Similarly, Lee [164] utilized SURF for feature point extraction from a low-resolution image, followed by Harr wavelet transformation, constituting the rough registration phase. The fine registration phase mirrored the approach advocated by Yu et al. More recently, Ye et al. [28] applied SR–SIFT for feature point extraction in the preliminary registration stage, aiming to eliminate significant translation, rotation, and scale differences.

To optimize the registration process further, the Harris algorithm was employed for feature point detection in both the reference and prealigned images, with the LSS method used for point matching [28]. To register large, high-resolution remote sensing images, a strategy combining the Harris–Laplace detector with the SIFT descriptor has been proposed. After initial registration, the image is subdivided into smaller, manageable blocks for fine-tuning [165]. Additionally, a novel two-step registration process has been introduced, initially calculating an approximate spatial relationship using deep features via a convolutional neural network, and subsequently adjusting the results based on locally extracted features [166]. Another technique merges feature point and feature line methods for image registration in scenarios with low-texture content, commonly encountered in computer vision applications [167]. Given that low- and repeated-texture regions are prevalent in remote sensing imagery, the inclusion of feature lines can augment the number of feature points available, underscoring the potential of integrating different geometric features for high-precision remote sensing image alignment [14].

Software-Based Registration Exploration

Numerous reviews have highlighted the growing array of image registration techniques, many of which build upon existing methods to accommodate increasingly large and complex images [11], [168]. However, there has been limited evaluation of the performance of embedded image registration modules within various software packages and tools designed for geometric image registration [169]. In this context, we explore several notable examples.

Renowned software packages such as ERDAS, ENVI, PCI Geomatica, ER Mapper, and ArcGIS offer a suite of tools for remote sensing image processing, including modules for image registration. ERDAS, having acquired ER Mapper, integrates both manual and automatic registration functionalities. ENVI, for instance, enables the registration of remote sensing images or the alignment of an image with a corresponding map, with users manually identifying tie points based on observable features across the images. While this process can be laborious and subjective, especially for images requiring wide field view registration, ENVI also facilitates automatic alignment. However, the accuracy of the tie points, whether manually or automatically extracted, may not always meet the required precision, particularly for high-resolution images with localized deformations.

ERDAS, developed by the ERDAS Corporation in the United States, offers more precise location accuracies for tie points and a wider array of transformation models compared to ENVI. It also incorporates elevation data into the registration process, enhancing the precision of alignments, particularly for mountainous remote sensing images. Both ArcGIS and PCI Geomatica, despite being primarily utilized for different applications, include image registration modules, employing various transformation models to achieve high-precision registration of complex remote sensing images. Nonetheless, the results can sometimes be suboptimal due to non-uniform distribution and insufficient numbers of tie points.

Newer software solutions, such as Pixel Information Expert developed by Beijing Aerospace Hongtu Information Technology, specialize in multimodal remote sensing image registration, addressing issues of dislocation in multisource, heterogeneous remote sensing images. Other software options, including both commercial and open-source packages, offer additional tools for geometric registration.

Given the critical nature of high-resolution image registration in remote sensing image processing, considerable emphasis has been placed on developing effective strategies. One such approach combines SURF with an adaptive

binning SIFT descriptor to extract dense tie points representing local geometric relationships, guiding the registration process to a precise result [170]. The MATLAB code for this algorithm, along with experimental data, is available at https://www.researchgate.net/publication/320354469_HRImReg. However, the code is encrypted, and the parameters are not adjustable, limiting its use to comparative experiments for evaluating proposed approaches. For simulation experiments assessing feature point detectors or evaluating mismatched elimination approaches with real data, the progressive sparse spatial consensus algorithm can be employed [171]. The code and experimental data are publicly accessible at https://github.com/jiayi-ma?tab=repositories, although modifications may be necessary for application to remote sensing images. Beyond these tools, a plethora of commercial and open-source software packages and tools are available for geometric registration, offering various perspectives and methodologies that warrant deeper exploration in future discussions. Regardless of the tool or method chosen, it is imperative to conduct a thorough evaluation of the registration approach to ensure the aligned image meets the necessary standards and requirements.

Assessment of Image Registration Precision

In aligning spatial data from remote sensing images, it is crucial to provide an accurate measure of how precise the registration is. This challenge of evaluating accuracy is a common theme across various studies in the field of remote sensing image registration. In this discussion, we focus on three key areas for assessing registration precision: the identification of tie points, the efficacy of the transformation model, and the measurement of alignment errors. Let's delve into the fundamental methods used in evaluating alignment.

Precision in Identifying Tie Points

The accuracy and number of tie points play a critical role in achieving precise image registration. It is vital to have an adequate number of redundant tie points, as well as to correctly compute the parameters for the chosen transformation model. We generally aim to utilize as many tie points as possible for this computation. Additionally, it is necessary to account for a residual $((\Delta x_i, \Delta y_i))$ for each feature point extracted, relative to the image's origin [172]. Given (N) tie points, the root-mean-square error (RMSE) can be calculated as follows:

$$\mathrm{RMSE}_{tp} = \sqrt{\frac{1}{N}\sum_{i=1}^{N}((\Delta x_i)^2 + (\Delta y_i)^2)}$$

This RMSE should be normalized to the pixel size for a standardized comparison. Moreover, evaluating the proportion of incorrect points (those with residuals exceeding a certain threshold) is essential. This evaluation can help in assessing the quality of the extracted feature points. Additionally, the distribution of tie points should be uniform, and several studies have suggested methods for extracting feature points within specific subregions to achieve this [22]. However, it's important to note that while tie points significantly impact registration accuracy, they are not the only factor.

Performance of the Transformation Model

The transformation model serves as an abstract representation of the geometric mapping function, transforming data from the sensed image to the reference image. Obtaining the actual geometric distortion between images is challenging without prior information, making it necessary to estimate the transformation to approximate the real geometric relationship. A portion of the matched feature points is used to estimate the mapping function, while the remaining points in the sensed image serve as test points to be transformed into the reference image system [172]. The residual, or the distance between the transformed coordinate and the corresponding point in the reference image, represents the precision of the estimated transformation model. This residual can be expressed as:

$$\mathrm{RMSE}_{\mathrm{N-T}} = \sqrt{\frac{1}{\mathrm{N-T}} \sum_{\mathrm{j=1}}^{\mathrm{N-T}} ((\mathrm{x} - \mathrm{Hx}')^2 + (\mathrm{y} - \mathrm{Hy}')^2)}$$

Here, (H) represents the estimated transformation model derived from (T) pairs of tie points, and (x, y) and (x', y') denote the corresponding points in the reference and sensed images, respectively. Additionally, a (Chi-square) goodness-of-fit test [172] can be applied to check if the residuals are uniformly distributed across all quadrants. However, it is crucial to be wary of "overfitting," where a model with too many degrees of freedom might show zero error, potentially leading to suboptimal registration results.

Alignment Error

Estimating the accuracy of registration alignment is crucial, and this has traditionally been done through visual inspections by experts in the field, a method that is highly effective yet subjective and lacks quantitative measures [11], [172]. Currently, this evaluation is often conducted using professional software tools like ENVI and ArcGIS, utilizing similarity metrics such as Mutual Information (MI), Normalized Mutual Information (NMI), and Cross-Correlation (CC) [50]. However, these metrics can be affected by changes in image information and variations in radiation levels. To provide a quantitative measure of alignment error, the Root Mean Square Error (RMSE) is calculated using feature points that have been manually identified by specialists, following the formula presented earlier [75]. Since there is no universally accepted reference image for remote sensing image registration, multiple criteria are typically used to evaluate the results, each with its own strengths and limitations.

Prospective Developments in Remote Sensing Image Registration

The domain of remote sensing image registration has witnessed numerous individual research endeavors, primarily focusing on the enhancement of robust feature descriptors and the mitigation of feature mismatches. With advancements in sensor technologies and evolving application demands, emerging opportunities and challenges necessitate innovative approaches in remote sensing image registration. We anticipate a shift towards more advanced strategies, including accelerated, integrated, heterogeneous, cross-scale, and intelligent image registration techniques, which we will elaborate upon below.

Advancements in Speed for Remote Sensing Image Registration

The continuous progress in sensor technology has led to remote sensing images with higher spatial resolutions, capturing a larger array of detailed features. This increase in detail, however, has made the path to real-time image registration more challenging, particularly when dealing with extensive images. Consequently, the process of constructing descriptors and matching features becomes notably time-intensive, especially for Wide Field of View (WFV) images. To address this, there is a suggestion to employ cloud platforms for remote sensing image registration, utilizing finite-state chaotic compressed sensing theory to enhance efficiency and approach real-time registration as closely as possible [43]. In addition to cloud computing solutions [81], specific hardware systems might also play a crucial role in hastening the image registration process. Currently, one of the more straightforward solutions is parallel computing [128], where an image is subdivided into various sections. The features within each section are then concurrently extracted and processed using parallel processors, following consistent methodologies for both feature extraction and transformation model construction. This parallelization approach is readily implementable on platforms such as MATLAB, facilitating a more efficient image registration process.

Integrated Strategies for Image Alignment

Advancements in imaging sensor technology have led to enhanced resolutions in remote sensing imagery, making local distortions more pronounced. Issues such as geometric distortions arising from terrain undulations and tall structures result in registration inaccuracies [28], posing challenges for applications of remote sensing images. For instance, when both flat and mountainous terrains are concurrently present in the reference and sensed images. When determining the pixel displacements necessary for spatial alignment. While the displacement magnitudes and directions in the flat areas are relatively consistent, they diverge significantly in the mountainous regions. In this scenario, a single-stage registration process employing a global mapping function falls short of accurately capturing the spatial relationship between the reference and sensed images, as does the application of a local transformation model.

Acknowledging the variability of displacements across different terrains, segmenting images into various regions and applying tailored registration methods can lead to more precise alignment, demonstrating the efficacy of integrating diverse techniques. Specifically, in flat regions, the transformation model is calculated using distinct tie features, enabling the estimation of displacements guiding pixels toward alignment, rather than direct acquisition of the aligned flat region. In contrast, for mountainous terrains, dense optical flow estimation, a concept borrowed from the field of computer vision, is employed to determine the displacement of each corresponding pixel. Subsequently, the displacement fields derived from the various terrain regions are seamlessly merged (for instance, utilizing the inverse distance weighted function for smooth transitions in image stitching) to generate a comprehensive displacement field for the entire image [163]. This approach represents an innovative amalgamation of varied registration methods, applied in a coordinated manner, and stands apart from the serially executed combined approaches discussed in the “Registration Based on the Combination Method” section. Consequently, regional registration, tailored to accommodate complex geometric relationships that vary with terrain, is poised to emerge as a prominent direction in remote sensing image registration. This approach maximizes the registration benefits of different methodologies across diverse terrain regions.

Integration of Diverse and Multiscale Image Alignment

The simultaneous and sequential acquisition of heterogeneous and cross-scale images provides a rich blend of information, enhancing our comprehension of entire scenes, whether for Earth observation or disaster response efforts. Nevertheless, challenges arise due to the substantial differences in spatial resolution, brightness levels, noise characteristics, and geometric properties, attributed to varied imaging techniques. Research endeavors have delved into spatial registration challenges, encompassing the alignment of optical and Synthetic Aperture Radar (SAR) images, the correlation of optical and infrared imagery, as well as the integration of satellite data with maps [28], [48]. These studies have underscored the necessity of developing robust descriptors capable of withstanding variations in intensity, noise, and other influential factors.

The pronounced scale disparities in cross-scale images, often exceeding fourfold resolution differences as seen between panchromatic and multispectral imagery, complicate the task of extracting geometric features from low-resolution images that align well with their high-resolution counterparts. Consequently, establishing tie features for cross-scale images to aid in the construction of transformation models, even in the context of high-precision registration, presents a formidable challenge. The quest for efficient and effective methods for heterogeneous and cross-scale image registration remains a pressing research frontier, warranting further exploration in the coming years.

A pertinent example can be found in the near-real-time registration of optical and SAR images, which has the potential to expedite the analysis of disaster-stricken areas, thereby aiding rescue efforts through timely comparisons of pre- and post-event imagery. Such applications are crucial for the swift coordination of rescue operations. To fulfill the demands of these high-stakes, real-time applications, the development of precise and efficient methodologies for heterogeneous and cross-scale image registration is imperative.4. Smart Remote Sensing Image Registration

The conventional approach of aligning multiple images on a frame-to-frame basis is both time-intensive and resource-heavy. A more efficient strategy involves designating a reference image and aligning all other images to this reference, thereby saving memory and improving computational efficiency. However, this method needs further refinement, especially for images with minimal overlap.

Intelligent Alignment of Remote Sensing Imagery

The task of aligning multiple remote sensing images can be approached by transforming the challenge of multi-image registration into a series of pair-to-pair alignments. This method, drawing inspiration from the simultaneous stitching of multiple frames, involves selecting a reference image to which all other images are aligned. In practice, this necessitates reading in the images to be registered, extracting the coordinates of their four corners, and subsequently determining the reference image through a comparative analysis of these coordinates. This approach stands out from frame-to-frame methods, as it requires the specification of only the reference image, eliminating the need for repeated input and output of intermediate results, thereby conserving memory and enhancing computational efficiency. This streamlined process, which we regard as a form of intelligent registration, is particularly advantageous for generating Wide Field of View (WFV) images. Nonetheless, the approach necessitates further refinement and intelligence when dealing with overlapping images.

In addition, there may be instances where the images to be registered share only minimal overlapping areas. Such limited overlap poses a significant challenge for achieving high-accuracy alignment, given the scarcity of geometric and intensity features available for the construction of the transformation model. Addressing this issue, particularly in the context of registering images with minimal overlapping regions, requires the development of intelligent solutions. These images are commonly utilized in the production of WFV images through stitching techniques, underscoring the need for innovative solutions in the future.

Consequently, the task of accurately aligning high-resolution, heterogeneous, and cross-scale remote sensing images, particularly when they exhibit large-scale, complex distortions, emerges as a critical area of focus for future research endeavors. In these complex scenarios, traditional single-registration methods may fall short of the required performance standards. Instead, a synergistic approach that combines various alignment techniques with high-performance computing holds considerable promise for achieving real-time, high-precision registration outcomes.

Conclusions

In this review, we have provided an extensive and detailed analysis of various approaches to aligning remote sensing images, covering intensity-based, feature-based, and hybrid methods. We have explored both traditional techniques and innovative applications of deep learning and optical flow methodologies. The effectiveness of different image registration software and tools has been critically assessed. Furthermore, we introduced innovative evaluation methods to facilitate accurate and reliable assessment. The ultimate goal of any registration method is to enhance the precision of alignment, which is a crucial preprocessing step in handling remote sensing images. This review has systematically reviewed numerous strategies developed for this purpose.

Nevertheless, the advent of high-resolution imagery has underscored the issue of local distortion inconsistencies, particularly those caused by skyscrapers and terrain variations, which are not adequately addressed by current transformation models. Additionally, the production of Wide Field of View (WFV) images is becoming a prevalent trend in satellite imagery, aiming to capture an entire Region of Interest (ROI) in a single frame. This trend, however, brings its own set of challenges, especially concerning real-time registration capabilities and memory requirements during the registration process. Looking ahead, we anticipate that future research in remote sensing image registration will focus on speeding up the registration process, employing combined methodologies, addressing the challenges of heterogeneous and cross-scale image registration, and developing intelligent registration solutions. Despite the progress made, numerous challenges persist, necessitating extensive further research. We are optimistic about the future of this field, especially considering the relatively low barriers to entry compared to the generation of Three-Dimensional Orthophoto Maps (TDOM).

A review of the state of art classification methods

Numerous investigations into land cover have been conducted over time, utilizing data from a variety of sensors, each with unique resolutions, and employing diverse techniques and data processing methods [173] [185] [212] [213]. The objective of these studies has predominantly been to map and monitor changes in land use and cover. The methodologies employed can be categorized into supervised, semi-supervised, and unsupervised classifications, while the classifiers themselves can be divided into parametric and non-parametric, rigid, and flexible, or pixel/subpixel and object-based approaches [183] [207].

Parametric classifiers, such as the maximum likelihood, minimum distance, and Bayesian classifiers, rely on probabilistic theories. They establish decision boundaries between classes using a predetermined number of parameters, which remain constant regardless of the sample size, and employ global criteria for classification [214]. On the other hand, non-parametric classifiers, including support vector machines (SVM) and artificial neural networks (ANN), determine class groupings based on digital numbers or spectral reflectance, in addition to other attributes like shape and texture. These classifiers operate independently of the image value distribution, focusing on the local data structure and necessitating a large number of samples for effective classification [215] [216] [217] [218].

Recent advancements in object pattern recognition, driven by artificial intelligence and machine learning, have played a significant role in the development of sophisticated non-parametric classifiers. These are now commonly found in both commercial and open-source GIS and Digital Image Processing software [216].

The pixel-based approach, exemplified by Random Forest and spectral matching techniques, utilizes spectral information of individual pixels to assign them to specific classes, based on the likelihood of pixel belonging to a particular class [216] [219]. In contrast, the Object-Based Image Analysis (OBIA) approach classifies land use and cover using geographic objects as the basic unit, reducing within-class variation and mitigating the "salt and pepper" effect of isolated misclassified pixels. OBIA also allows for the integration of additional information sources, such as texture, shape, and position, in the classification process [215] [216] [219]. However, selecting the appropriate segmentation scale and managing various steps in the process can introduce variability if not handled carefully.

The sub-pixel-based approach addresses limitations in pixel-based classification, particularly in differentiating land uses and cover within mixed pixels. This approach is well-suited for sensors with medium to low spatial resolutions and is commonly used in regional, continental, or even global mapping projects [211] [212] [220]. Various statistical and set theory-based algorithms, including Maximum Likelihood (Maxver), Linear Mixture Model (LSMM), Possibilistic C-Means (PCM), and Fuzzy C-Means (FCM), are employed for sub-pixel classification and are incorporated into various image processing software options, both proprietary and open source. However, selecting the most appropriate classifier remains a complex and challenging task, as each method has its own set of strengths and weaknesses, as illustrated in Table 1.

In this context, Ackom et al. [222] and Mohammady et al. [223] advocate for the adoption of hybrid approaches, which have grown increasingly potent and diverse thanks to the emergence of sophisticated and advanced classifiers.

Classification approach	Algorithm	Advantages	Disadvantage	Reference
Pixel-Based	Artificial Neural Networks	Manage well large feature space; Indicate strength of class membership; Resistant to training data deficiencies-requires less training data than DT	Needs parameters for network design; Tends to overfit data; Black box (rules are unknown); Computationally. Intense Slow training	[216]
Sub-pixel Based	Spectral Unmixing	Clear physical meaning and being able to estimate fractional distribution	Hard to find a proper endmember in larger scale	[230]
Object Based	Support Vector Machines (SVM)	Manages well large feature space; Insensitive to Hughes effect; Works well with small training dataset and does not overfit	Needs parameters: regularization and kernel; Poor performance with small feature space; Computationally intense	[216]

Table 2.1 classifiers and their Advantages and Disadvantage

Additionally, there is the option to integrate strategies capable of deducing vegetation cover proportions, commonly referred to as vegetation indices. Among the most frequently utilized indices are the Normalized Difference Vegetation Index (NDVI), Normalized Difference Water Index (NDWI), Soil-adjusted Vegetation Index (SAVI), Normalized Difference Built Index (NDBI), and the Spectral Mixture Analysis Modified Soil Adjusted Vegetation Index (MSAVI). However, it is crucial to acknowledge that the effectiveness of this methodology is contingent upon various factors, including the quality of the preprocessing, the expertise of the analyst, and the efficacy of the classifier.

When confronted with complex subjects, Gómez et al. [207] highlight the necessity of considering several criteria in the selection of an appropriate classification algorithm. These criteria encompass the type of data, the statistical distribution of classes, the desired level of accuracy, as well as practical considerations such as ease of use, speed, scalability, and interpretability. Adhering to these considerations is essential to ensure not only the attainment of satisfactory accuracy but also the judicious utilization of available resources, as detailed in Table 4.

Machine Learning Algorithms

Machine Learning (ML) encompasses algorithms and models designed to learn from data and make informed decisions in future scenarios. These algorithms are categorized into two primary types: Lazy (e.g., k-nearest neighbor, Case-based reasoning) and Eager (e.g., Decision Tree, Naive Bayes, Artificial Neural Networks). Furthermore, ML algorithms are broadly classified into four main categories: supervised learning, unsupervised learning, semi-supervised learning, and reinforcement learning [241] [242].

As outlined by Galván et al. [241], a substantial portion of machine learning algorithms (MLAs), whether they be based on trees, rules, or functions, are categorized as eager learning methods. This implies that these algorithms generalize and make predictions beyond the training data before being exposed to new instances. They serve as potent instruments for training Artificial Intelligence (AI) models, enhancing automation, and optimizing operational efficiency in complex systems such as robotics, autonomous driving, manufacturing, and supply chain logistics [242].

Classification tasks in ML can be Binary (involving two class labels), Multiclass (with more than two class labels), or multi-label (an extension of multiclass classification where classes are hierarchically structured, and examples may belong to multiple classes at each hierarchical level) [242] [243].

Numerous studies have applied machine learning classifiers to land use and land cover mapping [173] [176] [183] [217] [244]. Classifiers such as Classification and Regression Trees (CART), Random Forest (RF), k-Nearest Neighbor (k-NN), Support Vector Machine (SVM), Artificial Neural Network (ANN), Multinomial Logistic Regression (MLR), C5.0, and J48 (Decision Tree) have demonstrated superior efficiency compared to conventional methods.

Shetty [183] explains that classifiers like SVM identify a subset of training data as support vectors to optimally separate two classes with a hyperplane. CART constructs simple decision trees from training data, ANN mimics neural network patterns building multi-layered nodes for data processing, RF constructs multiple decision trees using random subsets of training data, and so on.

These classifiers have shown a 10% to 20% increase in accuracy when dealing with complex data spanning large areas [207]. Their success is attributed to their non-reliance on parametric statistical assumptions, making them well-suited for analyzing multimodal, noisy, or incomplete data, combining categorical and continuous auxiliary data, reducing pre-processing steps required in traditional methods, and performing efficiently in cloud computing environments such as Google Earth Engine (GEE) [175] [245].

GEE is a cloud-based platform, hosting multiple petabytes of data and providing parallel computing and data catalog services for global geospatial analysis. It aggregates data from various geospatial development agencies like the USGS and ESA, offering a wide array of data sets ranging from surface reflection data from Landsat to Sentinel data sets, global land cover data, and climate data sets. GEE supports image pre-processing and houses a vast repository of functions for various operations on images and vectors [183]. Li et al. [246] provide an example of ML applications in remote sensing in their article published in the Remote Sensing Journal.

Classification Approach	Method	Algorithm	Data/product/Place	Software/ Platform used	References
Pixel Based	Supervised	SVM	Sentinel-2, Cartosat-DEM, Multi-temporal, Vietnam India	GEE, OBT	[233] [234]
		MKNN	Landsat, single date, India	Not reported	[235]
		ML	Landsat, Time series, Turkey	IDRISI, ArcGIS	[236]
		ISODATA	Landsat/sentinel, Time series, Ethiopia Vietnam	Not reported Envi/ArcGIS	[237] [238]
		Hierarchical Clustering	IRS-P5, Single date, India	ERDAS IMAGINE	[239]
	Unsupervised	K-Mean	Landsat 8/Sentinel2/ALOS 2 PALSAR, Multi-temporal, Finland	Forestry TEP	[240]
		ML-ISODAT	Sentinel, time-series, Australia	GEE	[241]
	Hybrid	CA-Marcov Chain	Landsat, Multi-temporal, India	ERDAS IMAGINE, ENVI, ArcGIS	[242]
		ISODATA-Decision	Landsat, Multi-temporal, Ghana	QGIS	[221]
		LP-SVM (SMCF)	Rule Based Landsat, Multi-temporal, Iran.	ArcGIS	[222]
			Hyperspectral (not specified), China	Matlab	[227]
Sub pixel	SMA	LSMA	Landsat/MODIS/SRTM, Time series, Brazil	Not reported	[230]
		MESMA	Hyperspectral (APEX)/Sentinel-2, Single date Belgium	LAStools	[229]
	Fuzzy analysis	Fuzzy Rule Based	IRS-P6, India	Erdas IMAGINE	[243]

		Fuzzy C-Mean (FCM)	IKONOS, single date, Netherlands	Not reported	[244]
Object Based	OBIA	Decision Rule	Landsat/IRS/ASTER-GDEM, Multi-temporal, India	eCognition developer	[245]
		Nearest Neighbor	Landsat, Malawi	Not reported	[246]
		RF	Landsat/MODIS/Google Earth, Time Series, USA	Trimble eCognition Developer	[247]
	Knowledge Based	Expert rule	Landsat, Time Series, Brazil	GEE	[248]
		Expert-Knowledge	Gaofen (GF-1)/Ziyuan (ZY-3)/ASTER-GDEM, China	Not reported	[249]
			WorldView-2, Multitemporal. Italy	Not reported	[250]

Table 2.2 Distinct approaches and algorithms for handling spatial data.

ML-Maximum Likelihood; MKNN-Modified k-nearest Neighbors; TEP-Thematic Exploitation Platform; SMCF-Superpixel and Multi-Classifier Fusion; MESMA-Multiple Endmember Spectral Mixture Analysis; APEX-Airborne Prism Experiment; LSMA- Linear Spectral Mixture Analysis; NN-Nearest Neighbor; GEE-Google Earth Engine.

Time Series/Multi-Temporal, Multi-Scale/Multi-Source

Optical data time series with medium spatial resolution yield significant outcomes, particularly when contrasted with single-scene analyses. This approach demonstrates a robust capability to depict environmental phenomena, capturing both trends and discrete events, and facilitating the detailed characterization and identification of changes in land use and cover [212] [247] [248].

Chi et al. [182] outline traditional data fusion methodologies, categorizing them into pixel-level, feature-level, and decision-level fusion. However, the burgeoning field of big data in remote sensing encompasses diverse scales and formats. Huang and Wang [178] elaborate on Big Spatial Data (BSD), highlighting its potential to amalgamate data from varied sources, thereby yielding a holistic perspective. This integration process necessitates managing data from disparate formats, devices, or systems, and attributing geographic context to enable comprehensive analysis. Challenges arise in harmonizing data features that may significantly differ, such as spectral signatures in

optical remote sensing, electromagnetic radiation in microwave data, structural text features, or unstructured image features from digital cameras.

Leveraging multi-source data enhances land use and cover mapping, as well as classification accuracy [176] [185] [215] [246]. This enhancement is achieved by acquiring high-resolution samples and fusing products from different sensors (e.g., optical/optical or optical/radar), resulting in clearer target differentiation.

Häme et al. [230] employed Hierarchical Clustering to detect and identify land cover changes using paired data from Sentinel-2/Sentinel-2, Landsat-8/Sentinel-2, and Sentinel-2/ALOS 2 PALSAR over an area spanning 12,372 km^2 in Finland. Joshi et al. [249] conducted a comprehensive review of 112 studies focusing on the fusion of optical and radar data, which provide unique spectral and structural information for land cover and use assessments. Their analysis revealed that in 32 studies where the benefits of data fusion for land use analysis were assessed, a predominant majority (28 studies) reported enhanced results with data fusion compared to using single data sources.

MateoGarcia et al. [250] introduced and applied a methodology utilizing GEE for cloud masking (Cloud Mask) to map a specific biome type based on OLI/Landsat-8 data. The employed algorithms, FMask and ACCA, demonstrated significant quantitative performance improvements, enhancing classification accuracy by 4% to 5% and reducing commission errors by 3% to 10%. Additional applications and methodologies are presented by Adamo et al. [240] and Samal and Gedam [235].

Validation and Accuracy Assessment

Effective monitoring and management of territorial landscapes necessitate precise land cover information. The quest for accurate land use and land cover maps is a perpetual task for professionals in the field [183]. Validating land cover products is crucial, as it demonstrates the reliability of remote sensing products for informed decision-making. Providing evaluations and reports using suitable information metrics is vital for the user community [207]. Various factors, including the size and quality of training samples, thematic accuracy, classifier selection, and the study area's dimensions, significantly influence the precision of classified maps [179] [180] [183] [251].

Understanding these influencing factors is essential to determining the appropriate accuracy classification for a specific research problem [183]. The selection of samples should adhere to statistical criteria, encompassing the type and method of sampling. Mastella and Vieira [217], along with Shetty [183], note that simple and stratified random sampling are predominantly used in remote sensing, with a majority of validation indices relying on simple random sampling. However, some researchers advocate for systematic sampling methods when studying land use and land cover, citing their ability to yield accurate results, even though they do not provide an unbiased variance estimate [183].

Accuracy assessment stands out as a crucial component in the utilization of remote sensing data for map creation, as it enables the evaluation of different classifiers and the impact of sampling methods [176]. The literature advises

incorporating an error or confusion matrix in this process [179] [180], which aids in identifying class misclassifications and potential error sources [183] [207] [217]. Additionally, quantitative metrics derived from the confusion matrix, such as global accuracy, producer accuracy, user accuracy, Kappa index, Tau, and statistical Z, along with their respective confidence intervals, offer valuable insights. These metrics collectively assess how closely the classified map aligns with the actual conditions and provide a weighted measure of accuracy across different areas.

References

1.A. Wong and D. A. Clausi, "ARRSI: Automatic registration of remote-sensing images", IEEE Trans. Geosci. Remote Sens., vol. 45, no. 5, pp. 1483-1493, 2007.
2.X. Li, N. Hui, H. Shen, Y. Fu and L. Zhang, "A robust mosaicking procedure for high spatial resolution remote sensing images", ISPRS J. Photogram. Remote Sens., vol. 109, pp. 108-125, Nov. 2015.
3.H. Shen, X. Meng and L. Zhang, "An Integrated Framework for the Spatio-Temporal-Spectral Fusion of Remote Sensing Images", IEEE Trans. Geosci. Remote Sens., vol. 54, no. 12, pp. 7135-7148, 2016.
4.Y. Lu, P. Wu, X. Ma and X. Li, "Detection and prediction of land use/land cover change using spatiotemporal data fusion and the Cellular Automata–Markov model", Environ. Monitoring Assessment, vol. 191, no. 2, pp. 68,, 2019.
5.Z. Lv, T. Liu, C. Shi, J. A. Benediktsson and H. Du, "Novel land cover change detection method based on k-means clustering and adaptive majority voting using bitemporal remote sensing images", IEEE Access, vol. 7, pp. 34,425-34,437, Jan. 2019.
6.C. Yuan, F. Wang, S. Wang and Y. Zhou, "Accuracy evaluation of flood monitoring based on multiscale remote sensing for different landscapes", Geomatics Natural Hazards Risk, vol. 10, no. 1, pp. 1389-1411, 2019.
7.L. Yang and G. Cervone, "Analysis of remote sensing imagery for disaster assessment using deep learning: A case study of flooding event", Soft Comput., vol. 23, no. 24, pp. 13,393-13,408, 2019.
8.F. P. M. Oliveira and J. M. R. S. Tavares, "Medical image registration: A review", Comput. Methods Biomech. Biomed. Eng., vol. 17, no. 2, pp. 73-93, 2014.
9.M. A. Viergever, J. B. A. Maintz, S. Klein, K. Murphy, M. Staring and J. P. W. Pluim, "A survey of medical image registration", Med. Image Anal., vol. 33, pp. 140-144, Oct. 2016.
10.G. Haskins, U. Kruger and P. Yan, "Deep learning in medical image registration: A survey", Mach. Vis. Appl., vol. 31, no. 1, pp. 8,, 2020.
11.B. Zitová and J. Flusser, "Image registration methods: A survey", Image Vis. Comput., vol. 21, no. 11, pp. 977-1000, 2003.
12.C. Dalmiya and V. Dharun, "A survey of registration techniques in remote sensing images", Indian J. Sci. Technol., vol. 8, no. 26, pp. 1-7, 2015.
13.R. M. Ezzeldeen, H. H. Ramadan, T. M. Nazmy, M. A. Yehia and M. S. Abdel-Wahab, "Comparative study for image registration techniques of remote sensing images", Egyptian J. Remote Sens. Space Sci., vol. 13, no. 1, pp. 31-36, 2010.
14.M. P. S. Tondewad and M. M. P. Dale, "Remote sensing image registration methodology: Review and discussion", Proc. Comput. Sci., vol. 171, pp. 2390-2399, June 2020.
15.P. E. Anuta, "Spatial registration of multispectral and multitemporal digital imagery using fast Fourier transform techniques", IEEE Trans. Geosci. Electron., vol. 8, no. 4, pp. 353-368, 1970.
16.X. Xu, X. Li, X. Liu, H. Shen and Q. Shi, "Multimodal registration of remotely sensed images based on Jeffrey's divergence", ISPRS J. Photogram. Remote Sens., vol. 122, pp. 97-115, Dec. 2016.
17.J. Ma, H. Zhou, J. Zhao, Y. Gao, J. Jiang and J. Tian, "Robust feature matching for remote sensing image registration via locally linear transforming", IEEE Trans. Geosci. Remote Sens., vol. 53, no. 12, pp. 6469-6481, 2015.

18.N. Hanaizumi and S. Fujimur, "An automated method for registration of satellite remote sensing images", Proc. IEEE Int. Geosci. Remote Sens. Symp. (IGARSS), pp. 1348-1350, 1993.
19.W. F. Webber, "Techniques for image registration", Proc. LARS Symp., pp. 1-7, 1973.
20.D. I. Barnea and H. F. Silverman, "A class of algorithms for fast digital image registration", IEEE Trans. Comput., vol. C-21, no. 2, pp. 179-186, 1972.
21.S. i. Kaneko, Y. Satoh and S. Igarashi, "Using selective correlation coefficient for robust image registration", Pattern Recognit., vol. 36, no. 5, pp. 1165-1173, 2003.
22.H. Gonçalves, J. A. Gonçalves, L. Corte-Real and A. C. Teodoro, "CHAIR: Automatic image registration based on correlation and Hough transform", Int. J. Remote Sens., vol. 33, no. 24, pp. 7936-7968, Dec. 2012.
23.J. Inglada and A. Giros, "On the possibility of automatic multisensor image registration", IEEE Trans. Geosci. Remote Sens., vol. 42, no. 10, pp. 2104-2120, 2004.
24.J. Ma, J. C. Chan and F. Canters, "Fully automatic subpixel image registration of multiangle CHRIS/Proba data", IEEE Trans. Geosci. Remote Sens., vol. 48, no. 7, pp. 2829-2839, 2010.
25.Y. Wu, W. Ma, Q. Su, S. Liu and Y. Ge, "Remote sensing image registration based on local structural information and global constraint", J. Appl. Remote Sens., vol. 13, no. 1, pp. 1,, 2019.
26.G. Wolberg and S. Zokai, "Image registration for perspective deformation recovery", Proc. SPIE Automatic Target Recognit. X, vol. 4050, pp. 259-270, 2000.
27.D. P. Huttenlocher, G. A. Klanderman and W. J. Rucklidge, "Comparing images using the Hausdorff distance", IEEE Trans. Pattern Anal. Mach. Intell., vol. 15, no. 9, pp. 850-863, 1993.
28.Y. Ye and J. Shan, "A local descriptor based registration method for multispectral remote sensing images with non-linear intensity differences", ISPRS J. Photogram. Remote Sens., vol. 90, pp. 83-95, 2014.
29.Y. Hel-Or, H. Hel-Or and E. David, "Fast template matching in non-linear tone-mapped images", Proc. Int. Conf. Comput. Vision (ICCV), pp. 1355-1362, 2011.
30.Y. Bentoutou, N. Taleb, K. Kpalma and J. Ronsin, "An automatic image registration for applications in remote sensing", IEEE Trans. Geosci. Remote Sens., vol. 43, no. 9, pp. 2127-2137, 2005.
31.K. Taejung and I. Yong-Jo, "Automatic satellite image registration by combination of matching and random sample consensus", IEEE Trans. Geosci. Remote Sens., vol. 41, no. 5, pp. 1111-1117, 2003.
32.J. P. Kern and M. S. Pattichis, "Robust multispectral image registration using mutual-information models", IEEE Trans. Geosci. Remote Sens., vol. 45, no. 5, pp. 1494-1505, 2007.
33.H. m. Chen, M. K. Arora and P. K. Varshney, "Mutual information-based image registration for remote sensing data", Int. J. Remote Sens., vol. 24, no. 18, pp. 3701-3706, 2003.
43.D. Brunner, G. Lemoine and L. Bruzzone, "Earthquake Damage assessment of buildings using VHR optical and SAR imagery", IEEE Trans. Geosci. Remote Sens., vol. 48, no. 5, pp. 2403-2420, 2010.
35.X. Wang, W. Yang, A. Wheaton, N. Cooley and B. Moran, "Efficient registration of optical and IR images for automatic plant water stress assessment", Comput. Electron. Agriculture, vol. 74, no. 2, pp. 230-237, 2010.
36.S. Chen, X. Li, L. Zhao and H. Yang, "Medium-low resolution multisource remote sensing image registration based on SIFT and robust regional mutual information", Int. J. Remote Sens., vol. 39, no. 10, pp. 3215-3242, 2018.
37.L. Y. Zhao, B. Y. Lü, X. R. Li and S. H. Chen, "Multi-source remote sensing image registration based on scale-invariant feature transform and optimization of regional mutual information", Acta Phys. Sin., vol. 64, no. 12, pp. 124204,, 2015.
38.G. Hermosillo, C. Chefd'Hotel and O. Faugeras, "Variational methods for multimodal image matching", Int. J. Comput. Vis., vol. 50, no. 3, pp. 329-343, Dec. 2002.
39.R. N. Bracewell and R. N. Bracewell, The Fourier Transform and Its Applications, New York:McGraw-Hill, 1986.
40.H. Foroosh, J. B. Zerubia and M. Berthod, "Extension of phase correlation to subpixel registration", IEEE Trans. Image Process., vol. 11, no. 3, pp. 188-200, Mar. 2002.
41.X. Wan, J. G. Liu and H. Yan, "The illumination robustness of phase correlation for image alignment", IEEE Trans. Geosci. Remote Sens., vol. 53, no. 10, pp. 5746-5759, 2015.
42.X. Wan, J. Liu, H. Yan and G. L. K. Morgan, "Illumination-invariant image matching for autonomous UAV localisation based on optical sensing", ISPRS J. Photogram. Remote Sens., vol. 119, pp. 198-213, Sept. 2016.

43.Z. Liu, L. Wang, X. Wang, X. Shen and L. Li, "Secure remote sensing image registration based on compressed sensing in cloud setting", IEEE Access, vol. 7, pp. 36,516-36,526, Mar. 2019.
44.M. Xu and P. K. Varshney, "A subspace method for Fourier-based image registration", IEEE Geosci. Remote Sens. Lett., vol. 6, no. 3, pp. 491-494, 2009.
45.L. Lucchese, S. Leorin and G. M. Cortelazzo, "Estimation of two-dimensional affine transformations through polar curve matching and its application to image mosaicking and remote-sensing data registration", IEEE Trans. Image Process., vol. 15, no. 10, pp. 3008-3019, 2006.
46.P. Bao and D. Xu, "Complex wavelet-based image mosaics using edge-preserving visual perception modeling", Comput. Graph., vol. 23, no. 3, pp. 309-321, 1999.
47.H. Gang and Z. Yun, "Combination of feature-based and area-based image registration technique for high resolution remote sensing image", Proc. IEEE Int. Geosci. Remote Sens. Symp. (IGARSS), pp. 377-380, 2007.
48.Y. Ye, J. Shan, L. Bruzzone and L. Shen, "Robust registration of multimodal remote sensing images based on structural similarity", IEEE Trans. Geosci. Remote Sens., vol. 55, no. 5, pp. 2941-2958, 2017.
49.H. Yang, X. Li, L. Zhao and S. Chen, "A novel coarse-to-fine scheme for remote sensing image registration based on SIFT and phase correlation", Remote Sens., vol. 11, no. 15, pp. 1833, 2019.
50.Y. Han, F. Bovolo and L. Bruzzone, "An approach to fine coregistration between very high resolution multispectral images based on registration noise distribution", IEEE Trans. Geosci. Remote Sens., vol. 53, no. 12, pp. 6650-6662, 2015.
51.A. Plyer, E. Colin-Koeniguer and F. Weissgerber, "A new coregistration algorithm for recent applications on urban SAR images", IEEE Geosci. Remote Sens. Lett., vol. 12, no. 11, pp. 2198-2202, 2015.
52.G. Brigot, E. Colin-Koeniguer, A. Plyer and F. Janez, "Adaptation and evaluation of an optical flow method applied to coregistration of forest remote sensing images", IEEE J. Sel. Topics Appl. Earth Observ. Remote Sens., vol. 9, no. 7, pp. 2923-2939, 2016.
53.R. Feng, X. Li and H. Shen, "Mountainous remote sensing images registration based on improved optical flow estimation", ISPRS Ann. Photogramm. Remote Sens. Spatial Inf. Sci., vol. IV-2/W5, pp. 479-484, June 2019.
54.B. K. P. Horn and B. G. Schunck, "Determining optical flow", Artif. Intell., vol. 17, no. 1, pp. 185-203, 1981.
55.J. J. Gibson, The Perception of the Visual World, Oxford:Houghton Mifflin, 1950.
56.B. D. Lucas and T. Kanade, "An iterative image registration technique with an application to stereo vision", Proc. Imag. Understanding Workshop, pp. 121-130, 1981.
57.Z. Tu et al., "A survey of variational and CNN-based optical flow techniques", Signal Processing: Image Commun., vol. 72, pp. 9-24, Mar. 2019.
58.C. Liu, J. Yuen and A. Torralba, "SIFT Flow: Dense correspondence across scenes and its applications", IEEE Trans. Pattern Anal. Mach. Intell., vol. 33, no. 5, pp. 978-994, 2011.
59.T. Brox, A. Bruhn, N. Papenberg and J. Weickert, "High accuracy optical flow estimation based on a theory for warping", Proc. Eur. Conf. Comput. Vision (ECCV), pp. 25-36, 2004.
60.J.-Y. Xiong, Y.-P. Luo and G.-R. Tang, "An improved optical flow method for image registration with large-scale movements", Acta Autom. Sin., vol. 34, no. 7, pp. 760-764, 2008.
61.A. Plyer, G. Le Besnerais and F. Champagnat, "Massively parallel Lucas Kanade optical flow for real-time video processing applications", J. Real-Time Image Process., vol. 11, no. 4, pp. 713-730, 2016.
62.Y. Xiang, F. Wang, L. Wan, N. Jiao and H. You, "OS-Flow: A robust algorithm for dense optical and SAR image registration", IEEE Trans. Geosci. Remote Sens., vol. 57, no. 9, pp. 1-20, 2019.
63.C. Huo, C. Pan, L. Huo and Z. Zhou, "Multilevel SIFT matching for large-size VHR image registration", IEEE Geosci. Remote Sens. Lett., vol. 9, no. 2, pp. 171-175, 2012.
64.L. Yu, D. Zhang and E.-J. Holden, "A fast and fully automatic registration approach based on point features for multi-source remote-sensing images", Comput. Geosci., vol. 34, no. 7, pp. 838-848, 2008.
65.L. Hui, B. S. Manjunath and S. K. Mitra, "A contour-based approach to multisensor image registration", IEEE Trans. Image Process., vol. 4, no. 3, pp. 320-334, 1995.
66.H. Goncalves, L. Corte-Real and J. A. Goncalves, "Automatic image registration through image segmentation and SIFT", IEEE Trans. Geosci. Remote Sens., vol. 49, no. 7, pp. 2589-2600, 2011.

67.H. P. Moravec, Techniques towards automatic visual obstacle avoidance, no. 2, pp. 584, 1977, [online] Available: https://frc.ri.cmu.edu/~hpm/project.archive/robot.papers/1977/aip.txt.
68.C. Harris and M. Stephens, "A combined corner and edge detector", Proc. Alvey Vision Conf., vol. 15, pp. 147-151, 1988.
69.Y. Xiang, F. Wang and H. You, "OS-SIFT: A robust SIFT-like algorithm for high-resolution optical-to-SAR image registration in suburban areas", IEEE Trans. Geosci. Remote Sens., vol. 56, no. 6, pp. 3078-3090, 2018.
70.I. Misra, S. M. Moorthi, D. Dhar and R. Ramakrishnan, "An automatic satellite image registration technique based on Harris corner detection and Random Sample Consensus (RANSAC) outlier rejection model", 1st Int. Conf. on Recent Advances in Information Technology (RAIT), pp. 68-73, 2012.
71.S. M. Smith and J. M. Brady, "SUSAN–A new approach to low level image processing", Int. J. Comput. Vis., vol. 23, no. 1, pp. 45-78, 1997.
72.C. Leng, H. Zhang, B. Li, G. Cai, Z. Pei and L. He, "Local feature descriptor for image matching: A survey", IEEE Access, vol. 7, pp. 6424-6434, 2019.
73.W. He and X. Deng, "A modified SUSAN corner detection algorithm based on adaptive gradient threshold for remote sensing image", Proc. Int. Conf. Optoelectron. Image Process., vol. 1, pp. 40-43, 2010.
74.R. Feng, X. Li, W. Zou and H. Shen, "Registration of multitemporal GF-1 remote sensing images with weighting perspective transformation model", Proc. IEEE Int. Conf. Image Process. (ICIP), pp. 2264-2268, 2017.
75.R. Feng, Q. Du, X. Li and H. Shen, "Robust registration for remote sensing images by combining and localizing feature- and area-based methods", ISPRS J. Photogram. Remote Sens., vol. 151, pp. 15-26, May 2019.
76.Y. Duan, X. Huang, J. Xiong, Y. Zhang and B. Wang, "A combined image matching method for Chinese optical satellite imagery", Int. J. Digital Earth, vol. 9, no. 9, pp. 851-872, 2016.
77.P. K. Konugurthi, R. Kune, R. Nooka and V. Sarma, "Autonomous ortho-rectification of very high resolution imagery using SIFT and genetic algorithm", Photogram. Eng. Remote Sens., vol. 82, no. 5, pp. 377-388, 2016.
78.Q. Li, G. Wang, J. Liu and S. Chen, "Robust scale-invariant feature matching for remote sensing image registration", IEEE Geosci. Remote Sens. Lett., vol. 6, no. 2, pp. 287-291, 2009.
79.W. Ma et al., "Remote sensing image registration with modified SIFT and enhanced feature matching", IEEE Geosci. Remote Sens. Lett., vol. 14, no. 1, pp. 3-7, 2017.
80.M. Gong, S. Zhao, L. Jiao, D. Tian and S. Wang, "A novel coarse-to-fine scheme for automatic image registration based on SIFT and mutual information", IEEE Trans. Geosci. Remote Sens., vol. 52, no. 7, pp. 4328-4338, 2014.
81.C. A. Lee, S. D. Gasster, A. Plaza, C. Chang and B. Huang, "Recent developments in high performance computing for remote sensing: A review", IEEE J. Sel. Topics Appl. Earth Observ. Remote Sens., vol. 4, no. 3, pp. 508-527, 2011.
82.D. G. Lowe, "Distinctive image features from scale-invariant keypoints", Int. J. Comput. Vis., vol. 60, no. 2, pp. 91-110, 2004.
83.K. Mikolajczyk and C. Schmid, "A performance evaluation of local descriptors", IEEE Trans. Pattern Anal. Mach. Intell., vol. 27, no. 10, pp. 1615-1630, Oct. 2005.
84.K. Yan and R. Sukthankar, "PCA-SIFT: A more distinctive representation for local image descriptors", Proc. IEEE Comput. Soc. Conf. Comput. Vision Pattern Recognit. (CVPR), vol. 2, pp. 506-513, 2004.
85.Y. Zheng, Z. Cao and Y. Xiao, "Multi-spectral remote image registration based on SIFT", Electron. Lett., vol. 44, no. 2, pp. 107-108, 2008.
86.J. Morel and G. Yu, "ASIFT: A new framework for fully affine invariant image comparison", SIAM J. Imag. Sci., vol. 2, no. 2, pp. 438-469, 2009.
87.A. Sedaghat, M. Mokhtarzade and H. Ebadi, "Uniform robust scale-invariant feature matching for optical remote sensing images", IEEE Trans. Geosci. Remote Sens., vol. 49, no. 11, pp. 4516-4527, 2011.
88.A. Sedaghat and H. Ebadi, "Distinctive order based self-similarity descriptor for multi-sensor remote sensing image matching", ISPRS J. Photogram. Remote Sens., vol. 108, pp. 62-71, Oct. 2015.
89.H. Bay, T. Tuytelaars and L. Van Gool, "SURF: Speeded up robust features", Proc. Eur. Conf. Comput. Vision (ECCV), pp. 404-417, 2006.

90.W. Yan, H. She and Z. Yuan, "Robust registration of remote sensing image based on SURF and KCCA", J. Indian Soc. Remote Sens., vol. 42, no. 2, pp. 291-299, 2014.
91.X. Yuan, S. Chen, W. Yuan and Y. Cai, "Poor textural image tie point matching via graph theory", ISPRS J. Photogram. Remote Sens., vol. 129, pp. 21-31, July 2017.
92.R. Bouchiha and K. Besbes, "Automatic remote-sensing image registration using SURF", Int. J. Comput. Theory Eng., vol. 5, no. 1, pp. 88-92, 2013.
93.J. Chen et al., "WLD: A robust local image descriptor", IEEE Trans. Pattern Anal. Mach. Intell., vol. 32, no. 9, pp. 1705-1720, 2010.
94.E. Rosten and T. Drummond, "Machine learning for high-speed corner detection", Proc. Eur. Conf. Comput. Vision (ECCV), pp. 430-443, 2006.
95.M. Calonder, V. Lepetit, C. Strecha and P. Fua, "BRIEF: Binary robust independent elementary features", Proc. Eur. Conf. Comput. Vision (ECCV), pp. 778-792, 2010.
96.E. Rublee, V. Rabaud, K. Konolige and G. Bradski, "ORB: An efficient alternative to SIFT or SURF", Proc. Int. Conf. Comput. Vision (ICCV), pp. 2564-2571, 2011.
97.D. Ma and H. Lai, "Remote sensing image matching based improved ORB in NSCT domain", J. Indian soc. Remote Sens., vol. 47, no. 5, pp. 801-807, 2019.
98.P. F. Alcantarilla, A. Bartoli and A. J. Davison, "KAZE Features", Proc. Eur. Conf. Comput. Vision (ECCV), pp. 214-227, 2012.
99.P. Alcantarilla, J. Nuevo and A. Bartoli, "Fast explicit diffusion for accelerated features in nonlinear scale spaces", Proc. Brit. Mach. Vision Conf. (BMVC), pp. 1-11, 2013.
100.Y. Ye, M. Wang, S. Hao and Q. Zhu, "A novel keypoint detector combining corners and blobs for remote sensing image registration", IEEE Geosci. Remote Sens. Lett., vol. 18, no. 3, pp. 451-455, Mar. 2020.
101.X. Liu, Y. Ai, J. Zhang and Z. Wang, "A novel affine and contrast invariant descriptor for infrared and visible image registration", Remote Sens., vol. 10, no. 4, pp. 658, 2018.
102.Z. Ye et al., "Robust fine registration of multisensor remote sensing images based on enhanced subpixel phase correlation", Sensors, vol. 20, no. 15, pp. 4338,, Aug. 2020.
103.Y. C. Hsieh, D. M. McKeown and F. P. Perlant, "Performance evaluation of scene registration and stereo matching for cartographic feature extraction", IEEE Trans. Pattern Anal. Mach. Intell., vol. 14, no. 2, pp. 214-238, 1992.
104.S. Dongseok, J. K. Pollard and J. Muller, "Accurate geometric correction of ATSR images", IEEE Trans. Geosci. Remote Sens., vol. 35, no. 4, pp. 997-1006, 1997.
105.J. Inglada and F. Adragna, "Automatic multi-sensor image registration by edge matching using genetic algorithms", Proc. Int. Geosci. Remote Sens. Symp. (IGARSS), vol. 5, pp. 2313-2315, 2001.
106.W. Shi and A. Shaker, "The Line-Based Transformation Model (LBTM) for image-to-image registration of high-resolution satellite image data", Int. J. Remote Sens., vol. 27, no. 14, pp. 3001-3012, 2006.
107.T.-Z. Xiang, G.-S. Xia, X. Bai and L. Zhang, "Image stitching by line-guided local warping with global similarity constraint", Pattern Recognit., vol. 83, pp. 481-497, Nov. 2018.
108.C. Zhao and A. A. Goshtasby, "Registration of multitemporal aerial optical images using line features", ISPRS J. Photogram. Remote Sens., vol. 117, pp. 149-160, July 2016.
109.C. Li and W. Shi, "The generalized-line-based iterative transformation model for imagery registration and rectification", IEEE Geosci. Remote Sens. Lett., vol. 11, no. 8, pp. 1394-1398, 2014.
110.A. O. Ok, J. D. Wegner, C. Heipke, F. Rottensteiner, U. Soergel and V. Toprak, "Matching of straight line segments from aerial stereo images of urban areas", ISPRS J. Photogram. Remote Sens., vol. 74, pp. 133-152, Nov. 2012.
112.J. Canny, "A computational approach to edge detection", IEEE Trans. Pattern Anal. Mach. Intell., vol. PAMI-8, no. 6, pp. 679-698, 1986.
113.D. Marr and E. Hildreth, "Theory of edge detection", Proc. Roy. Soc. Ser. B-Biol. Sci., vol. 207, no. 1167, pp. 187-217, 1980.
114.R. G. v. Gioi, J. Jakubowicz, J. Morel and G. Randall, "LSD: A fast line segment detector with a false detection control", IEEE Trans. Pattern Anal. Mach. Intell., vol. 32, no. 4, pp. 722-732, 2010.

115.C. Akinlar and C. Topal, "EDLines: A real-time line segment detector with a false detection control", Pattern Recog. Lett., vol. 32, no. 13, pp. 1633-1642, 2011.
116.A. Goshtasby and G. C. Stockman, "Point pattern matching using convex hull edges", IEEE Trans. Syst. Man Cybern., vol. SMC-15, no. 5, pp. 631-637, 1985.
117.W. Dorigo, M. Hollaus, W. Wagner and K. Schadauer, "An application-oriented automated approach for co-registration of forest inventory and airborne laser scanning data", Int. J. Remote Sens., vol. 31, no. 5, pp. 1133-1153, 2010.
118.B. Sirmacek and C. Unsalan, "Urban-area and building detection using SIFT keypoints and graph theory", IEEE Trans. Geosci. Remote Sens., vol. 47, no. 4, pp. 1156-1167, 2009.
119.J. Flusser and T. Suk, "A moment-based approach to registration of images with affine geometric distortion", IEEE Trans. Geosci. Remote Sens., vol. 32, no. 2, pp. 382-387, 1994.
120.N. R. Pal and S. K. Pal, "A review on image segmentation techniques", Pattern Recognit., vol. 26, no. 9, pp. 1277-1294, 1993.
121.D. Xiaolong and S. Khorram, "Development of a feature-based approach to automated image registration for multitemporal and multisensor remotely sensed imagery", Proc. IEEE Int. Geosci. Remote Sens. Symp. Proc. Remote Sens.-A Sci. Vision Sustainable Develop. (IGARSS), vol. 1, pp. 243-245, 1997.
122.L. M. Fonseca and B. Manjunath, "Registration techniques for multisensor remotely sensed imagery", Photogram. Eng. Remote Sensing (PERS), vol. 62, no. 9, pp. 1049-1056, 1996.
123.A. Goshtasby, G. C. Stockman and C. V. Page, "A region-based approach to digital image registration with subpixel accuracy", IEEE Trans. Geosci. Remote Sens., vol. GE-24, no. 3, pp. 390-399, 1986.
124.A. Irani Rahaghi, U. Lemmin, D. Sage and D. A. Barry, "Achieving high-resolution thermal imagery in low-contrast lake surface waters by aerial remote sensing and image registration", Remote Sens. Environ., vol. 221, pp. 773-783, Feb. 2019.
125.A. Li, X. Cheng, H. Guan, T. Feng and Z. Guan, "Novel image registration method based on local structure constraints", IEEE Geosci. Remote Sens. Lett., vol. 11, no. 9, pp. 1584-1588, 2014.
126.S. Jiang and W. Jiang, "Hierarchical motion consistency constraint for efficient geometrical verification in UAV stereo image matching", ISPRS J. Photogram. Remote Sens., vol. 142, pp. 222-242, Aug. 2018.
127.J. S. Beis and D. G. Lowe, "Shape indexing using approximate nearest-neighbour search in high-dimensional spaces", Proc. IEEE Comput. Soc. Conf. Comput. Vis. Pattern Recognit. (CVPR), vol. 97, pp. 1000-1006, 1997.
128.Y. Ma et al., "Remote sensing big data computing: Challenges and opportunities", Future Gener. Comput. Syst., vol. 51, pp. 47-60, Oct. 2015.
129.G. Stockman, S. Kopstein and S. Benett, "Matching images to models for registration and object detection via clustering", IEEE Trans. Pattern Anal. Mach. Intell., vol. PAMI-4, no. 3, pp. 229-241, 1982.
130.G. Borgefors, "Hierarchical chamfer matching: A parametric edge matching algorithm", IEEE Trans. Pattern Anal. Mach. Intell., vol. 10, no. 6, pp. 849-865, 1988.
131.L. Livi and A. Rizzi, "The graph matching problem", Pattern Anal. Appl., vol. 16, no. 3, pp. 253-283, 2013.
132.L. Torresani, V. Kolmogorov and C. Rother, "Feature correspondence via graph matching: models and global optimization", Proc. Eur. Conf. Comput. Vision (ECCV), pp. 596-609, 2008.
133.Z. Liu, J. An and Y. Jing, "A simple and robust feature point matching algorithm based on restricted spatial order constraints for aerial image registration", IEEE Trans. Geosci. Remote Sens., vol. 50, no. 2, pp. 514-527, 2012.
134.Z. Xiong and Y. Zhang, "A novel interest-point-matching algorithm for high-resolution satellite images", IEEE Trans. Geosci. Remote Sens., vol. 47, no. 12, pp. 4189-4200, 2009.
135.H. Chang, G. Wu and M. Chiang, "Remote sensing image registration based on modified SIFT and feature slope grouping", IEEE Geosci. Remote Sens. Lett., vol. 16, no. 9, pp. 1363-1367, 2019.
136.S. Zhili and Z. Jiaqi, "Image registration approach with scale-invariant feature transform algorithm and tangent-crossing-point feature", J. Electron. Imag., vol. 29, no. 2, pp. 1-14, Mar. 2020.
137.M. A. Fischler and R. C. Bolles, "Random sample consensus: A paradigm for model fitting with applications to image analysis and automated cartography", Commun. ACM, vol. 24, no. 6, pp. 381-395, 1981.

138.K. Zhang, X. Li and J. Zhang, "A robust point-matching algorithm for remote sensing image registration", IEEE Geosci. Remote Sens. Lett., vol. 11, no. 2, pp. 469-473, 2014.
139.Y. Wu, W. Ma, M. Gong, L. Su and L. Jiao, "A novel point-matching algorithm based on fast sample consensus for image registration", IEEE Geosci. Remote Sens. Lett., vol. 12, no. 1, pp. 43-47, 2015.
140.B. Li and H. Ye, "RSCJ: Robust sample consensus judging algorithm for remote sensing image registration", IEEE Geosci. Remote Sens. Lett., vol. 9, no. 4, pp. 574-578, 2012.
141.H. Zhang et al., "Remote sensing image registration based on local affine constraint with circle descriptor", IEEE Geosci. Remote Sens. Lett., 2020.
142.F. Ye, Y. Su, H. Xiao, X. Zhao and W. Min, "Remote sensing image registration using convolutional neural network features", IEEE Geosci. Remote Sens. Lett., vol. 15, no. 2, pp. 232-236, 2018.
143.C. Farabet, C. Couprie, L. Najman and Y. LeCun, "Learning hierarchical features for scene labeling", IEEE Trans. Pattern Anal. Mach. Intell., vol. 35, no. 8, pp. 1915-1929, 2013.
144.W. Huang, L. Xiao, Z. Wei, H. Liu and S. Tang, "A new pan-sharpening method with deep neural networks", IEEE Geosci. Remote Sens. Lett., vol. 12, no. 5, pp. 1037-1041, 2015.
145.Y. Xing, M. Wang, S. Yang and L. Jiao, "Pan-sharpening via deep metric learning", ISPRS J. Photogram. Remote Sens., vol. 145, pp. 165-183, Nov. 2018.
146.G. J. Scott, M. R. England, W. A. Starms, R. A. Marcum and C. H. Davis, "Training deep convolutional neural networks for land–cover classification of high-resolution imagery", IEEE Geosci. Remote Sens. Lett., vol. 14, no. 4, pp. 549-553, 2017.
147.L. Ma, Y. Liu, X. Zhang, Y. Ye, G. Yin and B. A. Johnson, "Deep learning in remote sensing applications: A meta-analysis and review", ISPRS J. Photogram. Remote Sens., vol. 152, pp. 166-177, June 2019.
148.Y. Liu, D. Minh Nguyen, N. Deligiannis, W. Ding and A. Munteanu, "Hourglass-shapenetwork based semantic segmentation for high resolution aerial imagery", Remote Sens., vol. 9, no. 6, pp. 522, 2017.
149.H. Zhang et al., "Registration of multimodal remote sensing image based on deep fully convolutional neural network", IEEE J. Sel. Topics Appl. Earth Observ. Remote Sens., vol. 12, no. 8, pp. 3028-3042, 2019.
150.N. Merkle, W. Luo, S. Auer, R. Müller and R. Urtasun, "Exploiting deep matching and SAR data for the geo-localization accuracy improvement of optical satellite images", Remote Sensing, vol. 9, no. 6, pp. 586, 2017.
151.S. Wang, D. Quan, X. Liang, M. Ning, Y. Guo and L. Jiao, "A deep learning framework for remote sensing image registration", ISPRS J. Photogram. Remote Sens., vol. 145, pp. 148-164, Nov. 2018.
152.N. Merkle, S. Auer, R. Müller and P. Reinartz, "Exploring the potential of conditional adversarial networks for optical and SAR image matching", IEEE J. Sel. Topics Appl. Earth Observ. Remote Sens., vol. 11, no. 6, pp. 1811-1820, 2018.
153.H. L. Hughes, M. Schmitt and X. X. Zhu, "Mining hard negative samples for SAR-optical image matching using generative adversarial networks", Remote Sens., vol. 10, no. 10, pp. 1552,, 2018.
154.J. Zhang, W. Ma, Y. Wu and L. Jiao, "Multimodal remote sensing image registration based on image transfer and local features", IEEE Geosci. Remote Sens. Lett., vol. 16, no. 8, pp. 1210-1214, 2019.
155.N. Girard, G. Charpiat and Y. Tarabalka, "Aligning and updating cadaster maps with aerial images by multi-task multi-resolution deep learning", Proc. Asian Conf. Comput. Vision (ACCV 2018), pp. 675-690, 2019.
156.L. Li, L. Han, M. Ding, Z. Liu and H. Cao, "Remote sensing image registration based on deep learning regression model", IEEE Geosci. Remote Sens. Lett., 2020.
157.F. Liu, F. Bi, L. Chen, H. Shi and W. Liu, "Feature-area optimization: A novel SAR image registration method", IEEE Geosci. Remote Sens. Lett., vol. 13, no. 2, pp. 242-246, 2016.
158.X. Huang, Y. Sun, D. Metaxas, F. Sauer and C. Xu, "Hybrid image registration based on configural matching of scale-invariant salient region features", Proc. IEEE Comput. Society Conf. Comput. Vis. Pattern Recognit. (CVPR), pp. 167-167, 2004.
159.G. Hong and Y. Zhang, "Combination of feature-based and area-based image registration technique for high resolution remote sensing image", Proc. Int. Geosci. Remote Sens. Symp. (IGARSS), pp. 377-380, 2007.
160.N. E. Mekky, F. E.-Z. Abou-Chadi and S. Kishk, "Wavelet-based image registration techniques: A study of performance", Int. J. Comput. Sci. Netw. Security, vol. 11, no. 2, pp. 188-196, 2011.
161.S. Suri, P. Schwind, P. Reinartz and J. Uhl, "Combining mutual information and scale invariant feature transform for fast and robust multisensor SAR image registration", Proc. 75th Annu. ASPRS Conf., 2009.

162.Y. S. Heo, K. M. Lee and S. U. Lee, "Joint depth map and color consistency estimation for stereo images with different illuminations and cameras", IEEE Trans. Pattern Anal. Mach. Intell., vol. 35, no. 5, pp. 1094-1106, 2013.
163.R. Feng, Q. Du, H. Shen and X. Li, "Region-by-region registration combining feature-based and optical flow methods for remote sensing images", Remote Sens., vol. 13, no. 8, pp. 1475, 2021.
164.S. R. Lee, "A coarse-to-fine approach for remote-sensing image registration based on a local method", Int. J. Smart Sens. Intell. Syst., vol. 3, no. 4, 2010.
165.K. Sharma and A. Goyal, "Very high resolution image registration based on two step Harris-Laplace detector and SIFT descriptor", 2013 4th Int. Conf. Comput. Commun. Netw. Technol. (ICCCNT), pp. 1-5.
166.W. Ma, J. Zhang, Y. Wu, L. Jiao, H. Zhu and W. Zhao, "A novel two-step registration method for remote sensing images based on deep and local features", IEEE Trans. Geosci. Remote Sens., vol. 57, no. 7, pp. 4834-4843, 2019.
167.S. Li, L. Yuan, J. Sun and L. Quan, "Dual-feature warping-based motion model estimation", Proc. IEEE Int. Conf. Comput. Vision (ICCV), pp. 4283-4291, 2015.
168.S. Nag, Image registration techniques: A survey, Nov. 2017.
169.J. S. Bhatt and N. Padmanabhan, "Image Registration for meteorological applications: Development of a generalized software for sensor data registration at ISRO", IEEE Geosci. Remote Sens. Mag. (replaces Newslett.), vol. 8, no. 4, pp. 23-37, 2020.
170.A. Sedaghat and N. Mohammadi, "High-resolution image registration based on improved SURF detector and localized GTM", Int. J. Remote Sens., vol. 40, no. 7, pp. 2576-2601, Apr. 2019.
171.Y. Ma, J. Wang, H. Xu, S. Zhang, X. Mei and J. Ma, "Robust image feature matching via progressive sparse spatial consensus", IEEE Access, vol. 5, pp. 24,568-24,579, Oct .
172.H. Goncalves, J. A. Goncalves and L. Corte-Real, "Measures for an objective evaluation of the geometric correction process quality", IEEE Geosci. Remote Sens. Lett., vol. 6, no. 2, pp. 292-296, 2009.
173. Sidhu, N., Pebesma, E. and Camara, G. (2018) Using Google Earth Engine to Detect Land Cover Change: Singapore as a Use Case. European Journal of Remote Sensing, 51, 486-500. https://doi.org/10.1080/22797254.2018.1451782.
174. Probst, L., Pedersen, B. and Dakkak-Arnoux, L. (2017) Big Data in Earth Observation. https://ec.europa.eu/growth/tools-databases/dem/monitor/sites/default/files/DTM_Big%20Data%20in%20Earth%20Observation%20v1.pdf.
175. Gorelick, N., Hancher, M., Dixon, M., Ilyushchenko, S., Thau, D. and Moore, R. (2017) Google Earth Engine: Planetary-Scale Geospatial Analysis for Everyone. Remote Sensing of Environment, 202, 18-27. https://doi.org/10.1016/j.rse.2017.06.031.
176. Teluguntla, P., Thenkabail, P., Oliphant, A., Xiong, J., Gumma, M.K., Congalton, R.G., Yadav, K. and Huete, A. (2018) A 30-m Landsat-Derived Cropland Extent Product of Australia and China Using Random Forest Machine Learning Algorithm on Google Earth Engine Cloud Computing Platform. ISPRS Journal of Photogrammetry and Remote Sensing, 144, 325-340. https://doi.org/10.1016/j.isprsjprs.2018.07.017.
177. Mutanga, O. and Kumar, L. (2019) Google Earth Engine Aplications. Remote Sensing, 11, Article No. 591. https://doi.org/10.3390/rs11050591.
178. Liu, L., Zhang, X., Gao, Y., Chen, X., Shuai, X. and Mi, J. (2021) Finer-Resolution Mapping of Global Land Cover: Recent Developments, Consistency Analysis, and Prospects. Journal of Remote Sensing, 2021, 1-38. https://doi.org/10.34133/2021/5289697.
179. Jha, M.K. and Chowdary, V.M. (2007) Challenges of Using Remote Sensing and GIS in Developing Nations. Hydrogeology Journal, 15, 197-200. https://doi.org/10.1007/s10040-006-0117-1.
180. Gomes, V.C.F., Queiroz, G.R. and Ferreira, K.R. (2020) An Overview of Platforms for Big Earth Observation Data Management and Analysis. Remote Sensing, 12, Article No. 1253. https://doi.org/10.3390/rs12081253.
181. Huang, B. and Wang, J. (2020) Big Spatial Data for Urban and Environmental Sustainability. Geo-Spatial Information Science, 23, 125-140. https://doi.org/10.1080/10095020.2020.1754138.

182. Reeves, M.C., Washington-Allen, R.A., Angerer, J., Hunt, E.R., Kulawardhana, R.W., Kumar, L., Loboda, T., Loveland, T., Metternicht, G. and Ramsey, R.D. (2016) Land Resources Monitoring, Modeling, and Mapping with Remote Sensing. In: Prasad, S.T., Ed., Land Resources Monitoring, Modeling, and Mapping with Remote Sensing, CRC Press, Boca Raton, 237-275.
183. Congalton, R.G. and Green, K. (2009) Assessing the Accuracy of Remotely Sensed Data: Principles and Practices. 2nd Edition, CRC Press, Boca Raton. https://doi.org/10.1201/9781420055139.
184. Food and Agriculture Organization of the United Nations (2016) Map Accuracy Assessment and Area Estimation: A Practical Guide. National forest Monitoring Assessment Working Paper, No. 46, Food and Agriculture Organization of the United Nations, Rome. http://www.fao.org/3/a-i5601e.pdf.
185. Zhu, L., Suomalainen, J., Liu, J., Hyyppa, J., Kaartinen, H. and Haggren, H. (2018) A Review: Remote Sensing Sensors. In: Rustamov, R., Hasanova, S. and Zeynalova, M., Eds., Multi-Purposeful Application of Geospatial Data, IntechOpen, London, 19-42. https://doi.org/10.5772/intechopen.71049.
186. Zwinkels, J.C. (2016) Light, Electromagnetic Spectrum. In: Luo, R., Ed., Encyclopedia of Color Science and Technology, Springer Science + Business Media, New York, 2-8. https://doi.org/10.1007/978-1-4419-8071-7_204.
187. Butcher, G. (2016) Tour of the Electromagnetic Spectrum. 3rd Edition, National Aeronautics and Space Administration, Washington DC.
188. Bowker, D.E., Davis, R.E., Myrick, D.L., Stacy, K. and Jones, W.T. (1985) Spectral Reflectances of Natural Targets for Use in Remote Sensing Studies. National Aeronautics and Space Administration, Washington DC.
189. Coetzee, S., Ivánová, I., Mitasova, H. and Brovelli, M.A. (2020) Open Geospatial Software and Data: A Review of the Current State and A Perspective into the Future. ISPRS International Journal of Geo-Information, 9, Article No. 90. https://doi.org/10.3390/ijgi9020090.
190. Chi, M., Plaza, A., Benediktsson, J.A., Sun, Z., Shen, J. and Zhu, Y. (2016) Big Data for Remote Sensing: Challenges and Opportunities. Proceeding of the IEEE, 104, 2207-2219. https://doi.org/10.1109/JPROC.2016.2598228.
191. Shetty, S. (2019) Analysis of Machine Learning Classifiers for LULC Classification on Google Earth Engine. MSc. Thesis, University of Twente, Enschede.
192. Sajjad, H. and Kumar, P. (2019) Future Challenges and Perspective of Remote Sensing Technology. In: Kumar, P., Rani, M., Chandra Pandey, P., Sajjad, H. and Chaudhary, B.S., Eds., Applications and Challenges of Geospatial Technology, Springer International Publishing, Cham, 275-277. https://doi.org/10.1007/978-3-319-99882-4_16.
193. Xu, Y. and Huang, B. (2014) Spatial and Temporal Classification of Synthetic Satellite Imagery: Land Cover Mapping and Accuracy Validation. Geo-Spatial Information Science, 17, 1-7. https://doi.org/10.1080/10095020.2014.881959.
194. Maurya, S.P., Ohri, A. and Mishra, S. (2015) Open Source GIS: A Review. National Conference on Open Source GIS: Opportunities and Challenges, Varanasi, 9-10 October 2015, 150-155. https://www.researchgate.net/publication/282858368.
195. GIS Technical Advisory Committee (2017) Open Source GIS Software: A Guide for Understanding Current GIS Software Solutions. North Carolina Geographic Information Coordinating Council, Raleigh. https://files.nc.gov/ncdit/GICC-TAC-OpenSource-GIS-Software-20171201.pdf.
196. Steiniger, S. and Hay, G.J. (2009) Free and Open Source Geographic Information Tools for Landscape Ecology. Ecological Informatics, 4, 183-195. https://doi.org/10.1016/j.ecoinf.2009.07.004.
197. Teodoro, A.C., Ferreira, D. and Sillero, N. (2012). Performance of Commercial and Open Source Remote Sensing/Image Processing Software for land Cover/Use Purposes. Earth Resources and Environmental Remote Sensing/GIS Applications III, 8538, Article ID: 85381K. https://doi.org/10.1117/12.974577.
198. Correia, R., Duarte, L., Teodoro, A.C. and Monteiro, A. (2018) Processing Image to Geographical Information Systems (PI2GIS)—A Learning Tool for QGIS. Education Sciences, 8, Article No. 83. https://doi.org/10.3390/educsci8020083.

199. Anand, A., Krishna, A., Tiwari, R. and Sharma, R. (2018) Comparative Analysis between Proprietary Software vs. Open-Source Software vs. Free Software. 5th IEEE International Conference on Parallel, Distributed and Grid Computing (PDGC-2018), Solan, 20-22
190. Coetzee, S., Ivánová, I., Mitasova, H. and Brovelli, M.A. (2020) Open Geospatial Software and Data: A Review of the Current State and A Perspective into the Future. ISPRS International Journal of Geo-Information, 9, Article No. 90. https://doi.org/10.3390/ijgi9020090
191. Chi, M., Plaza, A., Benediktsson, J.A., Sun, Z., Shen, J. and Zhu, Y. (2016) Big Data for Remote Sensing: Challenges and Opportunities. Proceeding of the IEEE, 104, 2207-2219. https://doi.org/10.1109/JPROC.2016.2598228
192. Shetty, S. (2019) Analysis of Machine Learning Classifiers for LULC Classification on Google Earth Engine. MSc. Thesis, University of Twente, Enschede.
193. Sajjad, H. and Kumar, P. (2019) Future Challenges and Perspective of Remote Sensing Technology. In: Kumar, P., Rani, M., Chandra Pandey, P., Sajjad, H. and Chaudhary, B.S., Eds., Applications and Challenges of Geospatial Technology, Springer International Publishing, Cham, 275-277. https://doi.org/10.1007/978-3-319-99882-4_16
194. Xu, Y. and Huang, B. (2014) Spatial and Temporal Classification of Synthetic Satellite Imagery: Land Cover Mapping and Accuracy Validation. Geo-Spatial Information Science, 17, 1-7. https://doi.org/10.1080/10095020.2014.881959
195. Maurya, S.P., Ohri, A. and Mishra, S. (2015) Open Source GIS: A Review. National Conference on Open Source GIS: Opportunities and Challenges, Varanasi, 9-10 October 2015, 150-155. https://www.researchgate.net/publication/282858368
196. GIS Technical Advisory Committee (2017) Open Source GIS Software: A Guide for Understanding Current GIS Software Solutions. North Carolina Geographic Information Coordinating Council, Raleigh. https://files.nc.gov/ncdit/GICC-TAC-OpenSource-GIS-Software-20171201.pdf
197. Steiniger, S. and Hay, G.J. (2009) Free and Open Source Geographic Information Tools for Landscape Ecology. Ecological Informatics, 4, 183-195. https://doi.org/10.1016/j.ecoinf.2009.07.004
198. Teodoro, A.C., Ferreira, D. and Sillero, N. (2012). Performance of Commercial and Open Source Remote Sensing/Image Processing Software for Land Cover/Use Purposes. Earth Resources and Environmental Remote Sensing/GIS Applications III, 8538, Article ID: 85381K. https://doi.org/10.1117/12.974577
199. Correia, R., Duarte, L., Teodoro, A.C. and Monteiro, A. (2018) Processing Image to Geographical Information Systems (PI2GIS)—A Learning Tool for QGIS. Education Sciences, 8, Article No. 83. https://doi.org/10.3390/educsci8020083
200. Anand, A., Krishna, A., Tiwari, R. and Sharma, R. (2018) Comparative Analysis between Proprietary Software vs. Open-Source Software vs. Free Software. 5th IEEE International Conference on Parallel, Distributed and Grid Computing (PDGC-2018), Solan, 20-22 December 2018, 144-147. https://doi.org/10.1109/PDGC.2018.8745951
201. Mota, C. and Seruca, I. (2015) Open Source Software vs. Proprietary Software in Education. 10th Iberian Conference on Information Systems and Technologies, (CISTI), Aveiro, 17-20 Jun 2015, 1-6. https://doi.org/10.1109/CISTI.2015.7170544
202. Miller, A. (2011) Open Source vs. Proprietary Software in Developing Countries. https://www.academia.edu/777383/Open_Source_v_Proprietary_Software
203. Tesoriere, A. and Balletta, L. (2017) A Dynamic Model of Open Source vs. Proprietary R & D. European Economic Review, 94, 221-239. https://doi.org/10.1016/j.euroecorev.2017.02.009
204. Neteler, M., Beaudette, D.E., Cavallini, P., Lami, L. and Cepicky, J. (2008) GRASS GIS. In: Hall, G.B. and Leahy, M.G., Eds., Open Source Approaches in Spatial Data Handling, Vol. 2, Springer, Berlin, Heidelberg, 171-199. https://doi.org/10.1007/978-3-540-74831-1_9

205. Montesinos, S. and Fernández, L. (2012) Introduction to ILWIS GIS Tool. In: Erena, M., López-Francos, A., Montesinos, S. and Berthoumieu, J-.P., Eds., Options Méditerranéennes, No. 67, 47-52. http://om.ciheam.org/om/pdf/b67/00006595.pdf
206. Camara, G., Vinhas, L., Ferreira, K.R., de Queiroz, G.R., de Souza, R.C.M., Monteiro, A.M.V., de Carvalho, M.T., Casanova, M.A. and de Freitas, U.M. (2008) TerraLib: An Open Source GIS Library for Large-scale Environmental and Socio-economic Applications. In: Hall G.B., Ed., Open Source Approaches to Spatial Data Handling, Vol. 2, Springer, Berlin, Heidelberg, 247-270. https://doi.org/10.1007/978-3-540-74831-1_12
207. Olaya, V. (2004) A Gentle Introduction to SAGA GIS. 1.1 Edition, Olaya Victor and Pineda Javier Editors., Madrid, Spain.
208. Nanni, A., Descovi Filho, L., Virtuoso, M.A., Montenegro, D., Willrich, G., Machado, P.H., Sperb, R., Dantas, G.S. and Calazans, Y. (2012) Quantum GIS Guia do Usuário, Versao 1.7.4 'Wroclaw' (Available in). http://qgisbrasil.org
209. Moutahir, H. and Agazzi, V. (2012). The gvSIG Project. International Conference of GIS Users, Taza, 23-24 May 2012, 1-6.
210. dos Santos, A.R., Machado, T. and Saito, N.S. (2010) Spring 5.1.2 passo a passo: Aplicações práticas. CAUFES, Alegre. http://www.mundogeomatica.com.br/Livros/Livro_Spring_5.1.2_Aplicacoes_Pratic%20as/LivroSPRING512PassoaPassoAplicacaoPratica.pdf
211. Eastman, J.R. (2003) IDRISI Kilimanjaro Guide to GIS and Image Processing. Clark Labs Editor, Worcester, MA. https://www.academia.edu/24202322/IDRISI_Kilimanjaro_Guide_to_GIS_and_Image_Processing
212. Hexagon (2020) ERDAS IMAGINE 2020 Update 1. Hexagon, Stockholm. https://bynder.hexagon.com/m/4cce2965b2270e54/original/Hexagon_GSP_ERDAS_IMAGINE_2020_Release_Guide.pdf
213. Exelis Visual Information Solutions (2009) Getting Started in ENVI. Boulder, Colorado: Exelis Visual Information Solutions.
214. Earth Resource Mapping (1998, November) Customizing ER Mapper. ed. E.R.P.L. Mapping.
215. Hoja, D., Schneider, M., Müller, R., Lehner, M. and Reinartz, P. (2008) Comparison of Orthorectification Methods Suitable for Rapid Mapping Using Direct Georeferencing and RPC for Optical Satellite Data. The International Archives of the Photogrammetry, Remote Sensing and Spatial Information Sciences, 37, 1617-1624.
216. Esri (2004) What Is ArcGIS? Esri, Redlands.
217. Gómez, C., White, J.C. and Wulder, M.A. (2016) Optical Remotely Sensed Time Series Data for Land Cover Classification: A Review. ISPRS Journal of Photogrammetry and Remote Sensing, 116, 55-72. https://doi.org/10.1016/j.isprsjprs.2016.03.008
218. Briassoulis, H. (2007) Land-Use Policy and Planning, Theorizing, and Modeling: Lost in Translation, Found in Complexity? Environment and Planning B: Urban Analytics and City Science, 35, 16-33. https://doi.org/10.1068/b32166
219. Nedd, R., Light, K., Owens, M., James, N., Johnson, E. and Anandhi, A. (2021) A Synthesis of Land Use/Land Cover Studies: Definitions, Classification Systems, Meta-Studies, Challenges and Knowledge Gaps on a Global Landscape. Land, 10, Article No. 994. https://doi.org/10.3390/land10090994
220. Rogan, J. and Chen, D.M. (2004) Remote Sensing Technology for Mapping and Monitoring Land-Cover and Land-Use Change. Progress in Planning, 61, 301-325. https://doi.org/10.1016/S0305-9006(03)00066-7
221. Duverger, S. (2015) Metodologia para a criação de mapas temáticos de super-resolução com base em informações subpixel: Um estudo de caso na APA do Pratigi-BA. MSc. Dissertation, Universidade Estadual de Feira de Santana, Feira de Santana. https://s3.amazonaws.com/ppgm.uefs.br/soltan_final.pdf
222. Du, P., Liu, S., Liu, P., Tan, K. and Cheng, L. (2014) Sub-Pixel Change Detection for Urban Land-Cover Analysis via Multi-Temporal Remote Sensing Images. Geo-Spatial Information Science, 17, 26-38. https://doi.org/10.1080/10095020.2014.889268

223. Farda, N.M. (2017) Multi-Temporal Land Use Mapping of Coastal Wetlands Area using Machine Learning in Google Earth Engine. IOP Conference Series: Earth and Environmental Science, 98, Article ID: 012042. https://doi.org/10.1088/1755-1315/98/1/012042
224. Zanotta, D.C., Ferreira, M.P. and Zortea, M. (2019) Processamento de imagens de satélite. 1st Edition, O. de Textos, Sao Paulo.
225. Pena, J.M., Gutiérrez, P.A., Hervás-Martínez, C., Six, J., Plant, R.E. and López-Granados, F. (2014) Object-Based Image Classification of Summer Crops with Machine Learning Methods. Remote Sensing, 6, 5019-5041. https://doi.org/10.3390/rs6065019
226. Phiri, D. and Morgenroth, J. (2017) Developments in Landsat Land Cover Classification Methods: A Review. Remote Sensing, 9, Article No. 967. https://doi.org/10.3390/rs9090967
227. Mastella, A.F. and Vieira, C.A. (2018) Acurácia temática para classificação de imagens utilizando abordagens por pixel e por objetos. Revista Brasileira de Cartografia, 70, 1618-1643. https://doi.org/10.14393/rbcv70n5-44559
228. Cui, B., Cui, J., Hao, S., Guo, N. and Lu, Y. (2020) Spectral-Spatial Hyperspectral Image Classification Based on Superpixel and Multi-Classifier Fusion. International Journal of Remote Sensing, 41, 6157-6182. https://doi.org/10.1080
229. Xiong, J., Thenkabail, P.S., Tilton, J.C., Gumma, M.K., Teluguntla, P., Oliphant, A., Congalton, R.G., Yadav, K. and Gorelick, N. (2017) Nominal 30-m Cropland Extent Map of Continental Africa by Integrating Pixel-Based and Object-Based Algorithms Using Sentinel-2 and Landsat-8 Data on Google Earth Engine. Remote Sensing, 9, Article No. 1065. DOI: 10.3390/rs9101065.
230. Degerickx, J., Roberts, D.A. and Somers, B. (2019) Remote Sensing of Environment Enhancing the Performance of Multiple Endmember Spectral Mixture Analysis (MESMA) for Urban Land Cover Mapping Using Airborne Lidar Data and Band Selection. Remote Sensing of Environment, 221, 260-273. DOI: 10.1016/j.rse.2018.11.026.
231. Zhu, C., Zhang, X. and Huang, Q. (2019) Mapping Fractional Cropland Covers in Brazil through Integrating LSMA and SDI Techniques Applied to MODIS Imagery. International Journal of Agricultural and Biological Engineering, 12, 192-200. DOI: 10.25165/j.ijabe.20191201.4419.
232. Ackom, E.K., Amaning, K., Samuel, A. and Odai, N. (2020) Monitoring Land-Use and Land-Cover Changes Due to Extensive Urbanization in the Odaw River Basin of Accra, Ghana, 1991-2030. Modeling Earth Systems and Environment, 6, 1131-1143. DOI: 10.1007/s40808-020-00746-5.
233. Mohammady, M., Moradi, H.R., Zeinivand, H. and Temme, A.J.A.M. (2015) A Comparison of Supervised, Unsupervised and Synthetic Land Use Classification Methods in the North of Iran. International Journal of Environmental Science and Technology 12, 1515-1526. DOI: 10.1007/s13762-014-0728-3.
234. Nguyen, H.T.T., Doan, T.M., Tomppo, E. and McRoberts, R.E. (2020) Land Use/Land Cover Mapping Using Multitemporal Sentinel-2 Imagery and Four Classification Methods—A Case Study from Dak Nong, Vietnam. Remote Sensing, 12, Article No. 1367. DOI: 10.3390/rs12091367.
235. Rana, V.K. and Suryanarayana, T.M.V. (2020) Performance Evaluation of MLE, RF and SVM Classification Algorithms for Watershed Scale Land Use/Land Cover Mapping Using Sentinel 2 Bands. Remote Sensing Applications: Society and Environment, 19, Article ID: 100351. DOI: 10.1016/j.rsase.2020.100351.
236. Rajalakshmi, K., Murugan, D. and Ganesh Kumar, T. (2013) Supervised Methods for Land Use Classification. International Journal of Research in Information Technology, 1, 64-73. DOI: Not available.
237. Kaya, I.A. and Gorgün, E.K. (2020) Land Use and Land Cover Change in Tuticorin Coast Using Remote Sensing and Geographic Information System Land Use and Land Cover Change in Tuticorin Coast Using Remote Sensing and Geographic Information System. Environmental Monitoring and Assessment, 192, Article No.430. DOI: 10.1007/s10661-020-08411-1.
238. Gedefaw, A.A., Atzberger, C., Bauer, T., Agegnehu, S.K. and Mansberger, R. (2020) Analysis of Land Cover Change Detection in Gozamin District, Ethiopia: From Remote Sensing and DPSIR Perspectives. Sustainability, 12, Article No.4534. DOI: 10.3390/su12114534.

239. Kovyazin, V.F., Demidova, P.M., Lan Anh, D.T., Hung, D.V. and Quyet, N.Van. (2020) Monitoring of Forest Land Cover Change in Binh Chau-Phuoc Buu Nature Reserve in Vietnam Using Remote Sensing Methods and GIS techniques. IOP Conference Series: Earth and Environmental Science, 507, Article ID: 012014. DOI: 10.1088/1755-1315/507/1/012014.
240. Chethan, K.S., Sinchana, G.S. and Choodarathnakara, A.L. (2020) Classification of Homogeneous Sites Using IRS-P5 Satellite Imagery. International Conference on Computation, Automation and Knowledge Management (ICCAKM), Dubai, 9-10 January 2020, 184-189. DOI: 10.1109/ICCAKM46823.2020.9051510.
241. Hame, T., Sirro, L., Kilpi, J., Seitsonen, L., Andersson, K. and Melkas, T. (2020) A Hierarchical Clustering Method for Land Cover Change Detection and Identification. Remote Sensing, 12, Article No. 1751. DOI: 10.3390/rs12111751.
242. Brinkhoff, J., Vardanega, J. and Robson, A.J. (2020) Land Cover Classification of Nine Perennial Crops Using Sentinel-1 and -2 Data. Remote Sensing, 12, Article No.96. DOI: 10.3390/rs12010096.
243. Kumar, J., Biswas, B. and Walker, S. (2020) Multi-Temporal LULC Classification Using Hybrid Approach and Monitoring Built-up Growth with Shannon's Entropy for a Semi-Arid Region of Rajasthan, India. Journal of the Geological Society of India, 95, 626-635. DOI: 10.1007/s12594-020-1489-x.
244. Sharma, C.S., Behera, M.D., Mishra, A. and Panda, S.N. (2011) Assessing Flood Induced Land-Cover Changes Using Remote Sensing and Fuzzy Approach in Eastern Gujarat (India). Water Resources Management, 25, Article No. 3219. DOI: 10.1007/s11269-011-9853-7.
245. Zhang, Y., Du, Y., Li, X., Fang, S. and Ling, F. (2014) Unsupervised Subpixel Mapping of Remotely Sensed Imagery Based on Fuzzy C-Means Clustering Approach. IEEE Geoscience and Remote Sensing Letters, 11, 1024-1028. DOI: 10.1109/LGRS.2013.2285404.
246. Samal, D.R. and Gedam, S.S. (2015) Monitoring Land Use Changes Associated with Urbanization: An Object Based Image Analysis Approach. European Journal of Remote Sensing, 48, 85-99.
https://doi.org/10.5721/EuJRS20154806

3. Methodology

Overview of the coregisteration method

eFolki stands as an efficient and resilient technique for estimating optical flow, drawing its methodology from the gradient-based Lucas–Kanade (LK) method [1]. The inception of the eFolki [2] algorithm is firmly anchored in the FOLKI optical-flow estimator, a creation within the field of computer vision [3]. Its versatility is evident through its widespread utilization across various domains, notably in particle imaging velocimetry [4], particularly within the context of wind tunnels' fluid velocimetry. In these settings, the algorithm demonstrates its capacity to process vast datasets with both high precision and scalability.

The structure of eFolki is notably straightforward and amenable to parallelization, rendering it an optimal choice for deployment on massively parallel computing architectures, especially when tasked with managing large-scale images. The computational complexity and execution time of eFolki are directly proportional to the quantity of pixels present. Consequently, its practical implementation enables computations to be conducted at a rate of 6 ms per megapixel, maintaining a linear relationship with pixel count. To illustrate, processing all pixels in an image sized at 10,000 × 10,000 can be accomplished in a mere 600 ms when utilizing a Titan GPU.**A.**

Description of the Algorithm

To provide a straightforward explanation, we initiate our discussion by detailing the FOLKI optical flow method, followed by an introduction to the modifications made in the eFolki algorithm. We conclude with an analysis of the principal parameters associated with these algorithms, particularly emphasizing their significance when applied to optical images. For an in-depth exploration and justification of the various components of the eFolki algorithm, readers are directed to reference [2].

Consider the task of aligning two images, denoted as ($I1$) and ($I2$), which are situated on a two-dimensional plane (S) within the real number space (R^2). In optical terminology, the dense optical flow represents the requisite shift needed to align the two images. This shift is mathematically expressed as ($u: x \to u(x) \in R^2$). The Lucas-Kanade (LK) algorithm, a member of the local or window-based category of methods, determines ($u(x)$)as the value that minimizes a specific criterion calculated across a localized window centered at (x):

$$J(u;x) = \sum_{x' \in S} \omega(x' - x) \left(I1(x') - I2\big(x' + u(x)\big) \right)^2 \quad (1)$$

Here, (ω) denotes a separable weighting function, which can either be uniform or Gaussian, and is confined to a limited support (ω). Typically, (ω) is represented as a square window of dimensions ($(2r + 1) \times (2r + 1)$), with (r) being the parameter that determines the radius of the window.

The minimization process is executed using an iterative Gauss–Newton method, which incorporates a first-order Taylor expansion to approximate the image intensity variations around a previously estimated displacement, denoted as (u_k).This approach categorizes the Lucas-Kanade (LK) algorithm as gradient-based, distinguishing it from block matching techniques that perform exhaustive searches within confined regions. Furthermore,

contemporary iterations of the LK algorithm employ a multiresolution strategy, utilizing a pyramid of images to calculate (u) at different scales, adhering to a coarse-to-fine methodology.

In the context of the eFolki algorithm, two primary modifications are introduced. Firstly, the cost function (1) is altered to:

$$J(u;x) = \sum_{x' \in S} \omega(x' - x) \left(R(I_1)(x') - R(I_2)\big(x' + u(x)\big) \right)^2 \quad (2)$$

In this revised equation, $(R(I))$represents a rank function applied to image (I). This function determines the filtered value based on the local ordering of gray levels. The rank function is mathematically expressed as:

$$R(I)(x) = \#\{x' : x' \in S_R(x) \text{ with } |I(x)| > |I(x')|\} \quad (3)$$

Here, $(S_R(x))$denotes the neighborhood surrounding pixel (x). Through these modifications, eFolki introduces a novel approach to optical flow estimation, enhancing the robustness and accuracy of the process.

The rank transform imparts a nonlinear filtering effect, significantly condensing the dynamics of the signal. In practical terms, this transformation reduces a float signal with 232 levels to a signal possessing $(d^2 - 1)$levels, where (d) is the diameter of the rank filter window. This compression of the signal's gradient serves to enhance the robustness of motion estimation. It also facilitates the computation of motion between optical images that are relatively dissimilar.

The second major adjustment within the eFolki algorithm pertains to the adaptive resizing of the windows (ω), following a coarse-to-fine approach during the iterative phase at each level of multiscale resolution. This particular modification is necessitated by the use of a dyadic pyramid in the multiscale solving process. For instances of large motion, it becomes crucial to smoothly transition between different scales to ensure proper convergence of the algorithm.

For the optimal application of eFolki to optical images, it is imperative to carefully select and adjust four key parameters:

1. The weighting function (w);
2. The radius (r) of the window.
3. (K), representing the number of iterations at each pyramid level.
4. (J) , denoting the total number of levels in the pyramid.

These adjustments are crucial to tailor the algorithm for effective and accurate motion estimation within optical imagery.

The performance of coregistration can be effectively evaluated using a metric known as the forward–backward criterion [5]. This process entails calculating the displacement from image 1 to image 2, and subsequently from image 2 back to image 1, to derive the residual displacement, termed as the forward–backward flow. Ideally, this cumulative displacement should equate to zero. Consequently, the forward–backward error serves as a reliable measure of the accuracy of the estimated displacement, even in the absence of ground truth data.

This criterion proves instrumental in identifying the most appropriate window radius, (r). Empirical testing has revealed that larger window radii tend to yield superior results. While this may initially seem counterintuitive, it is primarily attributed to the fact that a broader window facilitates a smoother estimation of motion, as depicted in Fig. 2. In this illustration, displacement profiles are computed for various radii to align a pair of images, with an artificial 9-pixel shift introduced at pixel number 1750 in one of the images. Typically, for optical images with relatively straightforward displacement patterns, achieving the smoothest possible spatial function is advantageous. This, in turn, enhances the effectiveness of the forward–backward criterion, particularly when estimating displacement in both directions, from image 1 to image 2 and vice versa. This trend may also be influenced by the reduced susceptibility to speckle effects when utilizing larger window sizes.

Parallel testing conducted on the number of iterations yielded insights that deviate from those observed in optical imaging scenarios. Optimal results were attained with a limited number of iterations. Excessive iteration tends to make the function (u) overly conform to the data, attempting to discern details at higher frequencies, which ultimately proves detrimental to the criterion's effectiveness in assessing coregistration performance.

Data pre-processing

Our study utilized Level 2D sceneries from the PRISMA hyperspectral satellite, each containing 239 spectral bands across wavelengths of 402 to 2497 nm. With a 30-meter resolution, they are orthorectified to correct terrain distortions and atmospherically corrected to minimize environmental noise. The data is available in the efficient HDF5 format, which supports complex datasets and simplifies spectral data handling for analysis.

PRISMA
PRS_L2D_STD_20220818034527_20220818034531
PRS_L2D_STD_20211107034543_20211107034547
PRS_L2D_STD_20220326034528_20220326034533
PRS_L2D_STD_20221113034523_20221113034527
PRS_L2D_STD_20230208034531_20230208034535
PRS_L2D_STD_20200308034830_20200308034834

Table 3.1 PRISMA data we used for the co-registration process.

The EnMap Box plug-in for QGIS, developed under the EnMAP preparatory science program, was employed to process PRISMA hyperspectral imagery. This tool is equipped with functionalities for basic image processing and visualization, alongside sophisticated methods for image analysis applicable across diverse research domains [6]. Initially, the plug-in was utilized to transform the PRISMA scenes into geolocated files in the Geotiff format, a widely used standard in geospatial analysis that facilitates further processing and compatibility with various GIS software. Subsequently, for each pixel within our area of interest, we applied a specific equation [7] to translate the Digital Number (DN) values into actual reflectance measures. This step is crucial for accurate remote sensing analysis. The formula utilized is as follows:

$$\text{Reflectance} = L2Scale_{\text{Min}} + \left(\text{DN} \times \frac{L2Scale_{\text{Max}} - L2Scale_{\text{Min}}}{65535}\right)$$

Here, "XXX" denotes the specific dataset under consideration, which could be the panchromatic "PAN", the visible and near-infrared "VNIR", or the short-wave infrared "SWIR" bands. which is 0 for $L2Scale_{\text{Min}}$ and 1 for $L2Scale_{\text{Max}}$ according to the PRISMA product specification. This normalization is critical in adjusting for sensor-specific variances and the range of values captured by the sensor's 16-bit format.

Complementing the PRISMA data, Sentinel-2A Level 2A (L2A) scenes, accessible from the Copernicus Open Access Hub, were acquired for the identical study areas to assist in image co-registration. The Sentinel-2 scenes, captured via the Multi-Spectral Instrument (MSI), have a substantial coverage area of 100 x 100 km and include 13 spectral bands. These bands provide a multi-resolution view of the surface with spatial resolutions of 10, 20, and 60 meters, catering to various wavelengths ranging from 440 to 2190 nm. To ensure the highest quality of data, we selected scenes with minimal cloud interference, specifically those with cloud cover below 5%. Additionally, to maintain consistency with the PRISMA data, these Sentinel-2 scenes underwent both orthorectification and atmospheric correction processes, thereby standardizing the datasets and ensuring an accurate and reliable comparison for co-registration tasks.

Sentinel 2 Data	cloud cover
L2A_T48QVJ_ 2022_11_29	5.8
L2A_T48QVJ_ 2021_11_29	2.8
L2A_T48QVJ_ 2022_04_03	0.6
L2A_T48QVJ_ 2022_12_19	0.00
L2A_T48QVJ_ 2023_02_27	0.15
L2A_T48QVK_2020_03_09	0.04

Table 3.2.Sentinel 2 data we used for the co-registration process.

To maintain the integrity of the spectral information while aligning the spatial resolution of the Sentinel-2 datasets with that of the PRISMA tiles, which have a resolution of 30 x 30 meters, we employed the bicubic interpolation method. This approach is particularly adept at preserving the intensity values of each pixel during the resampling process, minimizing the loss of image quality. Bicubic interpolation, a more sophisticated technique than nearest

neighbor or bilinear interpolation, uses the values of surrounding pixels to calculate the new value of a pixel in a way that smoothly transitions from one pixel to another, which is crucial when detailed spectral information is needed for precise environmental analysis.

For the Sentinel-2 optical data, we applied a simple conversion to change the Digital Number (DN) values into reflectance measurements. Reflectance is often used in remote sensing because it directly relates to the characteristics of the surfaces being observed. This conversion is a standard step in preparing the data, making sure that Sentinel-2's information matches well with other types of data and is easier to work with. The formula we used for this conversion is basic but essential to make sure our data is consistent and can be compared with information from other sensors:

$$\mathrm{DN} = 10000 \times \mathrm{Reflectance}$$

Table 3 illustrates our approach to coregistering various bands and red band combinations from PRISMA data with the red band of Sentinel-2 imagery. We chose to downsample the Sentinel-2 data to match PRISMA's spatial resolution. This decision was made because upscaling PRISMA to Sentinel-2's resolution would unnecessarily extend computational time without enhancing performance, as there is no additional detail to be gained below the 30 x 30 m resolution of PRISMA.

PRISMA bands
Red
Blue
Green
Red bands (655.41876 ,664.9841, 674.46436, 684.13727) nm combined with max operator
Red bands (655.41876 ,664.9841, 674.46436, 684.13727) nm combined with sum operator
Red bands (655.41876 ,664.9841, 674.46436, 684.13727) nm combined with average operator

Table 3.3. PRISMA bands used for the coregisteration

Coregistration

Figure 1 presents the images prior to the registration process. Upon visual inspection, it is evident that the two images are misaligned, as indicated by the non-coinciding green and white lines, which should ideally overlap if the images were correctly registered. To address this misalignment, we employed the 'gefolki' Python code [8] to perform the co-registration. In this process, we designated the PRISMA scene as the slave image, referred to as ($I2$), and the Sentinel-2 image as the master image, denoted as ($I1$). The choice of Sentinel-2 as the master image was based on its broader spectral coverage and higher temporal resolution, which provides a stable reference framework for the registration. By applying the co-registration algorithm, we aimed to correct spatial discrepancies and achieve a precise overlay of the images, which is critical for subsequent analyses that require accurate pixel-to-pixel correspondence between the datasets.

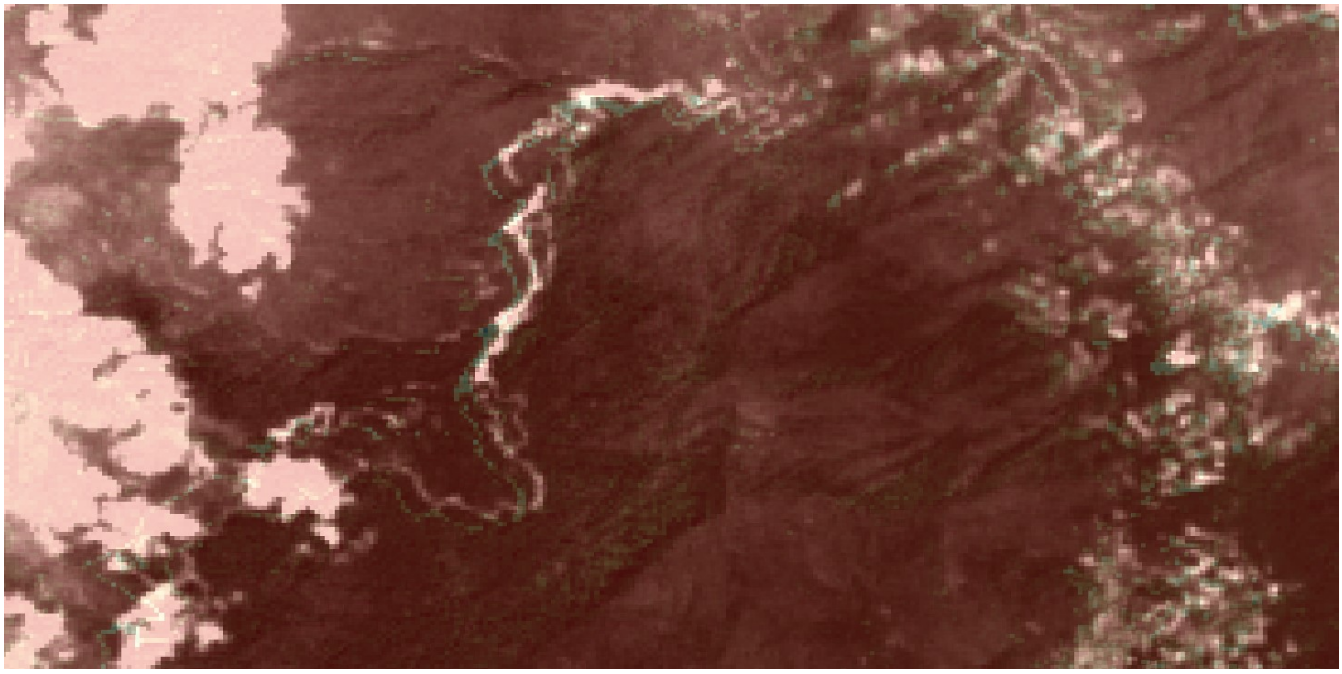

Figure 3.1Images before the co-registration

In the absence of Ground Control Points (GCPs) for our study area, which are often crucial for ensuring precise image alignment, we employed the parameter values specified in Table 3, we proceeded with the coregistration, wherein we assigned the weighting function a value of one. This decision was made under the premise that no single pixel holds greater significance over another within the scope of our analysis, ensuring uniformity in the treatment of each pixel during the process, thus promoting a uniform and unbiased registration.

Parameters	*Values*
r	*512,280,128,100,64*
j	*8,4,3,2*
k	*8,6,4*
R	*4*

Table 3.1 Gefolki parameters used for the coregisteration of PRISMA with Sentinal2 images.

From the experiments we did, we employed the same parameters for the co-registertion of the six PRISMA images the figures below show the images before and after coregisteration. The results of this co-registration are effectively demonstrated in Figure 2. This figure distinctly confirms the success of the co-registration, as it shows the green and white lines now perfectly coinciding, indicating accurate alignment of the images post-registration.

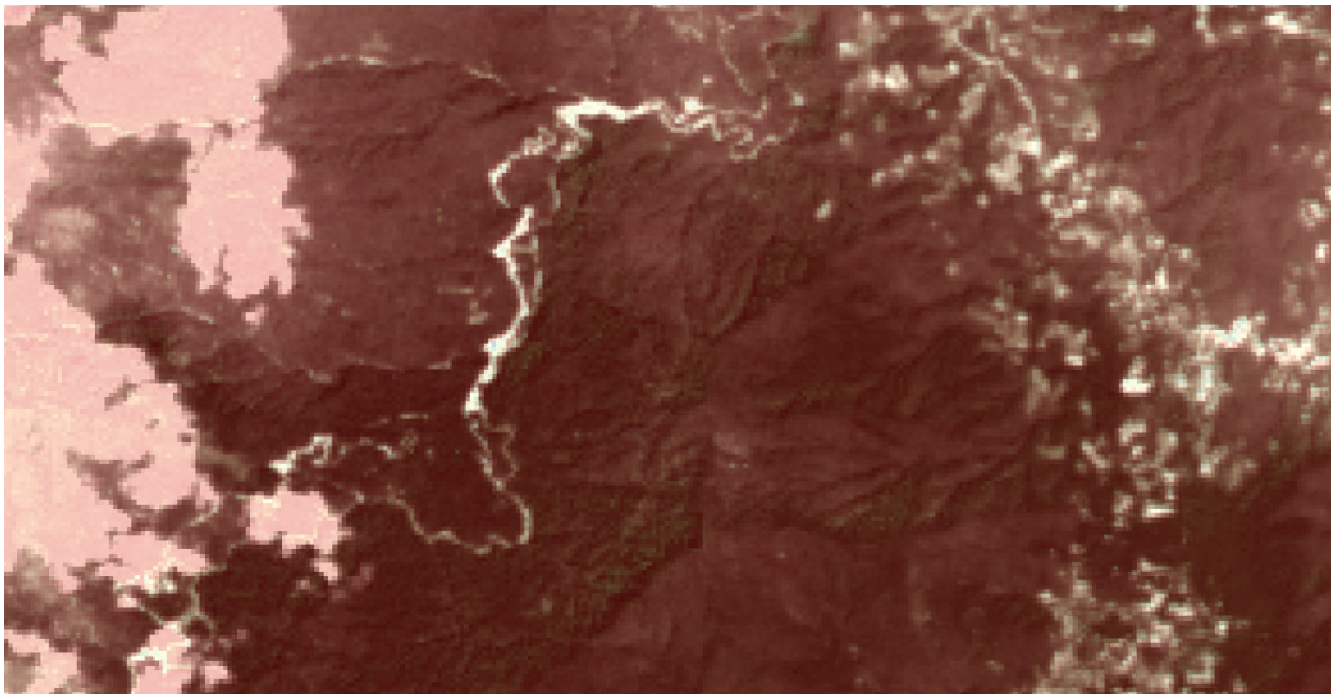

Figure 3.2 After the co-registration

Performance assessment

To evaluate the efficacy of our co-registration process, we implemented the forward-backward criterion, as outlined in [9]. This technique calculates the displacement from the first image to the second and then reverses the process. A key indicator of successful co-registration is that the total calculated movement approaches zero, implying that the images are accurately aligned. The forward-backward error thus becomes a vital quantitative measure of the co-registration's precision, especially useful in the absence of ground truth data for direct comparison.

The significance of this criterion lies in its ability to provide a numerical assessment of the co-registration's quality. It is particularly adept at uncovering subtle alignment issues that might not be immediately apparent through mere visual inspection of the images. By analyzing the forward-backward error, we gain a deeper understanding of the alignment accuracy, ensuring the co-registration meets the necessary standards for any subsequent analysis's dependent on the precise alignment of these images.

Figure 6 further complements this approach by visually depicting the error distribution resultant from the registration process. This graphical representation serves as an additional tool to evaluate and confirm the co-registration's reliability. A minimal error in this distribution is indicative of a high degree of precision in the alignment of the images, which is crucial for the integrity of any further applications or studies utilizing these co-registered images.

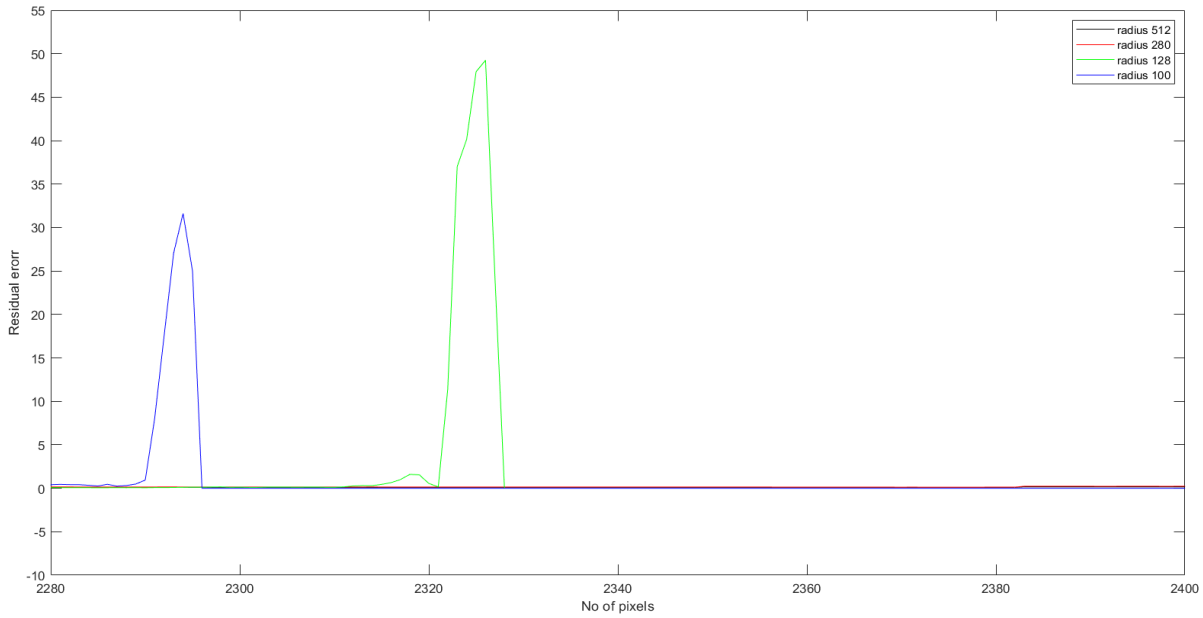

Figure 3.1 The residual error of the coregisteration using different radii.

The ideal window radius r can be determined using this criterion. As shown in Fig. 3, the displacement profiles were calculated for a variety of window radii in order to coregister our pair of images. At that point, estimating the displacement in both directions, from 1 to 2 and from 2 to 1, becomes advantageous for the criterion. This may seem counterintuitive, but it is mainly because the estimated motion is smoother when the window is wider. as shown in fig. 4,5 the histogram of the residual error for small and large window radius, it's also possible that these trends are caused by the facet's small windows will adapt to small-scale motion. Causing some confusion and lead to distortion in the output registered images as we examined in our experiments.

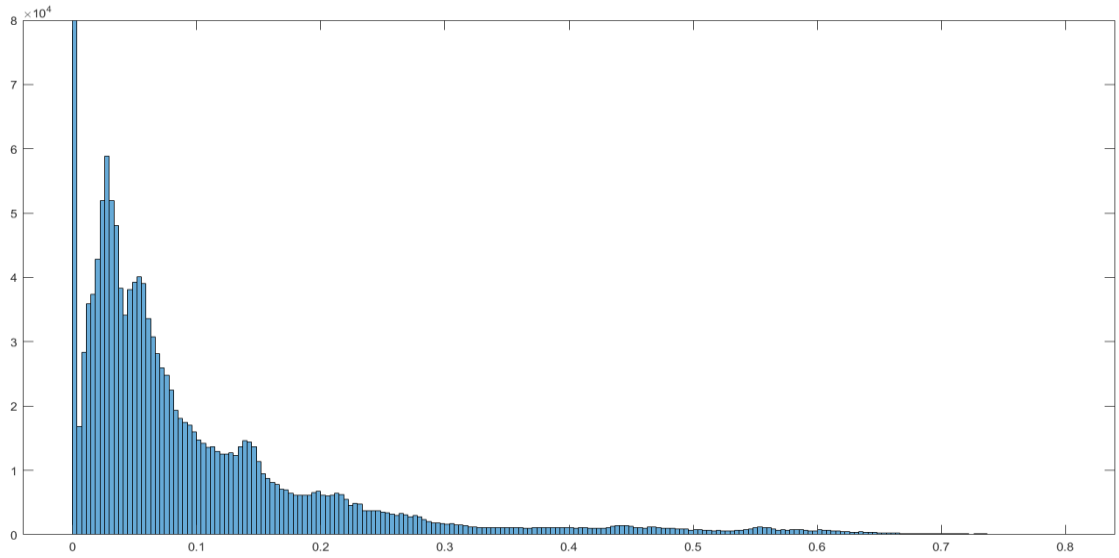

Figure 3.2 The histogram of the residual error using 100 pixels radius.

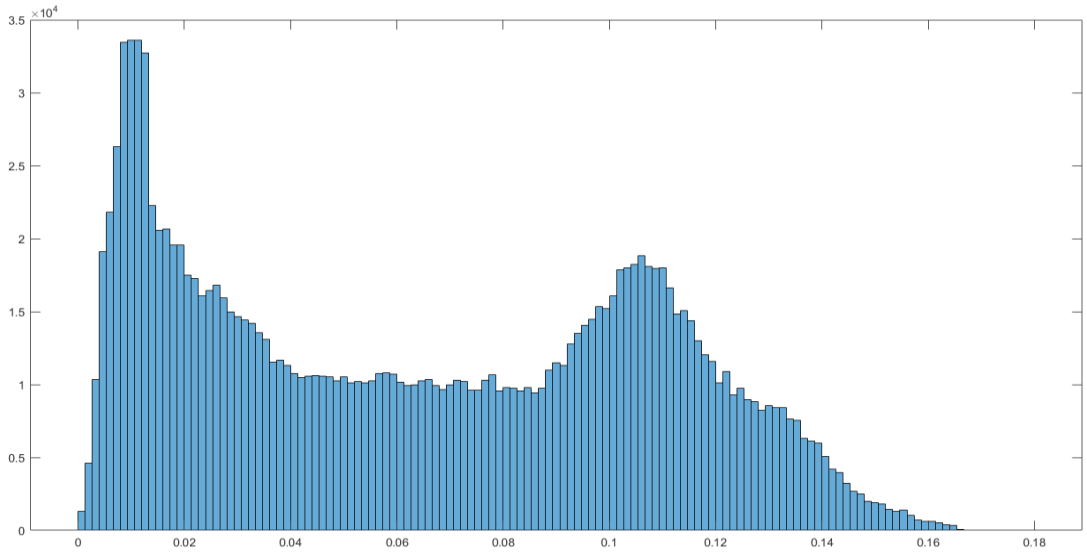

Figure 3.3 The histogram of the residual error using 512 pixels radius.

For the number of iterations, the same tests were run. Again, a higher number of iterations yields the best results. The registration has not been initialized by homologous points, so as we iterate more, we have new initial values with different starting points. As a result, the criterion avoids the local minimum, which is good for our final criterion. The higher the level of the pyramid, the worse the result, it has been demonstrated through testing that results stabilize at levels 4 and below, which is in accordance with the algorithm's manual that the level should be the smallest but greater than the maximum displacement to be estimated. Our results show a mean error of 0.065 pixels, and Figure 4 shows the spatial distribution of the residual error which lies between 0.02 pixels and never exceeds 0.18 pixels. The RMSE of the coregistration obtained is 2.31 m (0.0777 pixels) which is in The RMSE ranges between 2.3 m and 5.8 m of coregistration of optics in the literature [23].

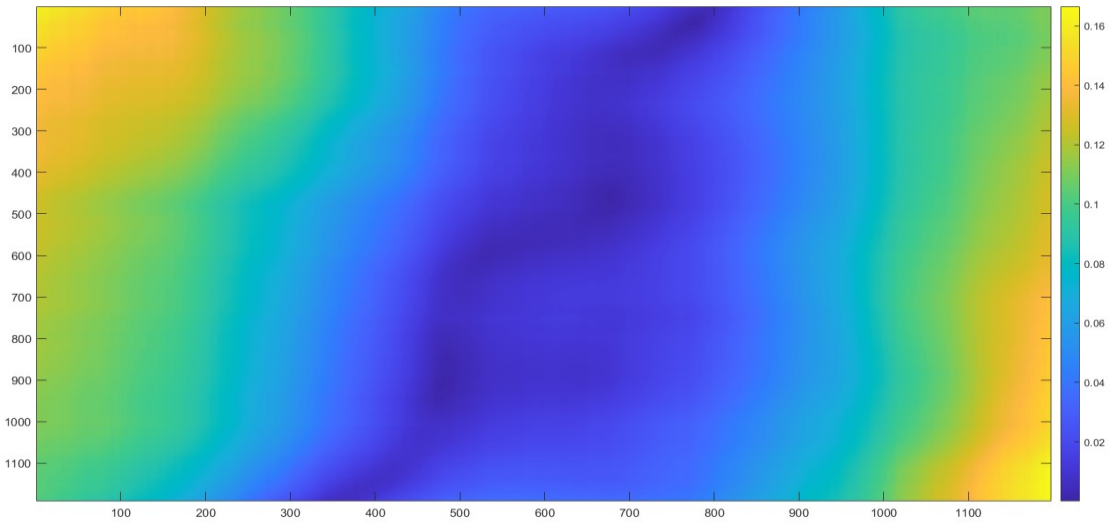

Figure 3.4 The spatial distribution of the norm of the residual error

Data preprocessing for landcover classification

In the preprocessing stage of our analysis, a critical step was addressing the quality of the PRISMA imagery, specifically the spectral bands characterized by a low signal-to-noise ratio (SNR). Bands with poor SNR can significantly impair the performance of classification models by introducing noise that may be misconstrued as meaningful data. To mitigate this issue and enhance the robustness of subsequent analyses, such bands must be carefully identified and excluded from the dataset.

The selection of bands for removal is not a one-size-fits-all procedure but rather a tailored approach that must consider the unique spectral characteristics of the study area and the specific classification objectives. For example, bands that may be irrelevant or counterproductive for distinguishing certain land cover classes could be vital for others. Therefore, the identification of bands to be excluded demands a thorough review of the spectral signatures pertinent to the desired classification outcomes.

In our research, we carefully reviewed the PRISMA data to identify any spectral bands that might negatively affect our classification work. Identifying noisy bands usually involves looking at each band's Histogram, a step that's detailed but slow and sometimes misses noisy bands. With the help of EnmapBox's statistical tools, we filtered out bands with unusual histogram patterns, like sharp peaks or skewed distributions as shown in fig 7. The following list details the bands we removed from our analysis due to their unsuitability: [1 to 36, 104 to 112, 147 to 150, 156, 157, 160 to 163, 227 to 233]. By refining our dataset in this manner, we aim to improve the overall effectiveness of our classification efforts.

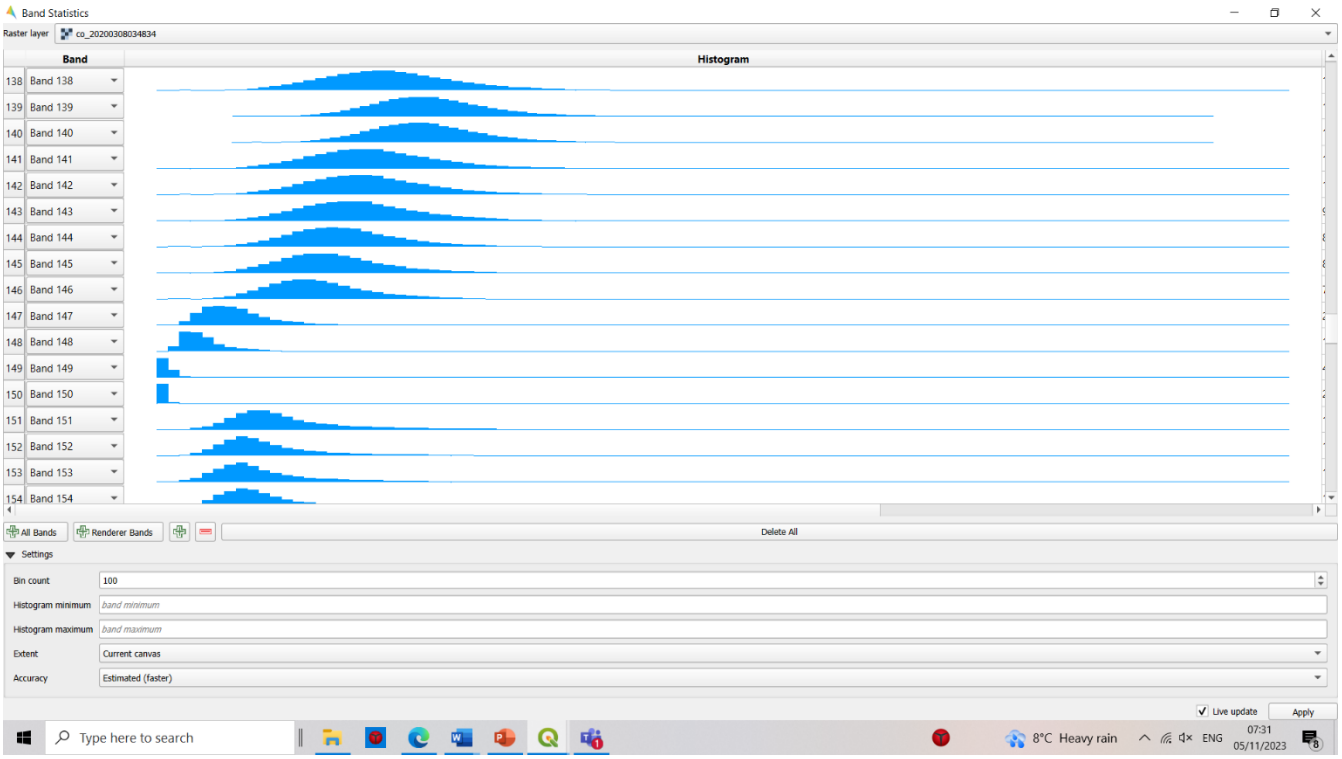

Figure 3.1 The histograms visualization of the PRISMA bands

Dataset creation

Creating an accurate dataset is paramount for any remote sensing classification task. To this end, we turned to the Dynamic World v1 platform within Google Earth Engine, which offers a near-real-time land cover mapping at a resolution of 10 meters. Our intention was to leverage this resource as a surrogate for ground truth, aligning our classification categories with the same number of land cover classes as provided by Dynamic World.

Given the temporal constraints and the necessity for temporal proximity between our PRISMA data and the Dynamic World dataset, we conducted a meticulous search within a specified time window. Our goal was to identify the closest match in terms of date and time to the PRISMA scenes. Although finding an exact temporal correspondence was not feasible, our methodological approach was to minimize the temporal gap, thereby ensuring the highest possible relevance and accuracy of the land cover data in relation to our PRISMA imagery. Fig shows an example of dynamic world images used for the creation of the dataset.

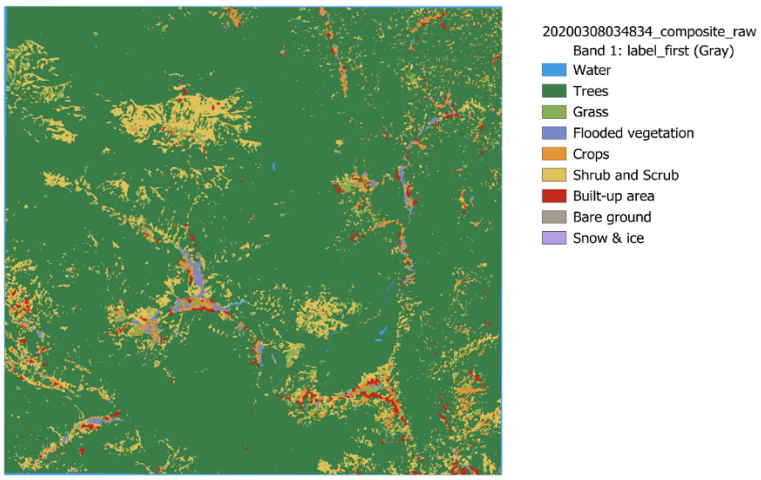

Figure 3.1 Dynamic World V1 (LC) dataset

We acknowledge that even small temporal discrepancies can lead to differences in land cover due to natural dynamics or human activities. Therefore, we paid special attention to the selection process, prioritizing dates that would likely reflect the land cover status as accurately as possible. This careful temporal alignment is critical, as it directly influences the reliability of the land cover data used for training and validating our classification models.

By doing so, we aimed to create a robust dataset that would serve as a solid foundation for our land cover classification, ensuring that our models are trained on the most accurate and representative ground truth data available within the constraints of our project timeline.

Dynamic World v1	Time span
20200308034834_composite_hillshade	01/03/2020 to 10/03/2020
20211107034547_composite_hillshade	07/11/2021 to 17/11/2021
20220326034533_composite_hillshade	01/03/2022 to 10/03/2022
20220818034531_composite_hillshade	18/08/2022 to 31/08/2022
20221113034527_composite_hillshade	03/11/2022 to 13/11/2022
20230208034535_composite_hillshade	08/02/2023 to 13/02/2023

Table 3.1 The dynamic world v1 data

To create a feature vector from Dynamic World scenes, we initially employed the ACATAMA plugin in QGIS for the sampling design. However, the ACATAMA plugin tended to overlook the less represented classes. As a result, we manually added samples for these underrepresented classes using the Semi-Automatic Classification Plugin (SCP).

Our goal was to outline nine different land cover classes. We worked directly with the raw Dynamic World data, without making any changes like overlaying or adjusting transparency.

In our first dataset, which we initially created, we collected 20 samples for most classes, except for the snow and ice class, where we had 18 samples. This dataset was imbalanced, meaning that it had varying numbers of samples for each land cover class, with some classes having more samples than others.

Subsequently, recognizing the importance of balance for training and evaluating our classification model, we created a second dataset. In this second dataset, we balanced the number of samples for each class by undersampling, ensuring that each land cover class had an equal representation of 15 samples. This balanced dataset allowed us to improve the fairness and accuracy of our classification model.

Additionally, we collected 5 samples from each class to create a separate test dataset. This test dataset served as an independent evaluation set to assess the performance of our land cover classification model.

We carefully drew polygons to represent each land cover class based on what we saw in the original Dynamic World data. This ensured that our vector features accurately reflected the real-world characteristics captured by the Dynamic World sensor.

The result was a set of precisely defined polygons that accurately represented how the nine land cover classes were distributed in our study area, using the original Dynamic World data. These polygon datasets, including the imbalanced initial dataset, the balanced second dataset, and the test dataset, played crucial roles in training, validating, and assessing the accuracy of our land cover classification model.

Classification model and its assessment

In our land cover classification process, we used the Dzetsaka plugin within QGIS to work with the datasets derived from Dynamic World V1 raw data. Initially, we employed both the Random Forest (RF) and Support Vector Machine (SVM) algorithms to classify the first, imbalanced dataset.

The RF algorithm constructs multiple decision trees during training and outputs the class that is most frequently predicted. SVM, on the other hand, is known for its powerful classification capabilities and outperformed the RF model in our specific scenario.

Recognizing SVM's superior performance, we trained and classified the balanced dataset using the SVM algorithm, resulting in classified images displayed in Figure 8, 9, and 10.

During this process, Dzetsaka provided us with confusion matrices for each model. These matrices helped us calculate overall accuracy, as well as user and producer accuracies, which are essential metrics for evaluating the classification performance.

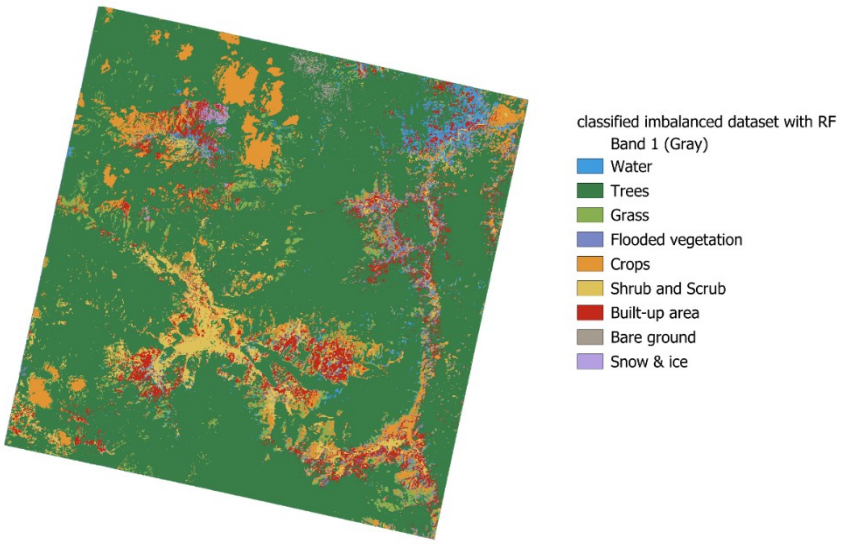

Figure 3.1 Classified PRISMA image using RF with imbalanced dataset.

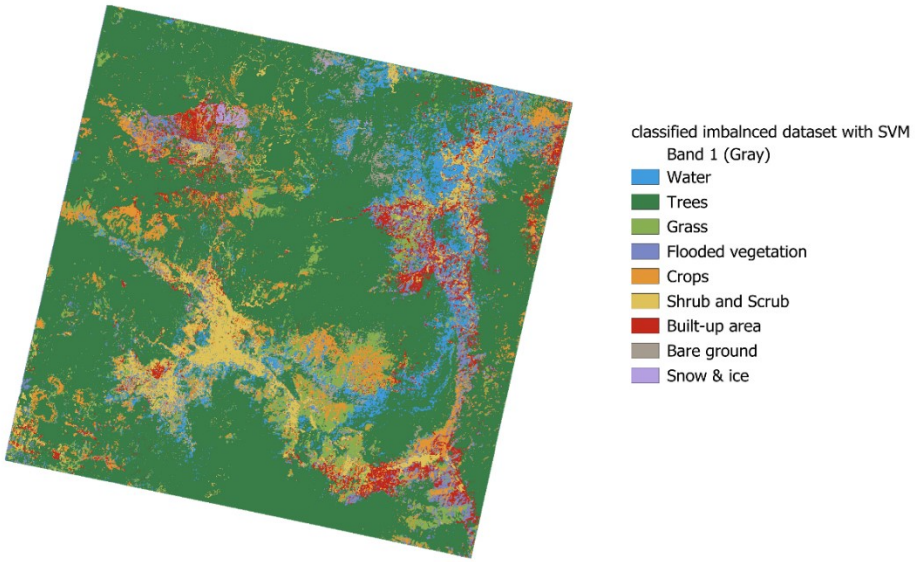

Figure 3.2 Classified PRISMA image using SVM with imbalanced dataset.

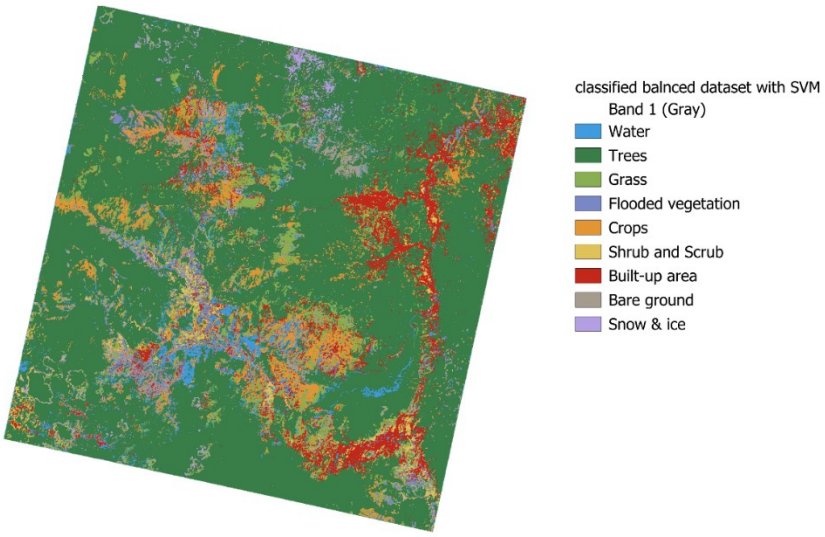

Figure 3.3 Classified PRISMA image using SVM with Balanced dataset.

References

1. B. D. Lucas and T. Kanade, “An iterative image registration technique with an application to stereo vision,” in Proc. IJCAI, 1981, vol. 81, pp. 674–679.
2. A. Plyer, G. Le Besnerais, and F. Champagnat, “Massively parallel Lucas Kanade optical flow for real-time video processing applications,” J. Real-Time Image Process., pp. 1–18, Apr. 2014.
3. G. Le Besnerais and F. Champagnat, “Dense optical flow by iterative local window registration,” in Proc. IEEE ICIP, 2005, vol. 1, pp. 137–140.
4. F. Champagnat et al., “Fast and accurate PIV computation using highly parallel iterative correlation maximization,” Exp. Fluids, vol. 50, no. 4, pp. 1169–1182, Apr. 2011.
5. P. Sand and S. Teller, “Particle video: Long-range motion estimation us ing point trajectories,” Int. J. Comput. Vision, vol. 80, no. 1, pp. 72–91, Oct. 2008.
6. F. Weissgerber, E. Colin-Koeniguer, and F. Janez, “Urban change detec tion by comparing SAR images at different resolutions and polarimetric modes,” in Proc. IEEE 10th EUSAR 2014, Berlin, Germany, Jun. 2014, pp. 1–4.
7. Chabrillat, S; Guanter, L.; Kaufmann, H.; Foerster, S.; Beamish, A.; Brosinsky, A.; Wulf, H.; Asadzadeh, S.; Bochow, M.; Bohn N.; Boesche, N.; Bracher, A.; Brell, M.; Buddenbaum, Cerra, D.; H.; Fischer, S.; Hank, T.; Heiden, U.; Heim, B.; Heldens, W.; Hill, J.; Hollstein, A.; Hostert, P.; Krasemann, H.; LaPorta, L.; Leitão, P.J.; van der Linden, S.; Mauser, W.; Milewski, R.; Mottus, M.; Okujeni, A.; Oppelt, N.; Pinnel, N.; Roessner, S.; Röttgers, R.; Schneiderhan, T.; Schickling, A.; Soppa, M.; Staenz, K.; Segl, K. (2022) EnMAP Science Plan. EnMAP Technical Report, GFZ Data Services. DOI: http://doi.org/10.48440/enmap.2022.001
8. PRISMA Algorithm Theoretical Basis Document (ATBD) Issue 1 Date 14/12/2021
9. SENTINEL-2 MISSION GUIDE
10. Guillaume Brigot, Elise Colin-Koeniguer, Aurélien Plyer, Fabrice Janez, "Adaptation and Evaluation of an Optical Flow Method Applied to Coregistration of Forest Remote Sensing Images", IEEE Journal of Selected Topics in Applied Earth Observations ans Remote Sensing, Volume 9, Issue 7, July 2016
11.P. Sand and S. Teller, “Particle video: Long-range motion estimation using point trajectories,” Int. J. Comput. Vision, vol. 80, no. 1, pp. 72–91, Oct. 2008.

4. Results

Result of the co-registration process

PRS_L2D_STD_20220326034528_20220326034533	RMSE (Pixels)
Red	0.11
Blue	0.29
Green	0.23
Red bands combined with max operator	0.11
Red bands combined with sum operator	0.11
Red bands combined with average operator	0.11

Table 4.1 coregistration result of PRS_L2D_STD_20220326034528_20220326034533

PRS_L2D_STD_20220818034527_20220818034531	RMSE (Pixels)
Red	0.03
Blue	0.56
Green	0.33
Red bands combined with max operator	0.03
Red bands combined with sum operator	0.04
Red bands combined with average operator	0.26

Table 4.2 coregistration result of PRS_L2D_STD_20220818034527_20220818034531

PRS_L2D_STD_20211107034543_20211107034547	RMSE (Pixels)
Red	0.98
Blue	0.55
Green	0.68
Red bands combined with max operator	0.94
Red bands combined with sum operator	0.93
Red bands combined with average operator	0.93

Table 4.3 coregistration result of PRS_L2D_STD_20211107034543_20211107034547

PRS_L2D_STD_20221113034523_20221113034527	RMSE (Pixels)
Red	0.35
Blue	0.80
Green	0.36
Red bands combined with max operator	0.31
Red bands combined with sum operator	0.32
Red bands combined with average operator	0.32

Table 4.4 coregistration result of PRS_L2D_STD_20221113034523_20221113034527

PRS_L2D_STD_20200308034830_20200308034834	RMSE (Pixels)
Red	0.07
Blue	0.27
Green	0.19
Red bands combined with max operator	0.07
Red bands combined with sum operator	0.07
Red bands combined with average operator	0.07

Table 4.5 coregistration result of PRS_L2D_STD_20200308034830_20200308034834

PRS_L2D_STD_20230208034531_20230208034535	RMSE (Pixels)
Red	0.07
Blue	1.82
Green	0.08
Red bands combined with max operator	0.07
Red bands combined with sum operator	0.07
Red bands combined with average operator	0.07

Table 4.6 coregistration result of PRS_L2D_STD_20230208034531_20230208034535

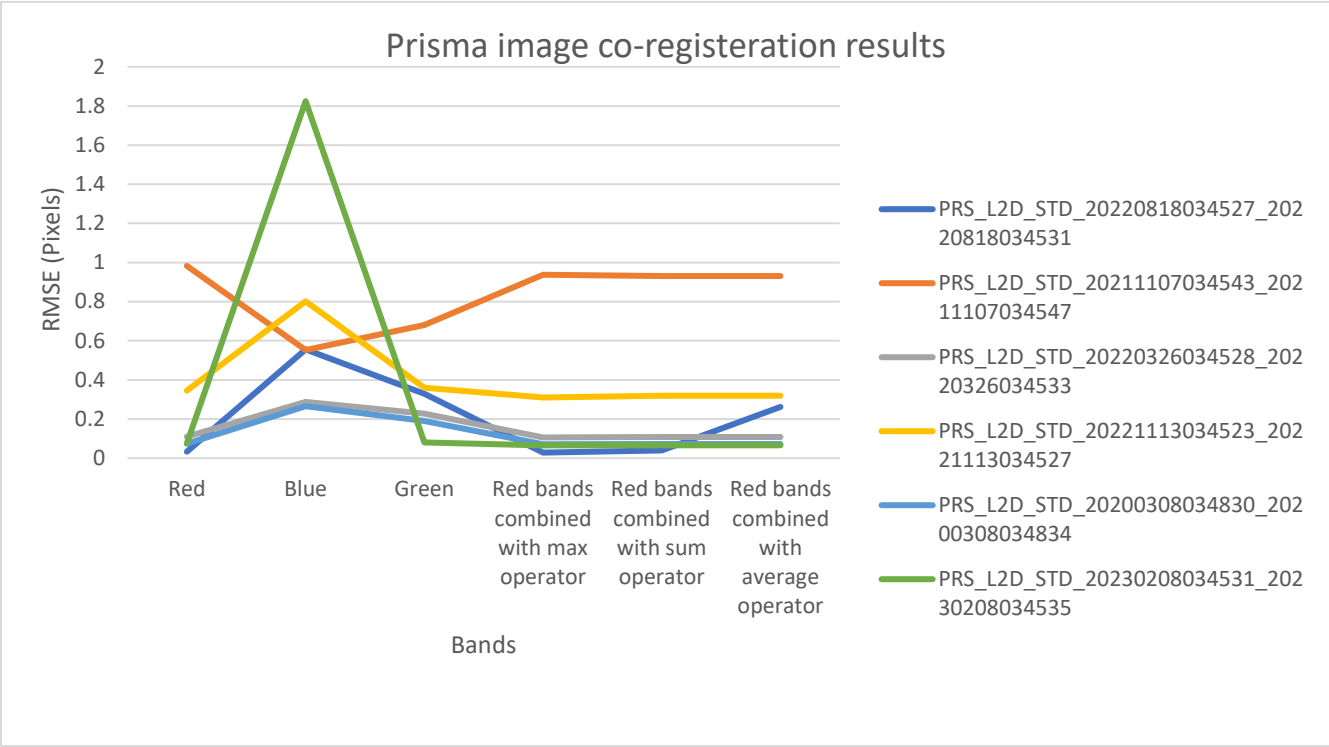

Figure 4.1 PRISMA image co-registeration results

Result of classification process

Actual \ Predicted	Water	Trees	Grass	Flooded Vegetation	Crops	Shrub and Scrub	Built	Bare	Snow and Ice	Total Actual
Water	29	1	0	3	5	5	10	4	0	57
Trees	35	5534	35	11	35	11	20	26	8	5715
Grass	3	1	36	0	1	0	4	0	0	45
Flooded Vegetation	2	0	1	8	1	3	2	4	0	21
Crops	3	7	1	8	73	5	2	2	1	102
Shrub and Scrub	4	2	3	9	4	114	10	5	0	151
Built	9	0	0	3	10	6	49	2	1	80
Bare	1	2	1	0	0	0	1	3	0	8
Snow and Ice	0	0	0	0	1	0	0	0	1	2
Total Predicted	77	5547	77	34	130	144	99	46	10	

Table 4.7 Random Forest Model Confusion Matrix for imbalanced dataset

Actual \ Predicted	Water	Trees	Grass	Flooded Vegetation	Crops	Shrub and Scrub	Built	Bare	Snow and Ice	Total Actual
Water	67	2	3	1	2	9	10	5	0	99
Trees	4	5531	13	5	25	4	1	8	2	5593
Grass	0	5	57	0	1	0	1	1	0	65
Flooded Vegetation	6	0	4	20	8	2	4	2	0	46
Crops	3	6	0	6	90	1	2	0	0	108
Shrub and Scrub	0	1	0	4	1	122	4	1	0	133
Built	6	0	0	6	3	5	76	4	0	100
Bare	0	2	0	0	0	1	0	25	3	31
Snow and Ice	0	0	0	0	0	0	0	0	6	6
Total Predicted	86	5547	77	42	130	144	97	46	11	

Table 4.8 SVM Model Confusion Matrix for imbalanced dataset

Actual \ Predicted	Water	Trees	Grass	Flooded Vegetation	Crops	Shrub and Scrub	Built	Bare	Snow and Ice	Total Actual
Water	26	2	2	0	0	2	0	0	1	34
Trees	5	4076	3	6	5	5	4	2	1	4109
Grass	0	0	41	0	0	1	6	0	1	52
Flooded Vegetation	0	0	0	11	3	0	0	0	0	18
Crops	0	0	0	1	38	3	1	1	1	50
Shrub and Scrub	2	1	0	0	2	40	0	0	0	51
Built	2	0	5	0	1	1	60	5	0	81
Bare	0	0	0	0	0	0	0	16	0	24
Snow and Ice	0	2	0	0	0	1	0	0	6	18
Total Predicted	36	4083	54	22	54	59	78	32	19	

Table 4.9 SVM Model Confusion Matrix for balanced dataset

Overall Accuracy Calculation

For both models, the overall accuracy is calculated with the formula:

$$\text{Overall Accuracy} = \frac{\text{Sum of diagonal elements (True Positives)}}{\text{Total number of predictions}}$$

Random Forest Overall Accuracy:

$$\text{Overall Accuracy} = \frac{29 + 5534 + 36 + 8 + 73 + 114 + 49 + 3 + 1}{57 + 5715 + 45 + 21 + 102 + 151 + 80 + 8 + 2} \approx 94.60\%$$

SVM Overall Accuracy:

$$\text{Overall Accuracy} = \frac{67 + 5531 + 57 + 20 + 90 + 122 + 76 + 25 + 6}{99 + 5593 + 65 + 46 + 108 + 133 + 100 + 31 + 6} \approx 96.97\%$$

SVM for balanced dataset Overall Accuracy:

$$\text{Overall Accuracy} = \frac{26 + 4076 + 41 + 11 + 38 + 40 + 60 + 16 + 6}{36 + 4105 + 52 + 15 + 44 + 50 + 75 + 16 + 9} \approx 0.9939 \approx 99.39\%$$

User's Accuracy (Precision)

User's Accuracy for each class is calculated as the number of true positives (diagonal element) divided by the total predicted for that class (column total).

$$\textbf{User's Accuracy (Precision)} = \frac{\textbf{True Positives (TP)}}{\textbf{TP} + \textbf{False Positives (FP)}}$$

Producer's Accuracy (Recall)

Producer's Accuracy for each class is calculated as the number of true positives (diagonal element) divided by the total actual occurrences of that class (row total).

$$\textbf{Producer's Accuracy (Recall)} = \frac{\textbf{True Positives (TP)}}{\textbf{TP} + \textbf{False Negatives (FN)}}$$

Class	User's Accuracy (Precision)
Water	33.72%
Trees	99.77%
Grass	46.75%
Flooded Vegetation	19.05%
Crops	56.15%
Shrub and Scrub	79.17%
Built	50.00%
Bare	6.52%
Snow and Ice	9.09%

Table 4.10 User's Accuracy (Precision) for Random Forest

Class	Producer's Accuracy (Recall)
Water	50.88%
Trees	96.83%
Grass	80.00%
Flooded Vegetation	38.10%
Crops	71.57%
Shrub and Scrub	75.50%
Built	61.25%
Bare	37.50%
Snow and Ice	50.00%

Table 4.11 Producer's Accuracy (Recall) for Random Forest

Class	User's Accuracy (Precision)
Water	77.91%
Trees	99.71%
Grass	74.03%
Flooded Vegetation	47.62%
Crops	69.23%
Shrub and Scrub	84.72%
Built	77.55%
Bare	54.35%
Snow and Ice	54.55%

Table 4.12 User's Accuracy (Precision) for SVM

Class	Producer's Accuracy (Recall)
Water	67.68%
Trees	98.89%
Grass	87.69%
Flooded Vegetation	43.48%
Crops	83.33%
Shrub and Scrub	91.73%
Built	76.00%
Bare	80.65%
Snow and Ice	100.00%

Table 4.13 Producer's Accuracy (Recall) for SVM

Class	Precision (User Accuracy)
water	72.20%
trees	99.30%
grass	79.30%
Flooded vegetation	73.30%
crops	86.00%
Shrub and scrub	80.00%
built	90.90%
bare	100.00%
Snow and ice	66.70%

Table 4.14 User's Accuracy (Precision) for SVM for balanced dataset

Class	Recall (Producer Accuracy)
water	72.20%
trees	99.30%
grass	79.30%
flooded vegetation	73.30%
crops	86.00%
Shrub and scrub	80.00%
built	90.90%
bare	100.00%
Snow and ice	66.70%

Table 4.15 Producer's Accuracy (Recall) for SVM for balanced dataset

Discussion

In assessing the co-registration accuracy through Root Mean Square Error (RMSE) metrics across various spectral bands—Red, Blue, Green—and combined Red with operations such as max, sum, and average, it is evident that lower RMSE values correlate with heightened accuracy. For instance, the dataset PRS_L2D_STD_20230208034531_20230208034535 and PRS_L2D_STD_20200308034830_20200308034834 exhibit exceptionally low RMSE values across all bands, indicative of a high-precision co-registration process. Conversely, datasets PRS_L2D_STD_20220818034527_20220818034531 and PRS_L2D_STD_20221113034523_20221113034527 demonstrate moderate RMSE values, signifying satisfactory but less optimal co-registration.

The dataset PRS_L2D_STD_20211107034543_20211107034547, however, manifests the highest RMSE values, signaling potential discrepancies in the co-registration accuracy. This divergence may stem from variable atmospheric conditions and cloud coverage at the time of image capture, which can introduce additional error sources do not present in the other datasets. Furthermore, the higher cloud coverage in the Sentinel-2 images corresponding to this period likely exacerbates the co-registration challenges, demanding a more nuanced approach to address these atmospheric inconsistencies.

In light of these observations, future research should incorporate atmospheric correction techniques and cloud masking strategies to mitigate the effects of varying cloud coverage and atmospheric conditions. Additionally, leveraging temporal analysis to align image acquisition dates with optimal atmospheric clarity could further refine the co-registration process. Such methodological enhancements will ensure the reliability of multi-temporal analyses and the robustness of subsequent land cover classifications.

In an analysis of the Random Forest and SVM models using their respective confusion matrices, distinct patterns emerge in terms of their performance across various classes. The Random Forest model exhibits a variable user's accuracy, with a notably high accuracy of nearly 100% for the 'Trees' class, but a substantially lower accuracy of 6.52% for the 'Bare' class. This disparity in accuracy across classes could be indicative of the model's challenges in dealing with class imbalances or complex decision boundaries. The overall accuracy of the Random Forest model stands at about 94.60%.

The producer's accuracy for the Random Forest model, which reflects its ability to correctly identify actual occurrences of each class, reveals similar disparities. The model's performance varies across different classes, suggesting potential overfitting issues or a lack of adaptability to certain class characteristics.

When comparing this to the SVM model, a notable improvement in user's accuracy is observed. The SVM model not only outperforms the Random Forest model in overall accuracy, with a figure of approximately 96.97%, but also shows enhanced user's accuracy across all classes. This is particularly evident in classes with limited sample sizes, such as 'Bare' (80.65% vs. 37.50%) and 'Snow and Ice' (100% vs. 50%). The higher accuracies in these classes suggest the SVM's superior ability to effectively delineate between different classes, even in scenarios of limited data.

Producer's accuracy for the SVM model, calculated similarly to that of the Random Forest model, also indicates a consistent improvement across all classes. This consistent performance across both user's and producer's accuracy metrics underscores the SVM model's robustness and its capability to handle the challenges posed by class imbalance and complex feature spaces more effectively than the Random Forest model.

The Random Forest model, while generally robust, shows a marked variability in its ability to accurately predict certain classes. This variability might stem from the model's tendency to overfit, especially when dealing with classes that have complex decision boundaries or that are underrepresented in the training data. For instance, the lower accuracy rates in classes like 'Water', 'Flooded Vegetation', and 'Bare' suggest difficulties in differentiating between classes that are potentially similar or not well-represented.

Conclusion

The co-registration process using the Gefolki algorithm and forward-backward method yielded varying degrees of accuracy across different datasets, as indicated by RMSE values. the PRS_L2D_STD_20200308034830_20200308034834 and PRS_L2D_STD_20230208034531_20230208034535 datasets stand out for their superior co-registration outcomes with Sentinel-2, as evidenced by the lowest RMSE values, particularly when employing the max operator in the red band analysis. The consistency of these images in yielding the best results across different metrics highlights its superior coregistration quality. The success of the coregistration of those images could be attributed to various factors, including optimal imaging conditions, effective coregistration techniques, or inherent characteristics of the scene that made alignment more precise. Understanding why this particular image performed the best could provide valuable insights for enhancing coregistration techniques in future applications.

In summary, the classification models performed well, with the SVM model on a balanced dataset showing superior accuracy. This suggests that the SVM model, particularly with a balanced dataset, is highly effective for land cover classification tasks when using coregistered PRISMA with Sentinel-2 images. Its ability to handle high-dimensional spaces effectively and to maintain robustness against overfitting is particularly beneficial, especially in cases where data for certain classes is limited. On the other hand, the Random Forest model, despite its overall good performance, might require further tuning and strategies to address its shortcomings in dealing with class imbalance and complex decision boundaries.

Recommendations

- **Optimization of Co-registration**: For datasets with higher RMSE values, investigate the causes and optimize the co-registration process to improve accuracy.

- **Temporal Consistency**: Examine the impact of temporal factors on co-registration and classification accuracy, considering seasonal changes and image acquisition times.

- **Algorithm Optimization**: While the Gefolki algorithm has shown satisfactory results, there might be room for further optimization, especially in the preprocessing stage to reduce RMSE.

- **Data Augmentation**: For classes with very few samples, such as 'Snow and Ice', using data augmentation techniques to increase the number of training samples could improve the Random Forest model's performance.

- **Feature Engineering**: For the Random Forest model, deeper analysis into feature selection and engineering might provide improved classification boundaries.

- **Model Tuning**: Both models would benefit from hyperparameter tuning; for SVM, exploring different kernel functions might yield better decision boundaries, while for Random Forest, adjusting the number of trees and depth could prevent overfitting.

- **Cross-validation**: Implement k-fold cross-validation to assess the models' robustness and their performance variance across different subsets of the data.

- **Ensemble Techniques**: Combining the predictions from both models through ensemble techniques might capitalize on their strengths and mitigate their weaknesses, potentially leading to a more accurate and robust classifier.

- **Address Class Imbalance**: Use techniques like SMOTE or adjust class weights in the SVM to handle the class imbalance problem better.

By adopting these recommendations, there is potential to improve both the co-registration accuracy and the predictive capabilities of the models, particularly for classes that are underrepresented in the dataset.

Appendix